MONITORING AND IMPROVEMENT OF MACHINING PROCESS OF CARBON FIBER REINFORCED POLYMER MATERIALS

by

Burcu Bilgiç

Submitted to the Graduate School of Engineering and Natural Sciences in partial fulfilment of the requirements for the degree of Master of Science

Sabanci University

Fall 2022-2023

Approved by

MONITORING AND IMPROVEMENT OF MACHINING PROCESS OF CARBON FIBER REINFORCED POLYMER MATERIALS

Burcu Bilgiç

Manufacturing Engineering, MSc. Thesis, 2022-2023

Thesis Supervisor: Asst. Prof. Dr. Lütfi Taner TUNÇ

Keywords: Carbon Fiber Reinforced Polymers, Machining, delamination assessment, image processing, drilling operation, edge trimming operation

Abstract

Carbon fiber reinforced plastic (CFRP) materials are an important class of advanced materials that are used in various applications due to their high strength-to-weight ratio and excellent performance characteristics. The machining of CFRP is an essential process for shaping and finishing these materials, and it requires specialized tools and techniques to achieve good results. Effective machining of CFRP is crucial for ensuring the quality and performance of the finished products, as well as for reducing production costs and increasing efficiency. In this study, different aspects of CFRP machining from airborne dust generation and vacuuming system to reduce the presence of dust and improve the suction performance to parameter selection for drilling and edge trimming operations for machining perfection is examined. Machining parameter and their effect on final product quality is investigated to oversee the correlation between final product quality and the selected parameters. Furthermore, image processing model which is a useful approach for assessing the machining quality of drilling CFRP, as it allows for the automatic inspection and analysis of the surface finish and dimensional accuracy of the drilled holes is developed. The importance of CFRP materials and the effective machining process of these materials cannot be overstated, and the use of image processing for quality assessment is proven to be an important tool for optimizing the machining process and achieving high-quality results.

KARBON FIBER TAKVIYELI POLIMER MALZEMELERIN ISLEME SURECININ IZLENMESI VE IYILESTIRILMESI

Burcu Bilgiç

Üretim Mühendisliği, Yüksek Lisans Tezi, 2022-2023

Tez Danışmanı: Dr. Öğr. Üyesi Lütfi Taner TUNÇ

Anahtar Kelimeler: Karbon fiber takviyeli polimer, talasli imalat, delaminasyon degerlendirme, goruntu isleme, delme islemi, kenar duzeltme operasyonu

Özet

Karbon fiber takviyeli plastik (CFRP) malzemeleri, yüksek kuvvet-ağırlık oranı ve mükemmel performans özellikleri nedeniyle çeşitli uygulamalarda yaygın olarak kullanılan önemli bir ileri malzeme sınıfıdır. CFRP'nin işleme işlemi, bu malzemeleri şekillendirme ve bitirme için esastır ve iyi sonuçlar elde etmek için özel araçlar ve teknikler gerektirir. CFRP'nin etkili işlemesi, bitirilen ürünlerin kalitesi ve performansını sağlamak, aynı zamanda üretim maliyetlerini azaltmak ve verimliliği artırmak için önemlidir. Bu çalışmada, hava toplarından oluşan toz üretimi ve tozun varlığını azaltmak ve emiş performansını iyileştirmek için vakum sistemine kadar CFRP işleme çeşitli yönleri incelenmektedir. İşleme parametrelerinin ve bu parametrelerin son ürün kalitesine etkisi araştırılır ve son ürün kalitesi ile seçilen parametreler arasındaki ilişki izlenir ve CFRP delme işleminin işleme kalitesini değerlendirmede yararlı bir yaklaşım olan görüntü işleme modeli geliştirilmiştir. Bu model, delinen deliklerin yüzey bitişi ve boyutsal doğruluğunun otomatik olarak incelenmesine ve değerlendirilmesine olanak sağlar. CFRP malzemelerinin ve bu malzemelerin etkili işleme işlemlerinin önemi asla vurgulanamaz ve görüntü işleme kalite değerlendirme için kullanımının, işleme işlemini optimize etmek ve yüksek kaliteli sonuçlar elde etmek için önemli bir araç olduğu kanıtlanmıştır.

ACKNOWLEDGMENTS

Firstly, I would like to express my gratitude to my thesis advisor Asst. Prof. Dr. Taner Tunç for his guidance, support and encouragement throughout my studies. His insightful feedback pushed me to work hard and do the best I can. I am very grateful for the opportunity of working with him.

I am very grateful for the support that I received from all of my friends. Many thanks to Sinem Kurnaz, Bora Gönül, Orkun Seçer, Saltuk Yıldız, Irfan Sargın and last but not least Ömer Altıntaş for their encouragement, friendship, and precious memories at the graduate school. Their contributions and dedications were essential to the success of this project.

Finally, I am very thankful to my family for the never-ending trust, love and support they had for me.

TABLE OF CONTENTS

LIST OF TABLES

LIST OF FIGURES

LIST OF ABBREVIATIONS

ANOVA	Analysis of Variance
CFRP	Carbon Fiber Reinforced Polymer
GLM	General Linear Model
DoE	Design of Experiment
MRR	Material Removal Rate
MDF	Medium density fibreboard
UD	Uni-Directional
RGB	Red Green Blue
RSM	Response Surface Methodology

Chapter 1

Introduction

In recent years, carbon fiber reinforced polymers (CFRPs) have become increasingly important in industries such as aerospace and construction due to their unique properties of being lightweight, high-performing, and resistant to corrosion. However, a significant drawback of these materials is their tendency to sustain damage during the machining process. This chapter focuses on researching ways to minimize and evaluate these damages. Specifically, the area of delamination and its effects on the material as well as methods to assess the severity of delamination are studied extensively in literature.

1.1 Background

Carbon fiber reinforced polymers (CFRPs) are becoming increasingly popular in various industries because they have the potential to save weight and improve efficiency. Their desirable properties include high resistance to corrosion, fatigue, and stiffness. As a result, the use of CFRP materials has been growing in various industries in recent years, and there is a push to develop new manufacturing processes for them.

In many industries, composite components need to be made in a near-net shape and conventional machining methods such as drilling, milling, and trimming are typically used to join parts. However, these machining operations can cause surface damage defects such as delamination, fiber pull-out, uncut fibers, and matrix cracking [1]. Research has shown that there is a connection between the mechanical performance of CFRPs and the surface damage defects caused by machining [2].

For certain industries, the strength and durability of components in use is vital, so it is essential to understand the surface profile and defects that occur during machining operations. For example, in the aerospace industry, tight tolerances are required, so controlling surface damage during machining is a crucial constraint for manufacturers. Additionally, efforts should be made to minimize the production of scrap or damaged material and lower production costs. Therefore, it is necessary to understand the basics of machining CFRPs, the mechanisms of chip formation, and the types of surface defects that occur during machining. Due to the non-homogeneous structure and anisotropic properties of fiber composites, their machinability characteristics are different from those of metals.

There is a significant interest in understanding how different machining parameters affect the surface damage structure of composite materials. Both academia and industry are interested in the relationship between machining parameters and the types of defects that occur during machining. Studies in literature have shown that factors such as feed rate, cutting speed, tool geometry, tool wear, material type, and fiber orientation can influence the forces generated during machining and the resulting surface quality. By identifying the correlation between these parameters and the types of damage, it is possible to improve the consistency and cost-effectiveness of manufacturing composite components.

The goal of this project is to develop a method to accurately measure and evaluate the damage structure and severity of delamination, understand the damage mechanism, and monitor and control the machining process parameters to improve surface quality. This research aims to improve the classification process for different types of damage and measurement methods for non-homogeneous multidirectional laminates, and to create predictive tools to assess the impact of machining parameters on surface quality and damage types. The results of this research will be useful for both industrial composite manufacturers and researchers.

1.2 Objective of the thesis

This project focuses on different types of machining operations performed on CFRP materials and how machining parameters affect machining-induced damage. This research is driven by the needs of industry and findings from academia. The initial step of the research is to evaluate the surface profile of the machined surface using experimental techniques and image processing methods.

The first part of this work looks at the issues found in the literature related to assessing delamination geometry, delamination type, measurement methods, and assessment formulations. As a result, this research evaluates a new assessment method for characterizing delamination geometry using image processing methods. This new approach aims to improve the accuracy of measurements and assessment methods by using image processing to quantify the severity of delamination. Additionally, by studying the delamination damage mechanisms and methods, the research aims to use the results to predict the impact of machining parameters on delamination geometry.

The aim of this project is to improve our understanding of the processes involved in machining carbon fiber reinforced plastic (CFRP), including the mechanism of cutting, the resulting surface quality, and the occurrence of delamination. A new method for evaluating delamination will be used in this project. By gaining a better understanding of these processes, we will be able to better characterise the surfaces produced by machining CFRP and continue to research new tools and techniques for machining these materials.

The project conducts a range of machining tests using different types of tools, such as drilling and edge trimming tools, as well as various types of CFRP materials with varying fiber orientations and thicknesses. The goal is to evaluate the impact of machining parameters on cutting force, delamination, and surface quality. The cutting forces are measured during the tests using a dynamometer, while drilling and edge trimming are performed on laminates with different fiber orientations, feed rates, cutting speeds, and varying levels of tool wear. The results of these tests will be used to quantify the effect

of different machining parameters on delamination and analyze the data to predict the outcome for various machining scenarios.

1.3 Literature Review

In literature, there have been various research on evaluating different machining process and process parameters on carbon fiber reinforced polymers and different studies propose different functions and evaluation techniques to improve the machining efficiency and quality. This study aims to present a comprehensive approach, which incorporates the best techniques from existing literature, to evaluate machining processes. By reviewing literature, it is clear that an image processing approach is needed to evaluate drilling quality in a machine shop setting, and a comparative method is needed to identify the most effective machining parameters for various machining operations. Therefore, this study will present different studies with various methods and focuses.

1.3.1 Carbon fiber introduction

Carbon fiber reinforced polymers (CFRPs) are widely used in aerospace structures, and their unique properties, such as high performance, light weight, high stiffness, and resistance to corrosion, make them an ideal choice for many other industries, such as construction, medical, and optical. [3].

In the aerospace industry, CFRP materials are frequently used in the construction of wing boxes, stabilizers, wings, and panels on aircraft. Examples of this type of application can be seen in Boeing and Airbus airliners [4]. Dreamliner, Boeing 767 and 787, Airbus A350 and A380 etc. increasingly uses CFRP materials. The material breakdown of Airbus can be seen in Figure 1[5].

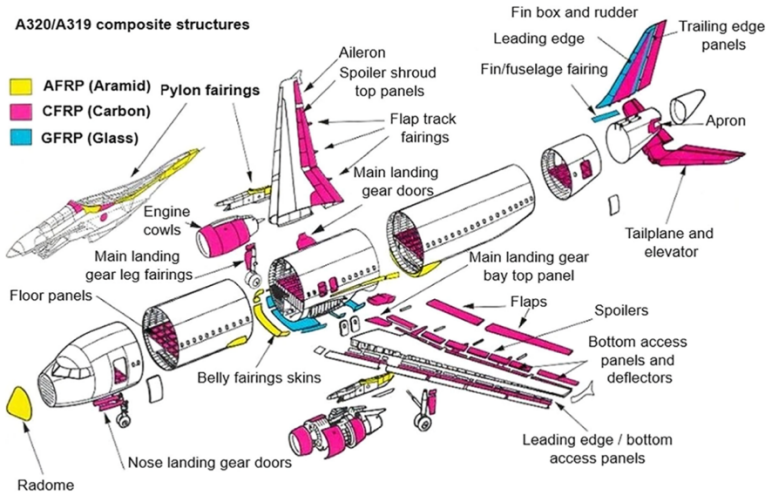

Figure 1: The material breakdown of Airbus A320/A319

CFRP materials are commonly used in many industries, but they are especially prone to damage caused by machining. To fully understand the process of machining these materials, it is necessary to study the failure mechanisms and material properties of carbon fiber composites.

Carbon fiber reinforced polymers (CFRPs) are composed of carbon fibers and a binding matrix material. Typically, the fiber volume fraction in industry is around 60%. The matrix material acts as a binder for the carbon fibers, distributing loads and protecting them from external damage. The carbon fibers are typically created from a polyacrylonitrile precursor by oxidizing and carbonizing it at high temperatures.

Typically, carbon fibers have a diameter of around 5-10 micrometers and are grouped together to form a "tow." These grouped fibers are then pre-impregnated with an epoxy matrix material to create pre-preg sheets. Additionally, grouped fibers can also be used in filament winding processes. Carbon fibers are preferred for mechanical applications over glass fibers due to their superior stiffness and strength characteristics. The matrix constituent is usually a thermoset or thermoplastic polymeric plastic. However, epoxy resins are the preferred choice for high-grade aerospace applications.

It is known that a large number of holes are required for joints in the assembly stage of the aircraft structural parts [6]. The number of holes required for a commercial aircraft is

known to be up to 1.5 to 3 million. This number is averagely 300.000 holes for a jet fighter [7] [8]. There exist challenges in drilling process of CFRP and these challenges are mostly arisen from the heterogeneous and anisotropic, abrasive, and hard nature of fibers. To understand the damages occurring during machining operations of CFRP materials, the structure of the material itself and the manufacturing process of the materials should be investigated. The classification of composites are summarised in Figure 2.

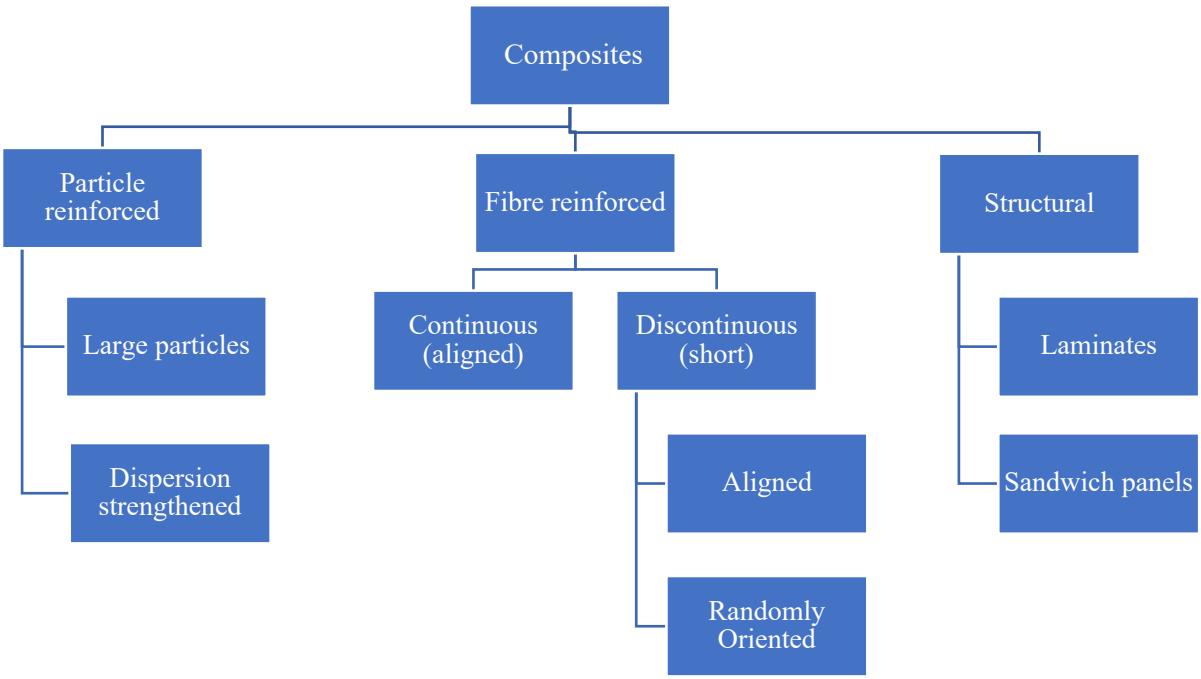

Figure 2: Classification of composite materials

CFRP materials are mainly constituted by pre-preg sheets of fibers by layering up these sheets in different orientations depending on the use cases. The nature of the pre-preg and the importance of the orientation is explained in the following section. Pre-preg sheets are made by immersing carbon fiber sheets in a resin bath, then storing them in a refrigerator until they are needed. During standard manufacturing methods, these refrigerated pre-preg sheets are cut to the desired shape and stacked on a mold surface in different orientations depending on the required mechanical properties, then vacuum-sealed and cured in an autoclave.. The vacuuming process is shown in Figure 3.

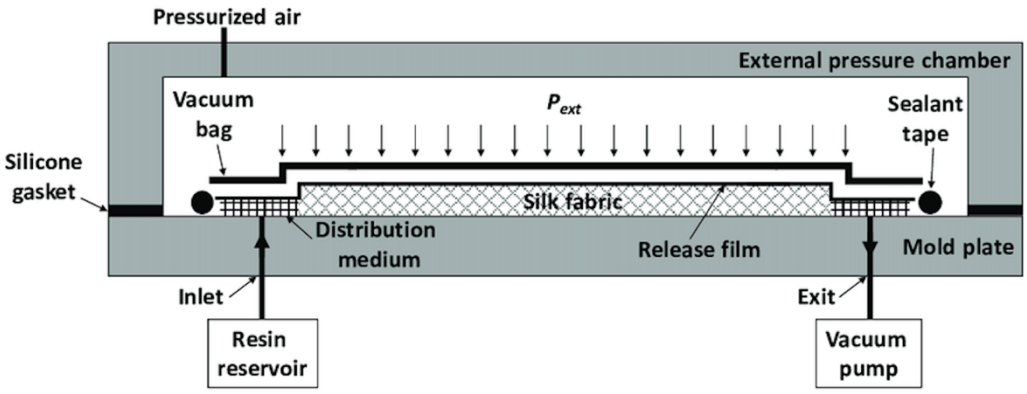

Figure 3: Vacuuming process

The pre-preg sheets are first cut to the correct dimensions and shape to fit the mold surface, then layered on top of the mold. A release agent is applied to the mold surface to prevent the pre-preg from sticking to it. The layered pre-pregs are then covered with a release film and sealed inside a vacuum bag. The bag is sealed around the edges using sealant tape. During the vacuuming process, a vacuum pump removes excess resin and any trapped air between the mold and release film, which helps to minimize voids and ensure consistent curing of the resin in the finished composite material.

There are different types of fiber geometry such as long chain fibrous composites, short chain, and woven composite materials. Long chain unidirectional carbon fiber composites are non-homogeneous and possess anisotropic properties. These properties give them a different modulus and strength in the fiber principal direction compared to the transverse fiber direction. The strength, volume fraction, quantity, and size of the fibers are the primary properties that determine the tensile strength of a composite material. Additionally, the strength of a fiber depends on its thickness and length, and longer or thicker fibers are more likely to have flaws, so their strength will be lower. Therefore, materials will have greater strength with a high fiber volume fraction. [9].

The structure of metals and composites are different, therefore, several damage modes can accumulate in CFRP materials leading to failure such as: fiber pull-out, fiber bridging, fiber/matrix debonding, fiber failure and matrix cracking.

The machinability of CFRP depends on the mechanical properties of fibers and resin, the fiber volume fraction, and the ply orientation. Additionally, the matrix glass transition temperature and the thermal conductivity of the matrix and fibers are known to be important factors in the machinability of CFRP.

The way the fibers and matrix bind together, as well as the rigidity of that bond, determines how the material will fail. Additionally, factors such as the orientation of the fibers, the pressure used during manufacturing, and the curing process are crucial for ensuring consistent material properties. However, factors such as manufacturing defects (e.g. empty spaces in the resin, wavy fibers, uneven distribution of fibers and matrix) can affect the mechanical properties of the composite.

1.3.2 Role of the fiber orientation in CFRPs

The fibers in CFRP materials have greater strength than the matrix, and typically around 70-90% of the material's load-bearing capacity comes from the fibers. The matrix primarily serves as a binding agent. This project uses fiber orientations of 0, 45, and 90 degrees. It's known that using different fiber orientations can make the composite material stable in all directions and prevent cracks from spreading. Typically, composites are layered symmetrically and balanced, with each layer being symmetrical through a center line, in order to ensure balanced mechanical properties and avoid warping due to variations in thermal expansion during the curing and cooling process.

In a nutshell, the direction of the fibers is known to be the responsible factor for damage tolerance and the orientations of fibers hence plays an important role in mechanical strength of CFRP material [10].

CFRP materials with unidirectional (UD) fibers are anisotropic, meaning they have the highest strength and stiffness in the direction of the fibers. However, in bidirectional fiber-oriented woven plies like plain weave fabrics, the fibers run in two different directions, resulting in varying strength characteristics in different directions [11].

Pre-preg plies are typically made from continuous fibers and can be aligned in unidirectional (UD) or bidirectional orientation to create thin plates of around 0.15mm in thickness. The strength design requirements depend on the applied load, its direction, the orientation of each pre-preg ply, and their sequence. To achieve optimal mechanical properties, it is important to properly select the pre-preg orientation. UD type of alignments in pre-preg are typically layered cross-ply to create a quasi-isotropic laminate, depending on the direction of the load. [12].

In actual production, the most commonly used stacking sequence for the plies is $0^{\circ}, -45^{\circ}, 45^{\circ}, \text{and } 90^{\circ}$ sequence, which simplifies the analysis and design of fastened joints. The plies oriented at 0° are intended to handle axial loads, those oriented at 45° are designed to resist shear loads, and those oriented at 90° are intended to handle side loads. This quasi-isotropic arrangement is close to have the optimum properties and used in the aerospace structures to endure the loads in axial and side directions [13]. This phenomenon is graphically represented in Figure 4 where different pre-preg orientation and layer structure are illustrated.

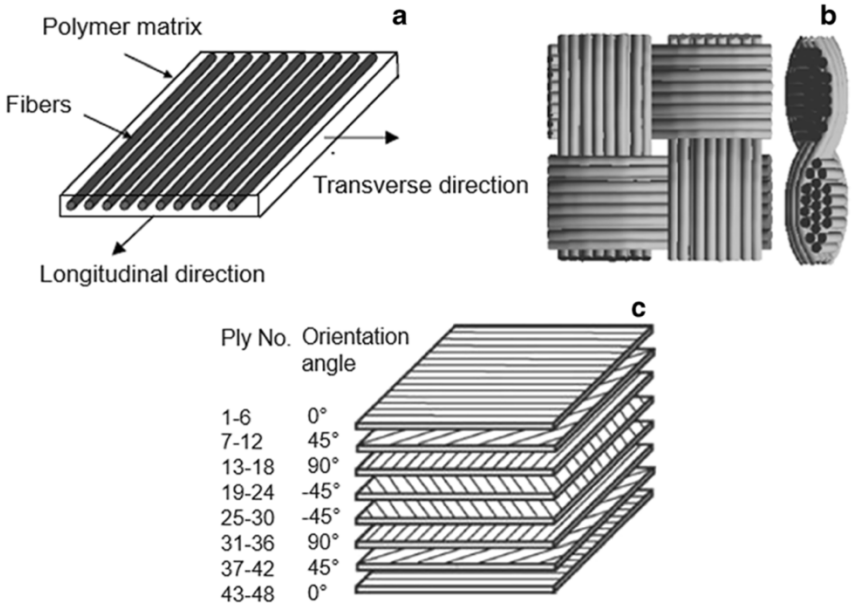

Figure 4: a) UD-ply laminate, b) woven-ply laminate, c) multi-orientated laminate with quasi-isotropic

The fibre orientation in CFRP highly effects the chip formation [4]. This effect is explained in section 2 composite machining in a detailed manner. It is noted that fiber orientation not only affects the chip formation and deformation types, but it also effects the surface of the drilled holes.

Wang et al. [15] experimented on epoxy-reinforced UD carbon fiber and stated that fiber orientation between 0° and 90° gives lower surface roughness however the surface roughness observed to be increasing with an increase of fibre orientation to 150°.

Previous studies, such as those by Palinikumar [16] and Gao et al. [17] have found that increasing the fiber orientation from 45° to 120°, and 135° leads to a rougher surface and poor surface profile. Additionally, Gao et al. [18] found that drilling holes into UD epoxy composites can cause more damage depending on the fiber orientation, with defects at the drilled hole becoming more severe as the fiber orientation increases from 90° to 180°.

1.3.3 Defects in CFRP machining

Researchers have stated that there exist different types of detect and problems that can be found during composite machining [19].

These phenomena can be listed as:

- Delamination
- Fuzzing
- Chipping
- Fiber/matrix debonding
- Spalling
- Fibre pull-out
- Uncut fibres
- Matrix cracking and burning
- Surface quality issues

Figure 5 illustrates some of the damages listed above [20].

Figure 5: Delamination, fiber frying, spalling, chipping and fuzzing [17]

In the industry, about 60% of all part rejections at the assembly stage are due to delamination and its effects on the dimensional accuracy and surface finish of machined holes. [21]. In addition, due to the high fiber content and strong resin system, CFRP materials can be highly abrasive and cause significant wear on cutting tools.

Early researchers found that, unlike when machining metals, a continuous chip is not produced when machining CFRP materials. Instead, dust-like or small fragmented chips are created when machining thermoset FRPs. 22].

It is well known that carbon fibers have a low tolerance to breaking due to their brittle and abrasive characteristics. Additionally, the matrix or thermosetting plastic has very little or no plastic deformation before failure. Therefore, when machining CFRP, the material is usually crushed or fractures sharply, making the cutting mechanism largely determined by the fibers' characteristics, debonding at the fiber-matrix interface, and the angles at which the fibers are cut. [13] [23].

Because of the challenging properties of CFRP materials, standard metal cutting tools tend to produce poor surface quality and low tool wear resistance when used to machine composites, due to the different wear mechanisms compared to metals. As machining composites is vastly different from machining metals, new practices and research must be developed to better understand the cutting mechanisms and improve surface quality.

One of the significant issues in the process of cutting fiber composites is the occurrence of delamination. In literature, there exist three main types of delamination. These types of delamination are shown and characterised in Figure 6.

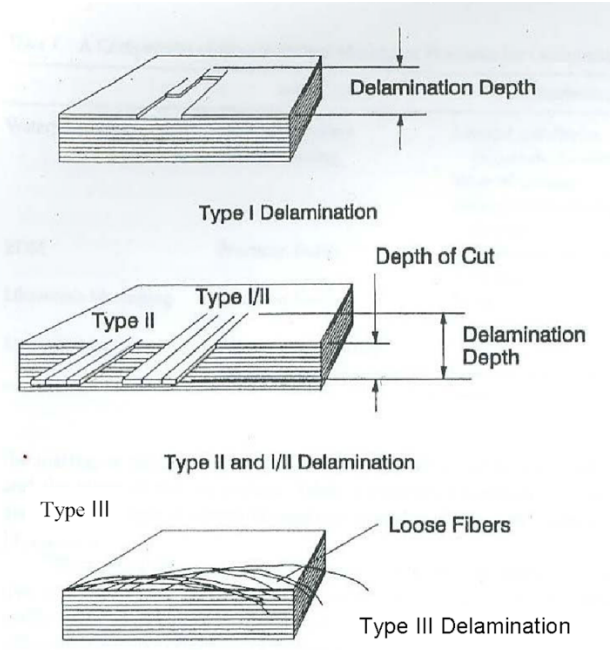

Figure 6: Delamination modes

Type I delamination is identified by the breakage and inward removal of fibers on the top surface from the machined surface. [19].

Type II delamination is identified by fibers that extend over the machined edge and fibers that have bounced back after being cut. Essentially, it is the presence of uncut fibers in the machined surface.

Type III delamination is characterized by cracks or fibers that are partially detached and run parallel to the machined surface. It is known that factors such as fiber orientation, tool geometry, type of machining operation, and machining parameters affect the extent and type of delamination. Studies have also shown that the orientation of fibers in relation to the cutting direction plays a crucial role in the chip removal process and surface damage. [24] [25] [19].

It is observed that the orientation of fibers in relation to the cutting direction plays a crucial role in the cutting process and the damage caused to the surface. Additionally, cutting forces have been shown to vary depending on the fiber orientation. The cutting mechanism changes depending on the fiber orientation, and each fiber orientation in relation to the cutting tool is illustrated in Figure 7.

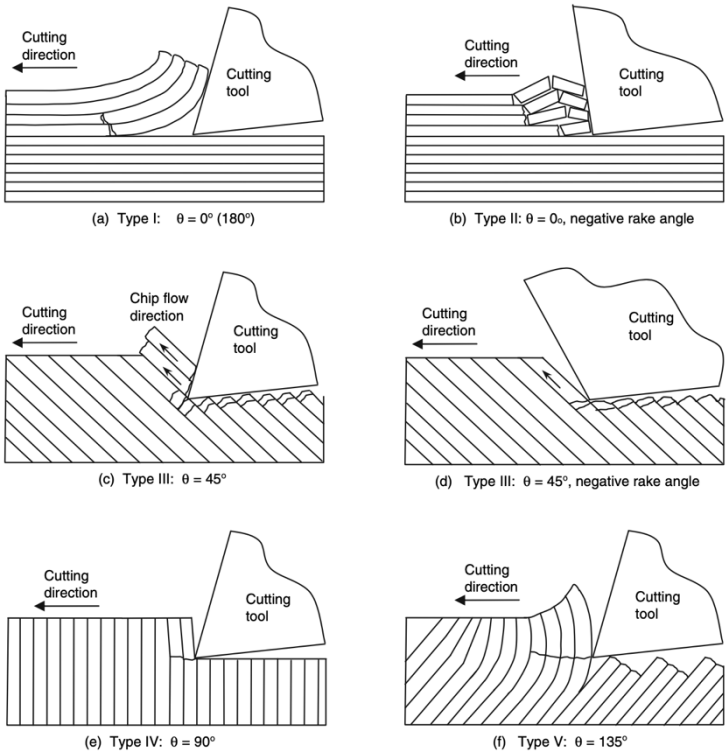

Figure 7: Fibre orientation in relation to cutting tool

In Figure 7(a), it is observed that in the 0° fibre orientation, the fibres are pushed up and the fibers are fractured on their cross section due to bending. The process of debonding or de-cohesion happens when the stress exceeds the physical bonding strength between fibers and the matrix interface. The fibers that have debonded from the fiber-matrix interface are bent upward, and a crack propagates along the interface until the fibers finally break [25].

In 90° fibre orientation, first, fibres are fractured perpendicularly due to the compression applied by the tool, Then there is a secondary breakage by interlaminar shear along the boundary of the fiber matrix for smaller particles [25]. Some plane displacement can be seen on the surface in the cutting direction due to small fracture particles. Koplev et al [22] stated that compared to 0° fibre orientation, irregular sized chips are produced. Furthermore, compared to 0° fibre orientation, overall cutting forces are larger in 90° fibre orientation due to the fact that all the fibres in that orientation should be compressed and sheared rather than bending case observed in 0° fibre orientation.

In the 45° orientation, fibres are sheared by the cutting tool tip and create a small dust-like chip while debonding from the matrix [19]. Furthermore, it is possible to observe that some individual fibres are pulled out from below the machined surface [26]. In terms of force fluctuations, they tend to fluctuate less compared to 0° fibre orientation.

In the 135° orientation, when fibers are facing the direction of the cutting tool, a combination of bending, crushing, and shearing fibers is observed. The fibers are first bent, and then a crack begins to spread beneath the surface along the boundary between the fibers and the matrix or the debonding area [24]. It is known that the due to the interfacial bonding strength between fibre and matrix, the interface is weak hence the crack can propagate easily. The surface is damaged because the fibers are crushed and broken. The surface roughness of 135° fibre orientation has been found to be worse than $0^{\circ}, 45^{\circ}, 90^{\circ}$ fibre orientations [22] [25].

1.3.4 Milling of CFRPs

Milling is a widely used manufacturing technique in industry to produce various flat or contoured surfaces such as slots, pockets, and shapes. [27]. During milling operations, the spindle rotates the tool and moves it into the workpiece. The milling tool typically has multiple cutting edges, and the spindle's axis of rotation can be either horizontal or vertical. [28]. During milling operations, the workpiece is cut with a varying depth due to the rotation of the cutting edge, which leads to a different cutting mechanism compared to turning processes.

In traditional milling, the tool rotates against the direction of the feed and the tool and workpiece are pushed away from each other because of the machining forces. It is observed that for each rotation of a single cutting edge, the chip thickness increases to its maximum before it is removed. [29] [22]. Therefore, the relationship between fiber orientation and the cutting tool edge changes as the tool rotates through the material, and unlike orthogonal turning, the relationship between fiber orientation and the cutting edge and chip thickness is not constant. Because of this inconsistency between fiber orientation and cutting tool edge interaction during tool rotation, machining forces fluctuate depending on each rotation cycle. It is observed that cutting forces increase as chip

thickness increases and the depth of cut determines the area to be removed and the number of fibers to be cut, while cutting speed, feed rate, and tool geometry determine chip thickness. [30].

Many researchers have conducted experiments on milling composite materials, as reported in literature. Karpat et al. [31] investigated slot milling operation of CFRP laminates and developed a model using cutting force coefficients. They observed that the cutting edge of the tool varies against the material fiber orientation as the tool rotates in slot milling. This is illustrated in Figure 8.

As expected, they observed that the cutting force coefficient represents the material's resistance to machining in the tangential and radial directions. Particularly, cutting forces in radial directions are higher when the fibre orientations are 0° and 90° compared to machining laminates with 45° and 135° fibre orientations. In addition to this, the maximum tangential cutting forces are observed in 135° fibre orientation and this phenomena is explained by "due to the combined effect of the instantaneous fibre cutting angle and the instantaneous chip thickness" [31]. More importantly, it is observed that delamination or uncut fibers are found to be a result of tool wear and fiber orientation, with the highest level of delamination occurring when the maximum tangential forces are present.

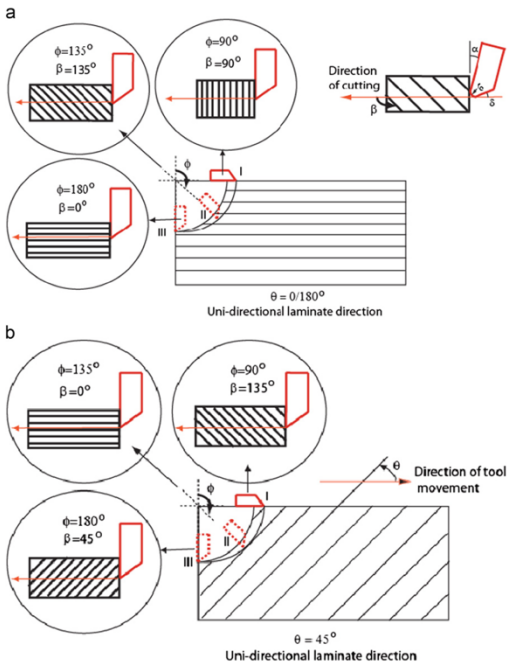

Figure 8: Tool cutting edge interaction with material fibre orientation in slot milling, adapted from REF [33]

Azmi et al. [30] conducted experiments on unidirectional glass-epoxy fiber with 16 layers to study the machinability of GFRP in terms of surface roughness, tool life, and machining forces by using Taguchi analysis. They performed end milling operations and took 3 measurements on the surface to analyze the average surface roughness. They found that feed rate had the most significant impact on surface roughness compared to cutting speed, and the resulting cutting force was mainly influenced by feed rate and cutting depth. Additionally, flank wear was found to be the most common wear mechanism observed during the test due to mechanical abrasion. As a result, tool wear, fiber orientation, cutting forces, and machining parameters have an effect on surface quality.

Two studies, Davim et al. [32] and Mathivanan et al. [33], analyzed the effects of feed rate, cutting speed, and material properties on machining forces, surface roughness, and delamination during end milling processes. Both studies found that machining forces increase with feed rate, and that surface roughness increases with feed rate and decreases with cutting speed.

Davim et al. found that delamination is also affected by feed rate. Mathivanan et al. found that machining forces have a linear correlation with feed rate and that cutting forces are higher when machining CFRP compared to GFRP due to its higher stiffness and strength. Hintze et al. [34] analysed the delamination formation on a woven plain weave having 0° and 90° fibre orientations. The author of the study found that the type of weave in the fabric can lead to varying levels of delamination during machining. Specifically, undulations in woven yarns were found to be a critical factor, with Type I/II delamination being the most common and dominant type observed.

In another study, Haddad et al [35] examined the effect of different machining methods such as water jet, abrasive diamond cutting, and standard burr tools on surface roughness, mechanical properties, and fatigue life. The results showed that the mechanical performance changes depending on the machining process and surface roughness. An increase in surface roughness decreases the strength of the component and it is important to minimize it to increase the strength and integrity of the parts. Ahmad et al [36] studied the effects of edge trimming on the surface roughness and delamination of CFRP. The researchers used a burr style router as the cutting tool and measured surface roughness

with a Mitutoyo profilometer. The study found that as the chip effective thickness increases, the frequency and depth of delamination also increases.

$$Chip\ effective\ thickness\ =\ a_{eff} = a_e \frac{V_f}{V_c} \quad (1)$$

Equation 1, given above is used to calculate the chip effective thickness where ae is the radial depth of cut, V_f is the feed rate and V_C is the cutting speed. It was observed that surface roughness in the longitudinal direction increases with an increase in chip effective thickness. An increase in feed rate increases chip effective thickness, while an increase in cutting speed decreases chip effective thickness. Therefore, the lowest feed rate and highest cutting speed result in the lowest chip effective thickness values. Additionally, Type I/II delamination was found to be the most common type. These findings were also reported by Ahmad et al. [37] who also found a relationship between chip effective thickness and surface roughness.

1.3.5 Drilling of CFRPs

Drilling is a commonly used method in the composite industry to join parts and is a vital final machining process for composite materials. However, composite materials are known to be difficult to machine, resulting in low drilling efficiency and unwanted delamination. Thus, improving the cost-effectiveness of current drilling processes and developing new ones is important for both literature and industry.

Typically, there are rigorous requirements for holes to meet surface and geometry standards, particularly in the aerospace industry. The quality of the holes is dependent on various factors such as material type, drilling conditions, and desired tolerances in the industry. It is essential for the position and diameter of the holes to be within tolerance limits for easy joining. Figure 9 shows the relevant factors that affect the hole quality of CFRP.

Figure 9: Factors affecting hole quality of CFRP

There exists alternative method for joining parts in composite such as bonded joints but since the bonded joints are permanent, they cannot be disassembled. Furthermore, the lifetime of bonded joints is not accurately known. Holes can be created during the lay-up and curing. However, the accuracy of the pre created holes are very low due to the distortion phenomena occurring in cooling process. although there exists different alternative to drilling process, due to the listed reasons, drilling of composite materials is still widely used in the industry and the drilling performance is crucial when the large number of drilling operation is required. The drilling performance of CFRPs is affected by factors such as material and tool selection, coolant, and type of machining operation. Therefore, the quality of drilling composite materials is highly dependent on the selection of process parameters. Additionally, using the optimal process parameters can help achieve the best drilling performance and reduce delamination. Figure 10 lists machining and tool related process parameters for drilling of CFRP and the online and offline output data classification.

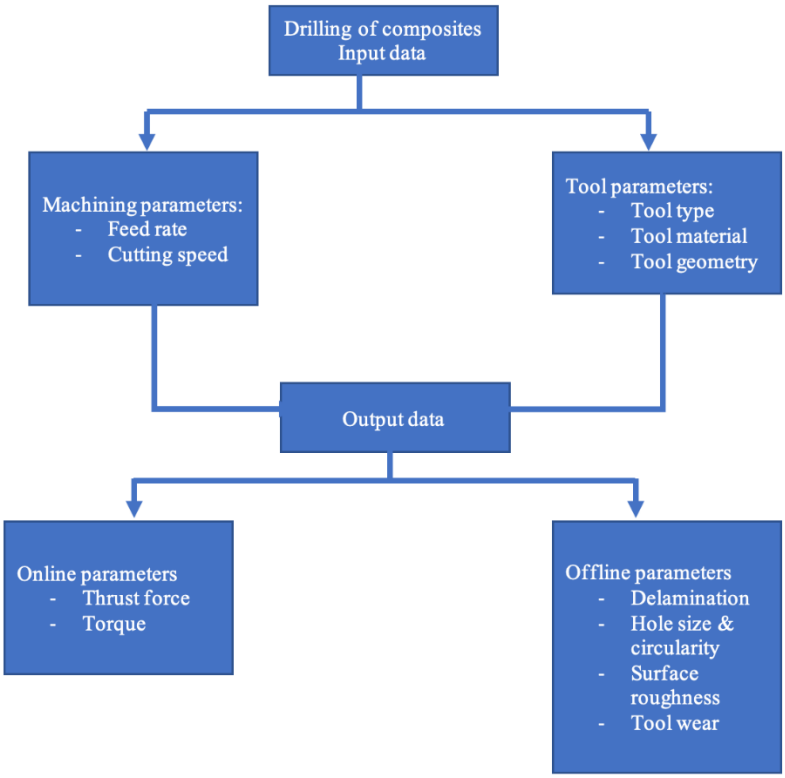

Figure 10: Process parameters and output data

Table 1 shows the relationship between machining parameters and drilling-induced delamination. The relationship between feed rate and delamination is discussed in the following chapter based on literature. However, the effect of cutting speed on drilling of CFRP is still a topic of debate [39].

Table 1: Impact of process parameters on delamination

Variation in machining parameter	Impact on delamination	References	
		Entry delamination	Exit delamination
Cutting speed (high)	Increases No/slight effect Decrease	[40] [41] [42] [43] [44] [40]	[45] [46] [42] [47] [44] [49] [50]
Feed rate (high)	Increases	[50] [47] [45] [42] [43]	[43] [44] [51] [52]

Many researchers have investigated the effect of input variables such as feed rate, cutting speed, and point angle of a twist drill bit on drilling-induced delamination in composite materials. The majority of literature shows that drilling-induced delamination increases with feed rate at any cutting speed, regardless of drill geometry. This is typically explained by an increase in thrust force during drilling as feed rate increases. The relationship between cutting speed and delamination is less clear, with different studies observing different trends. Some studies such as Davim et al. [53], [46], [54] and Kilickap [51] found a positive correlation, where delamination increases with cutting speed during conventional drilling. Others such as Khashaba [55] found a negative correlation, where delamination decreases with cutting speed during conventional drilling. Gaitonde et al. [56] found that during high-speed drilling of thin woven-ply CFRP composite laminates, drilling-induced delamination decreases with an increase in cutting speed.

Overall, the effect of feed rate on delamination during drilling operations is found to be more significant than that of cutting speed, and delamination occurs even at minimum feed rate according to most research.

Many researchers have analyzed the relationship between the angle point of a twist drill bit and delamination, but the results of their experiments vary. Gaitonde et al. [56] found that delamination tends to increase with an increase in the point angle of a twist drill bit for a cemented carbide tool during both conventional and high-speed drilling of woven CFRP composite laminates. However, Kilickap [7] found that delamination tends to decrease with an increase in the point angle of a twist drill bit for a steel tool during conventional drilling of UD-ply GFRP composite laminates. It is important to note that the researchers used different tools and fiber orientations, which could have affected the results.

1.3.6 Mechanism of drilling induced delamination

Delamination is an unwanted issue that occurs as a result of drilling operations and is defined as the separation between the layers of a composite material. It can significantly reduce the assembly tolerance and bearing strength, and has the potential to cause long-

term deterioration of performance under fatigue loads. Thus, delamination is widely recognized as the main damage encountered during drilling operations [8, 6, 9, 10].

In the literature, a significant amount of research has been devoted to studying delamination in composite drilling, with a focus on the top and bottom layers of composite plates. Thrust force has been identified as one of the main contributing factors to delamination during the drilling process [11].
In drilling processes, two types of drilling induced delamination is observed:

- Peel-up delamination: it is observed when the top ply of the laminate is pulled up by the cutting flutes. The laminate is bend due to the pulling force and get separated.
- Push-down (out): It is observed that when the bottom layer of the plate is pushed by the vertical thrust force, it bends. Because of the weak inter-laminar interface, bending can cause a crack to propagate along the interface [11].

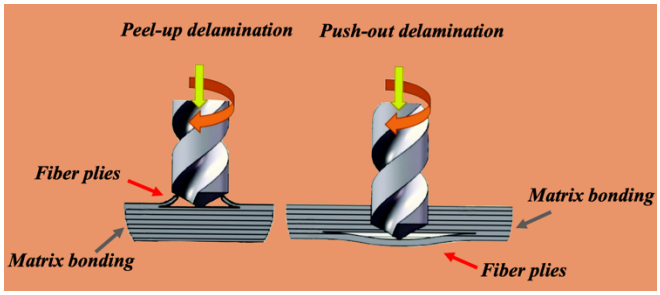

Figure 11: Delamination type occurring in drilling operation

It is known that increasing the feed rate results in an increase in uncut chip thickness and an increase in thrust force [11]. Therefore, feed rate is considered one of the primary causes of delamination. Additionally, tool wear and chisel edge size have been shown to contribute to the thrust force values, making them also effective in determining the severity of delamination [12]. This effect is mostly visible on the bottom layer of the composite, where push-out delamination is observed. To reduce delamination, one method is to decrease the feed rate near the hole exit [13].

Wen-chou chen [13] conducted experiments on drilling CFRP by using X-ray to analyze the size of the damage and delamination. The author coated the CFRP with

tetrabiomethane before using X-ray to analyze the hole dimension, and measured the thrust force and torque values with a dynamometer to observe the relation between thrust force and delamination. Furthermore, the effect of tool wear and drilling parameters were also investigated. It was observed that the delamination severity is mostly dominated by high thrust force, and by lowering the feed rate, torque and thrust force are reduced, resulting in a decrease in delamination. One important finding from the study was that the feed rate at the exit side of the part should be decreased during the drilling process to improve the hole quality. Furthermore, an increase in tool flank wear leads to an increase in thrust force and significant delamination at high spindle speeds.

In literature, burning of the matrix and fiber pull-out are also known to be problems that occur during drilling operations. Due to the low thermal conductivity of the matrix, the build-up temperature can be very high during drilling, and high build-up temperature can cause shrinkage of the hole. Once the tool is removed, there is a potential loss of dimensional accuracy due to high build-up temperature [11].

It has been found that there is relatively less research conducted into the milling process and the generated surface geometry during edge trimming, in contrast to the significant amount of research into drilling of CFRP, causes, strategies to reduce delamination, and to analyze the effect of machining parameters on tool life and delamination. In literature and practice, it is stated that delamination associated with push-out is much more severe than peel-up delamination, and most studies have focused on push-out delamination [14] [15] [16].

1.3.7 Assessment of delamination

In literature, there are several ways to evaluate the delamination damage around drilled holes in CFRP, and one of the most commonly used parameters is the delamination factor. Figure 12 illustrates the types of damage observed in CFRP during drilling operations, and Table 2 summarizes the different delamination evaluation criteria used in literature for drilling-induced delamination.

Table 2: Summary of evaluation criteria for drilling-induced delamination [17]

Delamination factor	Equation no.	Associated expression	Remarks
1D conventional delamination factor	Eq. 1	$F_d = \frac{D_{max}}{D_{nom}}$	D_{max}—maximum diameter of the delamination area D_{nom}—nominal diameter of the drilled hole
Minimum delamination factor	Eq. 2	$F_{dmin} = \frac{D_{min}}{D_{nom}}$	D_{min}—minimum diameter of the drilled hole
Delamination size	Eq. 3	$Delamination\ size = R_{max} - R$	R_{max}—radius of the maximum damage R—is the drilled hole radius
2D delamination factor	Eq. 4	$F_a = \left(\frac{A_{del}}{A_{nom}}\right)\%$	A_{del}—delamination area A_{nom}—nominal area of the drilled hole
Damage ratio	Eq. 5	$D_{RAT} = \frac{D_{MAR}}{A_{AVG}}$	D_{MAR}—hole peripheral damage area A_{AVG} – nominal drilled hole area
Delamination factor	Eq. 6	$F_d = \frac{A_d}{A}$	A_d – Area of the envelope of the damaged area, including the hole area
Adjusted delamination factor	Eq. 7	$F_{ad} = \alpha\left(\frac{D_{max}}{D_{nom}}\right) + \beta\left(\frac{A_{del}}{A_{nom}}\right)$	where α, β are parameters used as weights $\alpha = 1-\beta, \beta = \frac{A_{del}}{A_{max}-A_{nom}}$
Equivalent delamination factor	Eq. 8	$F_e = \frac{D_e}{D}$	$D_e = \sqrt{\frac{4(A_{del}+A_{nom})}{\pi}}$
3D delamination factor	Eq. 9	$F_v = \frac{1}{p}\sum_{k=1}^{p} F_a^k$	where $F_a^k = \frac{A_d^k}{A_{nom}}$ signifies the 2D delamination factor of the kth CFRP layer. A_d^k—delaminated area of the kth CFRP layer A_{nom}—the nominal drilled hole area P—the total number of the delaminated layers

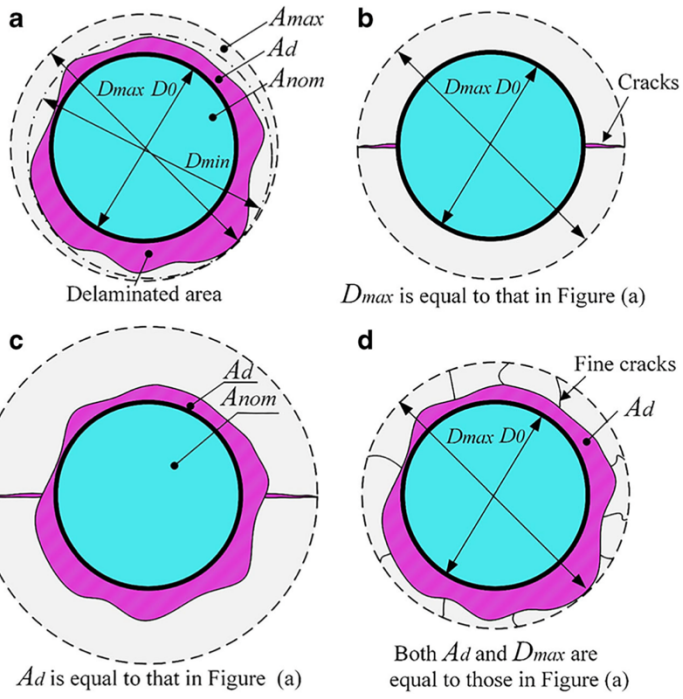

Figure 12: Drilling induced hole damage of CFRP: a) uniform, b) cracks, c) uniform with cracks, d) uniform with fine cracks [17]

The first delamination factor is introduced by Chen and the one-dimensional delamination factor is defined as the ratio of the maximum diameter (D_{max}) of the delamination zone to the nominal diameter (D_{nom}) of the drilled hole

$$F_d = \frac{D_{max}}{D_{nom}} \quad (1)$$

However, F_d formulation is a one-dimensional delamination factor and does not accurately represent the extent of delamination caused by a few fibers being peeled up or pushed down to a distinct significant width. It does not depict the real delamination zone and the area of the delamination in the drilled hole periphery.

Faraz [17] introduced the two-dimensional delamination factor (F_a) and suggested that the two-dimensional delamination factor is a reasonable formulation to depict the level of delamination damage.

$$F_a = (\frac{A_{del} - A_{nom}}{A_{nom}})\% \quad (2)$$

Where A_{del} is the delamination area and A_{nom} is the nominal area of the hole.

Another formulation to assess the severity of the delamination is introduced by Davim [18].

The adjusted delamination factor (F_{da}) based on digital image analysis also includes the size of the crack contribution and the damage area to evaluate the delamination severity occurring after the drilling operations.

$$F_{da} = \alpha \frac{D_{max}}{D_{nom}} + \beta \frac{A_{max}}{A_{nom}} \quad (3)$$

A_{max} in the equation 3 is the area of the maximum diameter of the delamination zone (D_{max}).

The α and β parameters are used to tailor and weight the equation depending on the delamination severity.

In literature, even though the two-dimensional delamination factor and adjusted delamination factor is more accurate to depict the delamination severity, F_d is observed to be used more frequently than F_a and F_{da} due to the practical use of the equation.

Additionally, there are other methods for delamination evaluation such as visual or non-destructive techniques.

Visual inspection is a simple method to detect composite defects such as visible delamination, cutting tool marks and other types of surface defects. However, in some cases, defects are located inside the machined or drilled surface and cannot be properly examined. In such situations, non-destructive techniques are crucial for assessing and inspecting the damage. Scott et al. [19] summarized the commonly used non-destructive techniques, including ultrasonic testing and thermography. Table 3 compares the commonly used methods for inspecting damage in CFRP

Table 3: Comparison of major inspection methods [20]

Damage	Delamination	Fiber breakage	Matric cracks	Surface defects	Damage size	Distance from surface
Deply	✓✓	✓	✓	✓✓	✓✓	✓✓
Fractography	✓✓✓	✓✓	✓	✓✓	✓✓	✓✓✓
Visual inspection	✓✓	✓	✓	✓✓✓	✓	✓
Ultrasonic	✓✓	XXX	XXX	XX	✓✓	✓✓
Radiography imaging	✓	✓✓	✓✓	O	✓✓	✓✓
Thermal imaging	✓	XX	XX	XX	✓	XX
Acoustic emission	XX	XX	XX	XXX	XXX	XXX

✓✓✓ = very good, ✓✓ = good, ✓ = fair, XXX = very poor, X X = poor, O = none

1.3.8 Approaches to reduce delamination

Many researchers in literature have found that the effect of thrust force on delamination is critical. To avoid drilling-induced delamination, the thrust force should not exceed the critical thrust force level. Thrust force is determined by the properties of the workpiece

material, parameters of the drill bit, and the uncut fiber thickness under the drill bit [21] [22] [13].

In industry, to prevent the push-out delamination, use of support plate under composite laminate is one of the commonly used approaches. Capello [23] stated that the use of support plate under the composite laminate during the drilling drastically reduced the drilling induce delamination. It is important to note that he indicated that the support is used to prevent the inflection rather than providing any mechanical strengthening. In a nutshell, by limiting the workpiece dynamics, it is possible to significantly reduce the delamination.

Another way to reduce delamination is by using special drill bits such as straight flute, step, core, and step-core drill bits. It is known that conventional twist drill bits generate high thrust force, making it difficult to generate delamination-free holes [24][10]. Special drill bits have a higher threshold for drilling feed rates without delamination, thus achieving higher drilling efficiency [25].

Chapter 2

Drilling Operations and Experimental Procedure

Hole making is known to be the one of the most time-consuming processes in industry. Furthermore, for some applications such as aerospace, hole quality is very crucial and tight tolerance is expected for manufacturing excellence. The assessment of drilling induced damage is highly dependent to the inspection method and approach used to mathematically asses the severity. Table 2, Table 3 and Figure 12 provides a general

overview of commonly used inspection techniques and available methods in terms of their capacity of mathematically identifying different type of damages.

Furthermore, there exist hole quality inspection criteria: surface roughness, delamination, circularity, hole size and burr formation. With the image processing model developed in this study, 3 criteria out of 5 can be examined, the delamination, circularity, and hole size to assess the quality of the hole in machine shop environment.

This chapter explains the detail of the image processing technique developed for evaluation of hole quality after drilling process and the result of this technique is examined.

2.1 Materials

The CFRP samples are supplied by KORDSA in the shape of plies with 300mm x 300 mm. CFRP plate consists of 20 prepreg plies of plain weave 4K yarn with 50% carbon fibre to epoxy content ratio and thickness of 0.2 mm per ply. The plies were manufactured using an autoclave process after stacking each layer up in a specific orientation. For the sake of the drilling operation and ease of the delamination assessment, plies are stacked in 0° orientation resulting in a unidirectional CFRP plate having 4.8mm of thickness.

2.2 Equipment and Test Setup

During the drilling tests, force data along X, Y and Z directions are collected by KISTLER 9129AA type dynamometer in order to link the delamination results with the force variation occurred during the drilling operations. Dynamometer is fixed to the fixture and the cutting test sample of CFRP unidirectional plate is attached to the dynamometer. To eliminate the bending of the CFRP material, to have extra stiffness and protect the surface of the dynamometer, a wooden MDF layer having the thickness of 20 mm and a glass fiber composite plate having a thickness of 5 mm is attached in between the dynamometer and the cutting sample.

Real-time force data gathered from dynamometer is visualized in LabView environment. After recording the force data along X, Y and Z direction, results are also visualized in MATLAB environment to compare the effect of cutting force with the severity of the delamination occurring in each drilling test. The experimental setup design for drilling operations, UD CFRP plate attachment to glass fiber plate, MDF layer and KISTLER dynamometer and real-time data collection window developed in LabView is shown in Figure 13, Figure 14, and Figure 15 consecutively.

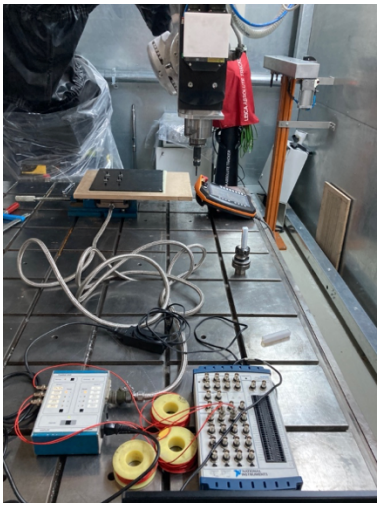

Figure 13: Experimental setup design for drilling operations

Figure 14: UD CFRP plate attached to glass fiber and MDF layer

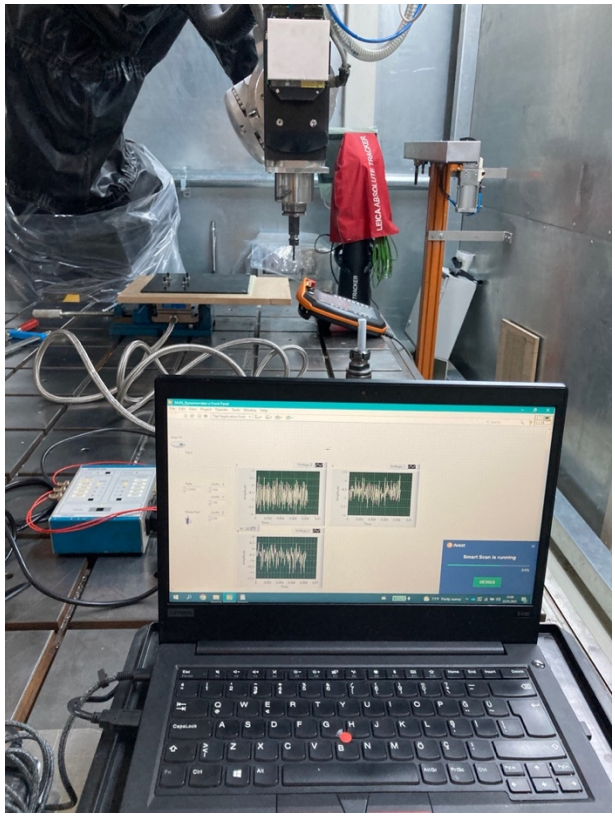

Figure 15: Real-time force collection and LabView project window

2.3 Cutting tools

The drilling tests are performed with a 9,55 mm Sandvik drilling tool of 854.1-0952-05-A0 N20C solid carbide drill with 4 cutting edges. The tool was unused and only used during the drilling tests.

The tool condition and the tool wear of each cutting edge observed after drilling test from different angles are given in Figure 16, Figure 17, Figure 18, and Figure 19.

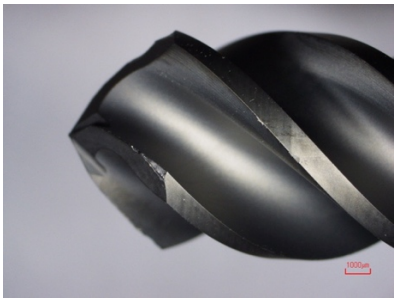

Figure 16: Tool wear after drilling operation 0°

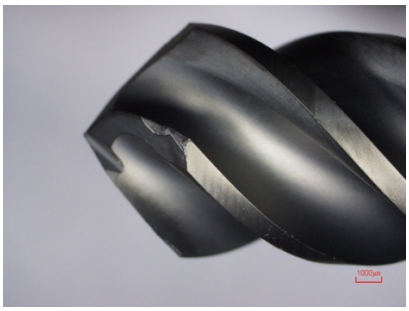

Figure 17: Tool wear after drilling operation 90°

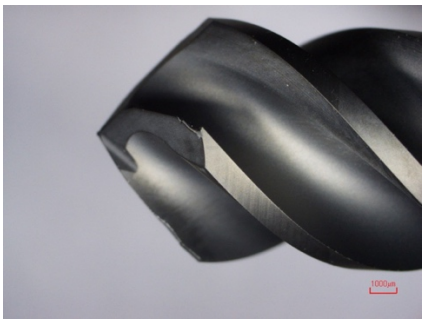

Figure 18: Tool wear after drilling operation 180°

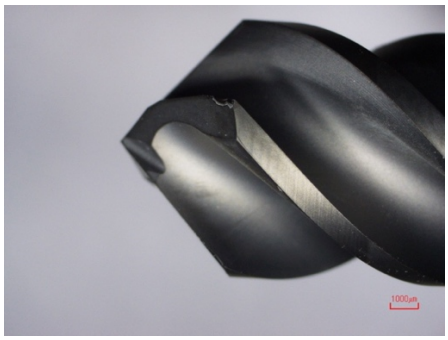

Figure 19: Tool wear after drilling operation 270°

2.4 Experimental Methodology

To study the relationship between drilling operation parameters and hole quality, a design of experiments was conducted. In the design of experiments, parameters were matched with each other to obtain coherent results.

After the test matrix was created and the toolpath was generated, twenty tests were carried out by providing specific ranges for three main parameters: feed rate, spindle speed, and cutting speed. The parameters used to develop the design of experiments and the full factorial test matrix are given in Table 4 , and Table 5.

Table 4: DoE values for drilling operations

Parameter	**Unit**	**Values**
Feed rate	mm/rev/teeth	0.04, 0.08, 0.12, 0.14, 0.20
Spindle speed	rpm	2000, 3000, 5000, 6670
Cutting speed	m/min	60, 90, 150, 200

Table 5: Test matrix for selected parameters of drilling operation

Test No	**Spindle Speed**	**Vcut**	**Feed Rate**	**Vfeed**
1	2000,87	60,00	0,04	80,03
2	2000,87	60,00	0,08	160,07
3	2000,87	60,00	0,12	240,10
4	2000,87	60,00	0,14	280,12
5	2000,87	60,00	0,20	400,17
6	3001,30	90,00	0,04	120,05
7	3001,30	90,00	0,08	240,10
8	3001,30	90,00	0,12	360,16
9	3001,30	90,00	0,14	420,18
10	3001,30	90,00	0,20	600,26
11	5002,17	150,00	0,04	200,09
12	5002,17	150,00	0,08	400,17

13	5002,17	150,00	0,12	600,26
14	5002,17	150,00	0,14	700,30
15	5002,17	150,00	0,20	1000,43
16	6669,56	200,00	0,04	266,78
17	6669,56	200,00	0,08	533,56
18	6669,56	200,00	0,12	800,35
19	6669,56	200,00	0,14	933,74
20	6669,56	200,00	0,20	1333,91

Chapter 3

Digital Image Processing

Digital image processing is a term used to focused in developing a system or a program that is able to perform processing on an image. There exist different tools to develop image processing models depending on the complexity and the focus of the model. Most of the image processing toolbox allows wider range of algorithms to be developed and applied to the input data to avoid problems such as noise and distortion etc. The image processing model developed in this study is mainly used to quantify the drilling quality in machine shop environment and distinguish the effect of machining parameters without using advanced camera technologies. In this chapter, the main focus and the building block of the model to assess and quantify the drilling quality is detailly examined.

3.1 Image processing methodology for drilling operations

There are many tools available to conduct image processing depending on the aim of the approach. Image processing procedures are either associated to an observer-based methodology or an automatic algorithm developed that can be easily developed in image processing Toolbox provided by MATLAB. The image processing approach generated for drilling operations is a combination of both observer-based and automatic algorithm where the model should be tailored beforehand by the user to define the distance between the sample and the camera, and the resolution of the captured image as the critical inputs of the model. The algorithm should take these inputs to calculate the area of the selected region of the image. Furthermore, since this algorithm only works with CFRP material, for the sake of this experiment, the user should add or eliminate some of the image enhancement function for other type of materials such as glass fiber etc.

In general, image processing models to analyse an image involves processes to extract meaningful information from its fundamental components. These processes can include finding shapes, detecting edges, removing noise, and calculating statistics. Hence, image analysis is an umbrella term that covers a range of technique having the subcategories of:

- Image enhancement to prepare images for display or analysis
- Image segmentation to isolate regions and objects of interest
- Morphological filtering for noise removal
- Region analysis to extract statistical data

The image processing model used in this study includes functions from all the subcategories that are listed above.

The image processing approach developed for drilling operations consists of numerous and sequentially connected image processing function to build a flow of image analysis and to quantify the delamination area and the delamination factor. This flow of image processing function mainly consists of RGB to Gray scale image processing, morphologic operations and contour detection and boundary extraction. To construct the image processing approach that consists of block of image processing operations

and subfunctions of image processing functions, MATLAB image processing toolbox and some of the embedded functions within the Toolbox is used. Table 6 gives the full list of image processing functions used to develop this approach.

Table 6: Functions list used in image processing approach

Function used in image processing approach	**Function syntax**	**Syntax explanation**
Image Complementing	J = imcomplement(I)	The complement of the image I is calculated and the result is returned in J. In the output image, darker areas become lighter and lighter areas become darker.
RGB to Gray scale	I = rgb2gray(RGB)	The true color image RGB is converted to a grayscale image I by removing the hue and saturation information while keeping the luminance.
Brightness adjustment	J = imadjust(I)	The intensity values in the grayscale image I are mapped to new values in J by adjusting the contrast. By default, the function "imadjust" increases the contrast of the output image J by saturating the bottom 1% and the top 1% of all pixel values.
Histogram adjustment	J = histeq(I)	Contrast is enhanced using histogram equalization, which transforms the grayscale image I so that the histogram of the output grayscale

		image J is distributed evenly over 64 bins.
Image binarization	BW = imbinarize(I)	This function describes the process of creating a binary image from a 2-D or 3-D grayscale image I by using a globally determined threshold value. All values above the threshold are replaced with 1s and all other values are set to 0s.
Image thresholding	thresh = multithresh(A)	A single threshold value "thresh" is calculated for image A using Otsu's method. This threshold value can be used as an input argument in the function "imquantize" to convert an image into a two-level image.
Binary image opening	J = imopen(I,SE)	The morphological opening operation is applied to the grayscale or binary image I using a structuring element SE. This operation is a combination of erosion followed by dilation, using the same structuring element for both processes.
Boundary Tracing	B = bwboundaries(BW,conn,options)	The exterior boundaries of objects are traced, with options of either including or not including the boundaries of holes inside other objects. The options can either be 'holes' or 'noholes' to specify the desired outcome.

Boundary extraction & area calculation	J = imdilate(I,SE) total = bwarea(BW)	Dilates the grayscale, binary, or packed binary image I using the structuring element SE.

Figure 20 shows the complete flow created to assess the machining induced damages (such as delamination, fibre pull-out etc.) occurring inside of the hole.

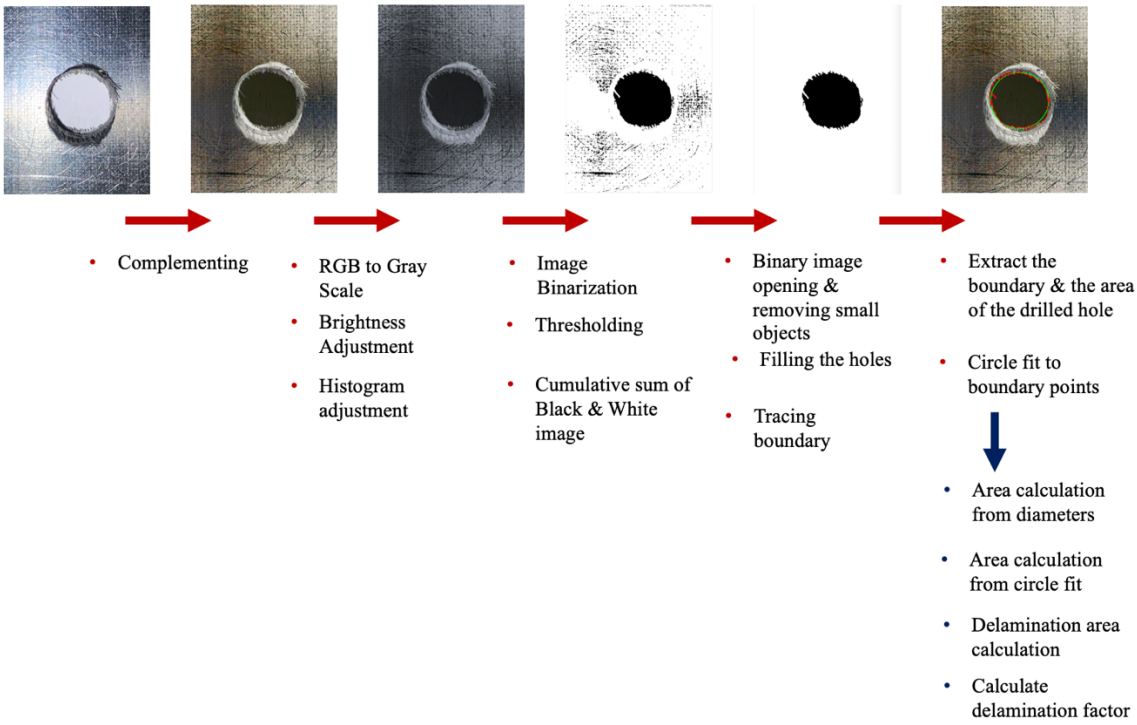

Figure 20: The flow of the image processing model developed for drilling operations

As it is already listed in chapter 3.1, it is essential to understand that image functions used to develop such model follows a sequence. Each function requires different types of input that cannot be gathered without using other types of image functions. The listed functions are therefore explained detailly in the following section in the used order.

3.2 Image processing functions

The complete list of image processing functions used to develop the assessment model is given in chapter 3.1. this section is dedicated to examining the details of the functions and the importance of the sequence of these functions in use.

The captured image is uploaded to the model in RGB form where the colour is defined by having separate intensities of 0 to 255 for red, green, and blue. The RGB coordinate system of the original image is shown in Figure 21.

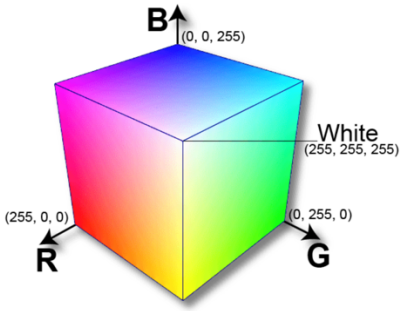

Figure 21: RGB coordinate system

The image processing model starts with image complementing. Image complementing is the process of subtracting each pixel values from the maximum pixel value. The region of interest in drilling of CFRP materials is the drilled hole and the contour of the hole, hence image complementing is used to make the drilled hole area black and the material

itself bright. Figure 22 shows the image complementing process applied to the original image and the resulting image.

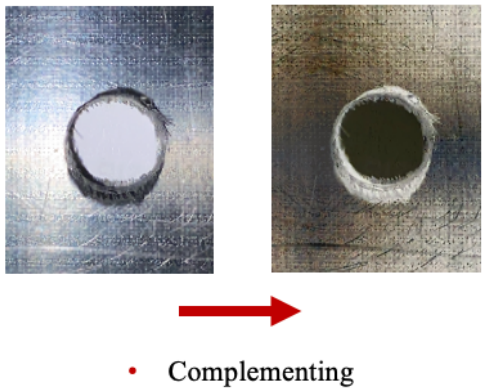

Figure 22: Image complementing process

After complementing the original image to a new RGB image, it is converted to Gray scale image. RGB to Gray scale image is mainly applied for:

1- To decrease the size of the image
2- To decrease the complexity of the operations performing on the image
3- To perform histogram analysis and find threshold values
4- To binarize the image
5- To generate a distinguishable contour from binarized image

Brightness adjustment is applied to the gray scaled image. Brightness adjustment is known to be a contrast adjustment method used to remap image intensity values to have a sharp difference between black and white regions. Image with a good contrast, highlights look brighter, and shadows looks darker. These contrast adjustment functions such as brightness adjustments are primarily applied to grayscale image to have a distinguishable pattern in histogram of the image.

There exist different types of function that can primarily be applied to grayscale image such as “imadjust, imcontrast, imsharpen, imreducehaze, adapthisteq etcç” in MATLAB image processing toolbox. For the sake of the model developed in this study, the “imadjust, imcontrast” are used.

Histogram adjustment or equalization is used to produce an output image with pixel values evenly distributed through a range. By starching the histogram of the gray scale image, the accuracy of the binarization process that will be applied in the next step is increased and the contour that will be generated from the binarization process is more reliable due to the histogram adjustment.

Different results of brightness adjustment, histogram adjustment and contour adjustment are shown in figure 23 with the corresponding histogram plots.

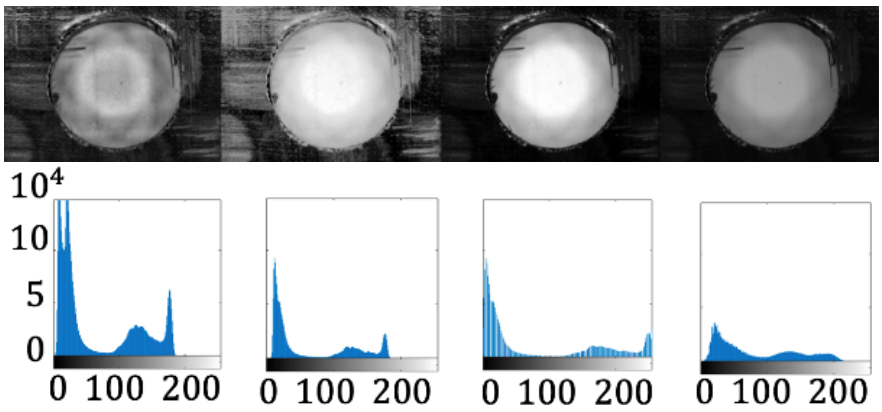

Figure 23: Brightness, histogram, and contour adjustments for different scenarios

Figure 24 shows the initial input image and the final output after applying the RGB to Gray Scale, Brightness adjustment and histogram adjustment processes.

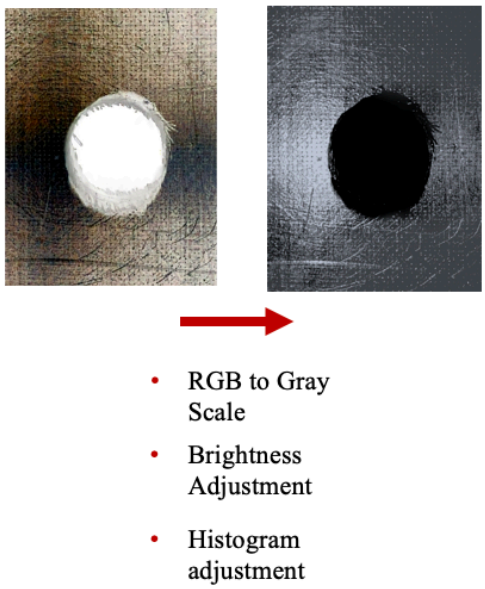

Figure 24: Processed RGB image

Binarization of an image is the process of converting it into a bi-level document image through thresholding. This process separates the pixels into two categories: black and white. By having only these two categories, the image can be easily segmented into foreground and background.

Image thresholding is used to partitioning the image into a foreground and background. Since the CFRP material and the captured image of the drilled hole are segmented, and they need to be isolated to extract the hole contour. Image thresholding can only be applied to binarized images and it is mostly effective in images with high level of contrast. By applying, brightness adjustment, histogram adjustment and image binarization, the efficiency of thresholding is increased.

Cumulative sum of the black and white pixel is used to understand how many pixels is darker than the corresponding pixel values in the horizontal axis and the portion of the hole size in the total size of the captured image.

Figure 25 shows the result image after applying image binarization, thresholding and cumulative sum of Black and White image.

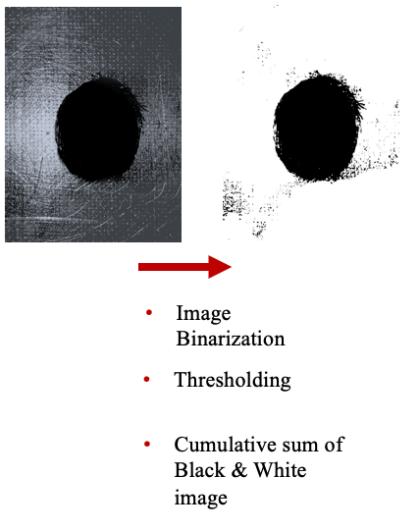

Figure 25: Processed gray scale image

Opening operation is a block of morphological operations that can be applied to binary or intensity image. The binary image opening operations applied in this model performs an erosion operation followed by a dilation operation on the binary image using predefined structuring element by ‘strel function’.

Opening operation is especially = crucial for the contour distinguishment of the original image. CFRP materials has gray or black surface with high reflection quality making the captured image hard to observe the delamination region. By performing opening operations, the delamination region is separated by the shadows caused by the lightning of the production area.

Within the image processing toolbox, imfill function is used to fill the small holes generated due to the texture of the composite material. Even though the algorithm is boost up for finding larger circle, or the actual drilled hole contour, the small circles can be intersect with the big circle contour and the circularity analysis of the main circle is corrupted. Filling the small holes is hence an important process before finding and extracting the machining region.

There exist different boundary tracing functions embedded in MATLAB image processing toolbox. For every function for boundary tracing, the nonzero pixels in the binary image belongs to an object, in this case the object is CFRP material itself, and the pixel with the values 0 constitute the background, in this case the area inside the drilled hole. For boundary tracing, the model used ‘bwboundaries’ function to return the coordinates of the border pixel of all the objects in the image.

The boundary in the image is then compared according to their size and the maximum boundary is defined as the main boundary where the other small circle like boundaries is filled. ‘regionprops’ function is used to measure the properties of an image region; in this case it is used for the diameter and the circularity of the drilled hole. Figure 26 shows the resulting image after applying binary image opening and removing small objects, filling the holes and tracing boundary operations.

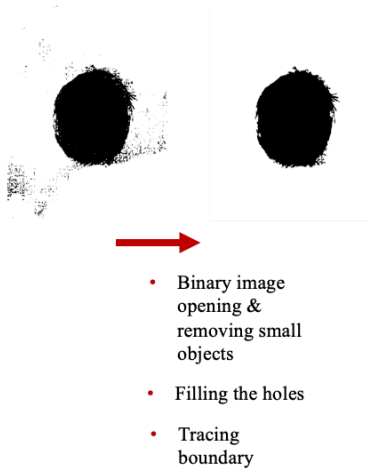

Figure 26: Processed black & white image for boundary extraction

After establishing the main contour and the pixel coordinates along the continuous contour, the maximum and minimum diameter are found by fitting a circle. ‘Fircircle’ function is used to fit a circle to the N points where the geometric error (sum of the squared distances from the points to the fitted circle) is minimised by using nonlinear least squares or Gauss Newton method. From the circle fit and the boundary extraction, model calculated the area from fitted circle and area from the diameters of the maximum and minimum radius. Boundary extraction and circle fit processes are shown in Figure 27.

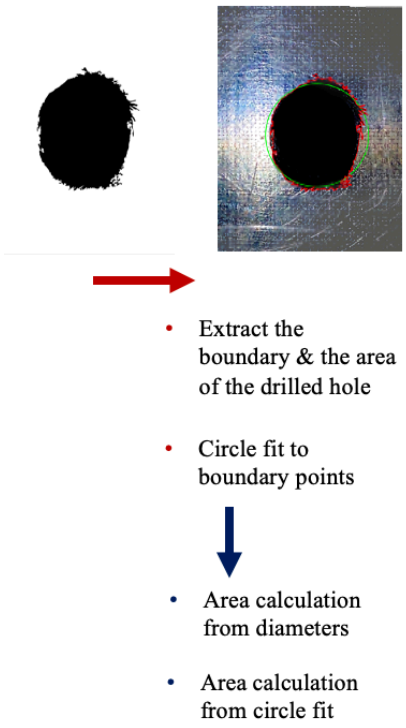

Figure 27: Boundary extraction & circle fit

The methodology for the delamination area is the same as the quantification of the inside of the area. The extracted contour is added to the original image to make the inside of the drilled hole black and combine it with the delamination region to find the outer contour. So, the process for outer contour defers from the inside contour by one additional process of combination of original image with the extracted contour of the drilled hole. The process of image overlaying is shown in Figure 28 and the process of boundary extraction is shown in Figure 29.

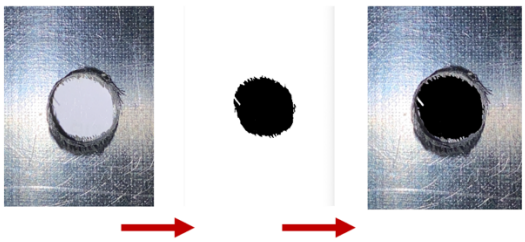

- In order to combine the outer contour with inner contour, image overlaying is done by taking the original image and the extracted contour of the drilled hole

```
idx=find(B(:,:,1)~=0&B(:,:,2)~=0&B(:,:,3)~=0);
%find ~black pixels in extracted contour image
C=B;
C(idx)=A(:,:,idx);%set ~black pixels to
original image's pixels
C(2*idx)=A(:,:,idx);
C(3(idx)=A(:,:,idx);
imshow(C);
```

Figure 28: Image overlaying of the drilling contour and the original contour

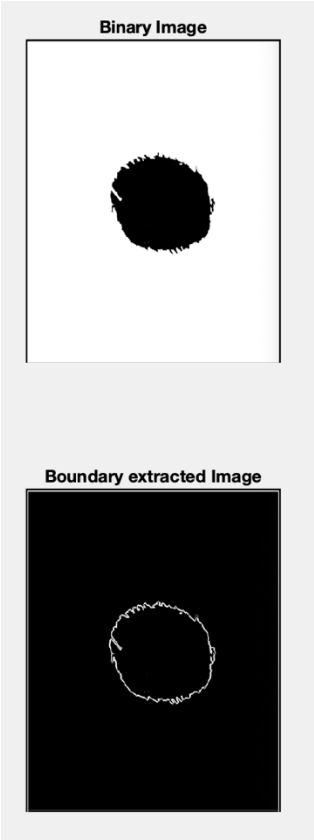

Figure 29: Boundary extraction from binary image

The image processing steps for the contour outside of the drilled hole is exactly the same with the image processing steps developed for the contour inside of the drilled hole. The

delamination factor calculations are done after extracting the outer contour of the drilled hole at the end of the contour extraction step. The image processing steps are shown in figure 30, after the image overlaying process of the original image and the extracted contour.

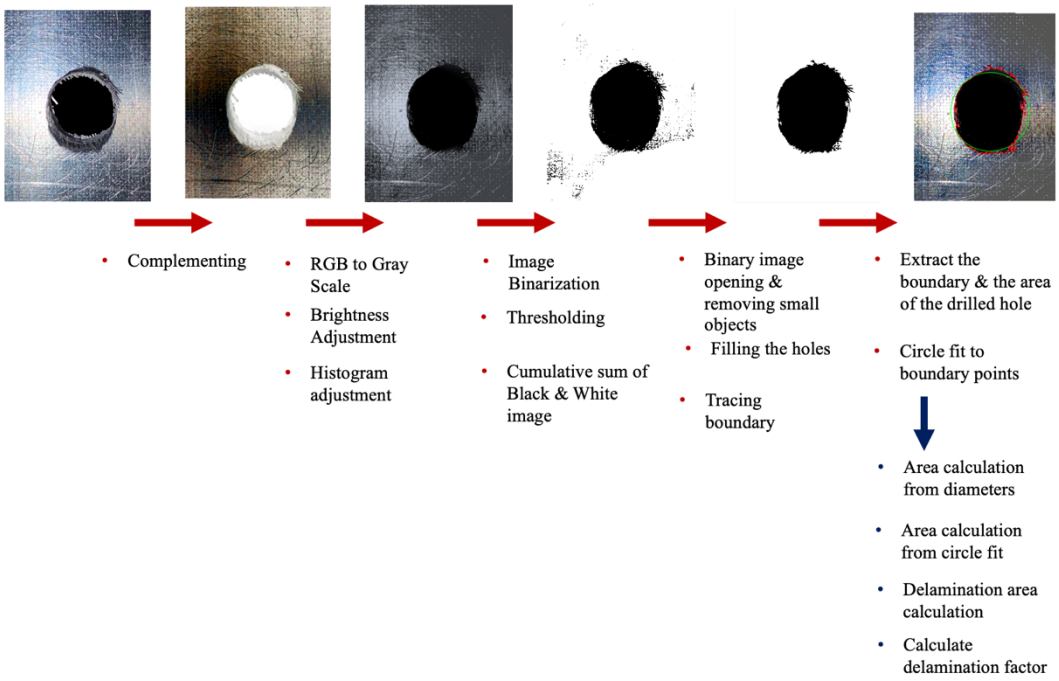

Figure 30: Image processing steps for outer contour of the drilling operation

The delamination area is calculated by extracting the outer contour of the delamination zone and by knowing the drilled hole nominal diameter, minimum and maximum diameter. By comparing the nominal area of the hole to the area of the extracted outer contour, the delamination factors, which have been discussed in literature, can be calculated. The delamination factor formulations vary in their complexity, functionality, and representation, but in order to evaluate the effect of machining parameters on delamination severity, commonly used delamination factors are calculated using the nominal area, maximum and minimum hole diameter, and delamination area.

3.3 Delamination quantification of drilling operations

It is known that different types of damages can be observed th CFRP machining and they severely deteriorate the performance of the material. Delamination is one of the commonly observed damage types that is known to be highly correlated with the performance of the material and the final quality of the machining surface. Furthermore, peel-up and push-out delamination are the major delamination types occurring in drilling operations. As it is already discussed in literature review, several researchers are developed different strategy to group delamination types and different mathematical formulations to assess the severity of the damage. Formulations that are used in this study are detailly examined and listed below. Figure 31 shows the peel-up and push-out delamination representation and Figure 32 shows the assessment parameters used to quantify the damage.

Figure 31: Peel-up and Push-out delamination in drilling operation

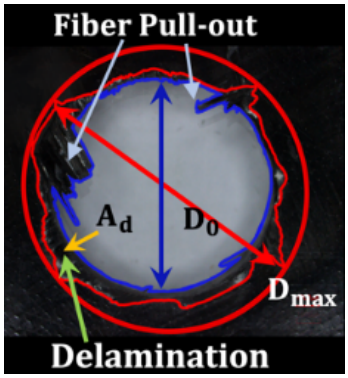

Figure 32: Damage and quality assessment parameters

By using image processing model developed to calculate min & max delamination diameter and inside & outside area are calculated and used to determine the best delamination formula retrieved from literature. The full list of diameter related result from image processing model is given in Table 7, and the full list of area related results from image processing model is given in

Table 7: Image processing model results related to diameter

Test no	Diameter max	Diameter min	Delamination Diameter max	Delamination Diameter min
1	12,2154	8,6893	18,8496	12,7179
2	12,4652	8,8552	18,3584	12,4155
3	12,5396	8,9525	17,535	12,3301
4	12,645	9,0098	17,511	12,2113
5	12,6527	9,0483	18,5244	12,7103
6	12,2699	8,7067	17,5752	12,278
7	12,6058	8,9882	18,1616	12,6608
8	12,8202	9,0956	17,4235	12,2074
9	12,9487	9,2419	17,2056	12,1114
10	13,137	9,3571	17,1524	12,0772
11	12,5277	9,0238	17,3841	12,2079
12	12,4376	9,1209	17,5557	12,1544
13	12,7937	9,2141	18,7254	12,2472
14	13,1473	9,3955	17,2107	12,0581
15	13,387	9,599	17,3376	12,0204
16	12,9801	9,3373	17,4854	12,1754
17	12,9853	9,3462	17,5849	12,3553
18	13,0797	9,3481	17,0661	12,101
19	13,3334	9,5615	17,1577	12,0183
20	13,3956	9,6187	16,9851	11,9961

Table 8: Image processing result related to area

Test no	Area inside	Area outside	Area Delamination	Fiber Area
1	59,3	127,033	55,44	12,29

2	61,5869	121,0653	49,47	10,01
3	62,948	119,4057	47,81	8,65
4	63,756	117,1145	45,52	7,84
5	64,3014	126,8824	55,29	7,29
6	59,5388	118,3977	46,80	12,06
7	63,45	125,8965	54,30	8,14
8	64,9761	117,0404	45,45	6,62
9	60,083	115,207	43,61	11,51
10	68,7655	114,5573	42,96	2,83
11	63,9548	117,051	45,46	7,64
12	65,3378	116,027	44,43	6,26
13	66,6782	117,8041	46,21	4,92
14	69,331	114,1956	42,60	2,26
15	72,3679	113,4813	41,89	0,77
16	68,4755	116,4274	44,83	3,12
17	68,6057	119,8944	48,30	2,99
18	68,633	115,0084	43,41	2,96
19	71,8028	113,4435	41,85	0,21
20	72,6653	113,0234	41,43	1,07

From the result of the image processing, delamination area is calculated by subtracting nominal area from area outside and fiber area is calculated by subtracting area inside from nominal area, hence these results are step by step used to generate delamination related inputs to use in different formulations.

In this study, 3 different delamination formulation from literature are used to assess the damage severity hence the drilled hole quality. These equations are listed as:

$$F_d = \frac{D_{max}}{D_{nom}} \tag{1}$$

In equation1, D_{max} is the maximum diameter of the delamination area and D_0 is the nominal hole diameter. This formulation provides a rough factor as it does not account the area of damage and irregularities in the delamination area are not quantified.

$$F_d = F_d + \frac{A_d}{(A_{max} - A_0)}(F_d{}^2 - F_d) \quad (2)$$

In equation 2, adjusted damage factor includes the delamination area so that various damages having the same diameter, but different damage areas can be distinguished.

$$F_{ed} = \frac{D_e}{D_0} \quad (3.1)$$

where,

$$D_e = \left[\frac{4(A_d + A_0)}{\pi}\right]^{0.5} \quad (3.2)$$

In equation 3.1, equivalent delamination factor, F_{ed}, defined as the ratio of an equivalent delamination diameter, D_e, to the nominal hole diameter, D_0 is used to calculate the delamination factor where D_e is correlated with nominal area and delamination area as expressed in equation 3.2.

3.4 Results of delamination quantification

As it is already discussed in chapter 3.3, there exist several mathematical expressions to quantify delamination depending on drilling condition and focus of the experiment. In this study, 4 assessment formulations are selected from literature that is given in Table **1** to quantify delamination damage and select best performing formulation for similar machining parameters. This section aims to quantify the delamination damages of the drilled hole that are conducted and explained in chapter 2 and compare the results of different delamination formulation by using the results of the image processing approach such as delamination diameter, delamination area and fiber length.

3.4.1 Result of equation 1

Equation 1 reflets the maximum drilled hole diameter over nominal diameter. Results shows that the maximum delamination diameter over nominal diameter is observed in test 1 and test 13. The related drilling parameters and the results of equation 1 is represented by response surface method.

$$F_d = \frac{D_{max}}{D_{nom}} \tag{1}$$

Delamination diameter is generated in image processing model for 20 conducted test and each result is used to calculate F_d , where the nominal diameter is the same value for each test and defined by the diameter of the drilling tool.

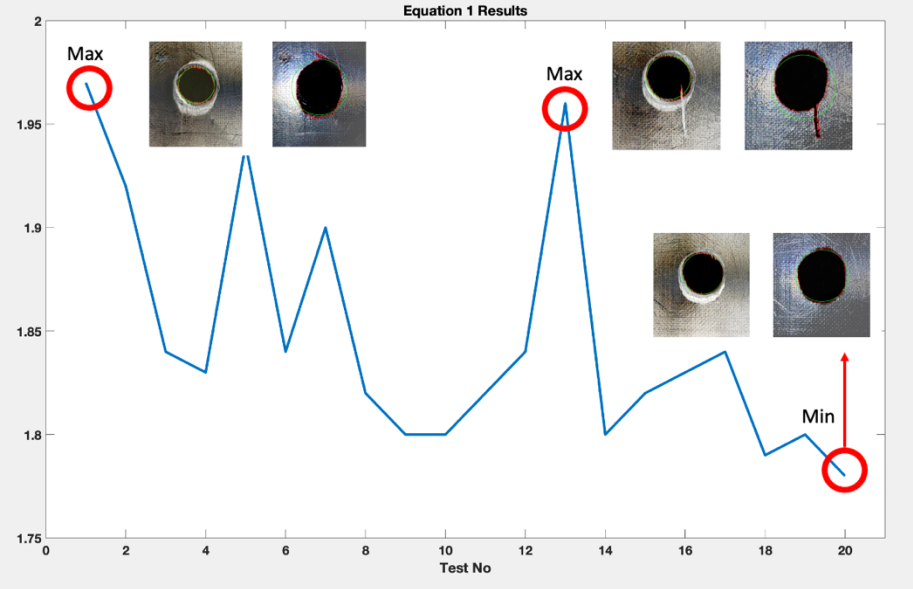

Figure 33: Conducted test number and $\boldsymbol{F_d}$ value

Figure 33 shows F_d values calculated for each test and the maximum and minimum F_d values are indicated according to corresponding test number to further analyse the root cause of the maximum and minimum delamination factor. Furthermore, to examine the effect of machining parameters to F_d calculations, surface response of the cutting speed, feed rate, cutting force and the F_d are generated.

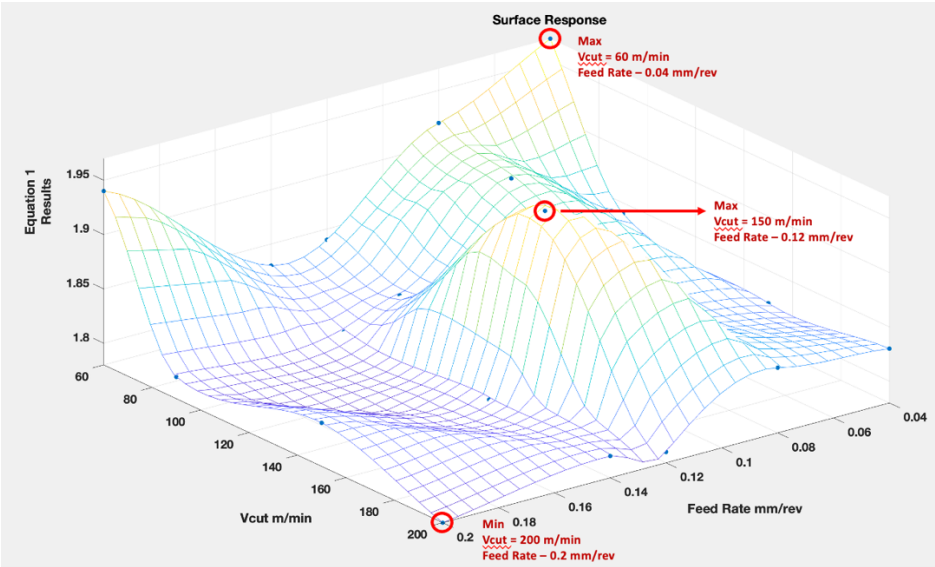

Figure 34: Surface response of $\boldsymbol{F_d}$ (equation 1)

Figure 34 shows that the maximum delamination diameters over nominal diameter are observed in low cutting speed of 60 m/min and feed rate of 0.04 mm/rev and moderate cutting speed of 150 m/min and feed rate of 0.12 mm/rev.

The minimum delamination diameter over nominal diameter is observed in cutting speed of 200m/min and feed rate of 0.2 mm/rev. It is safe to say that F_d values shows a decreasing tendency of delamination for high cutting speed compared to moderate and lower cutting speed values.

3.4.2 Result of equation 2

Equation 2 reflets the delamination size as a difference of maximum radius of delamination area to nominal radius.

$$Delamination\ size = R_{max} - R \tag{2}$$

Delamination diameter is generated in image processing model for 20 conducted test and each result is used to calculate $delamination\ size$, where the nominal diameter (R) is the same value for each test and defined by the diameter of the drilling tool and R_{max} is the maximum delamination diameter.

Results shows that the maximum delamination size in mm is observed in test 1 and test 13. It is convenient to observe the similar results that has been observed in equation 1. Figure 35 shows that the minimum delamination size in mm is observed in test number 10 and 20. The related cutting parameters and the results of equation 2 is represented by response surface method in Figure 36.

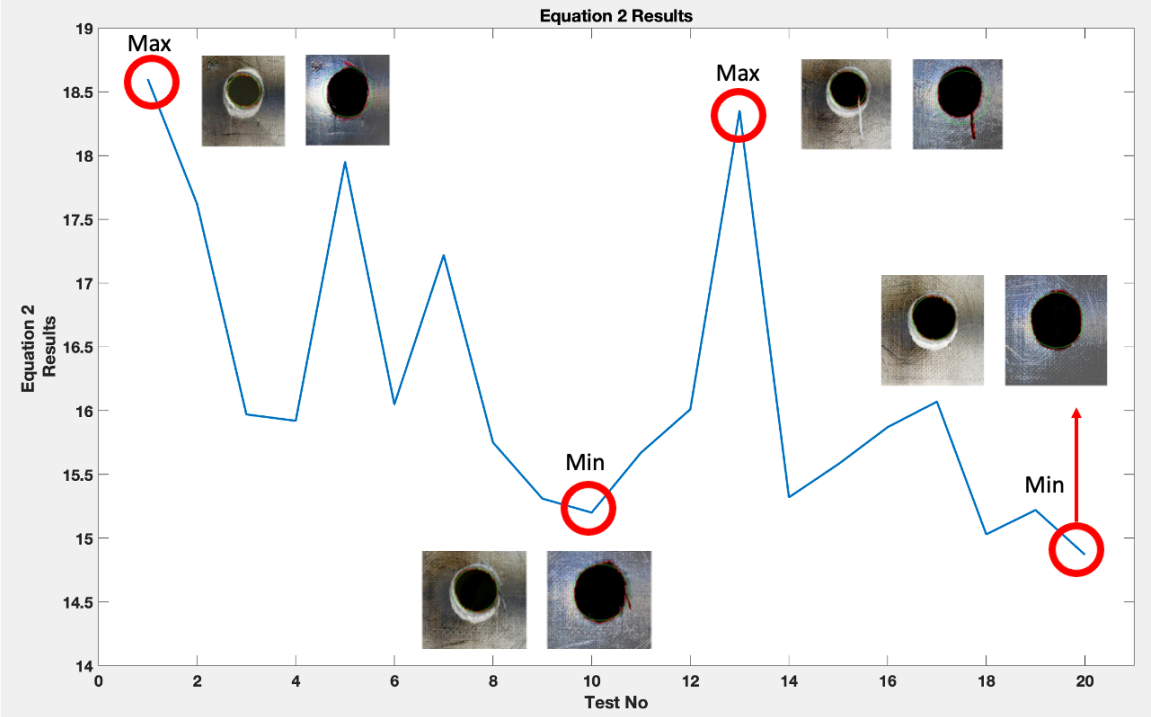

Figure 35: Conducted test number and *Delamination size* value

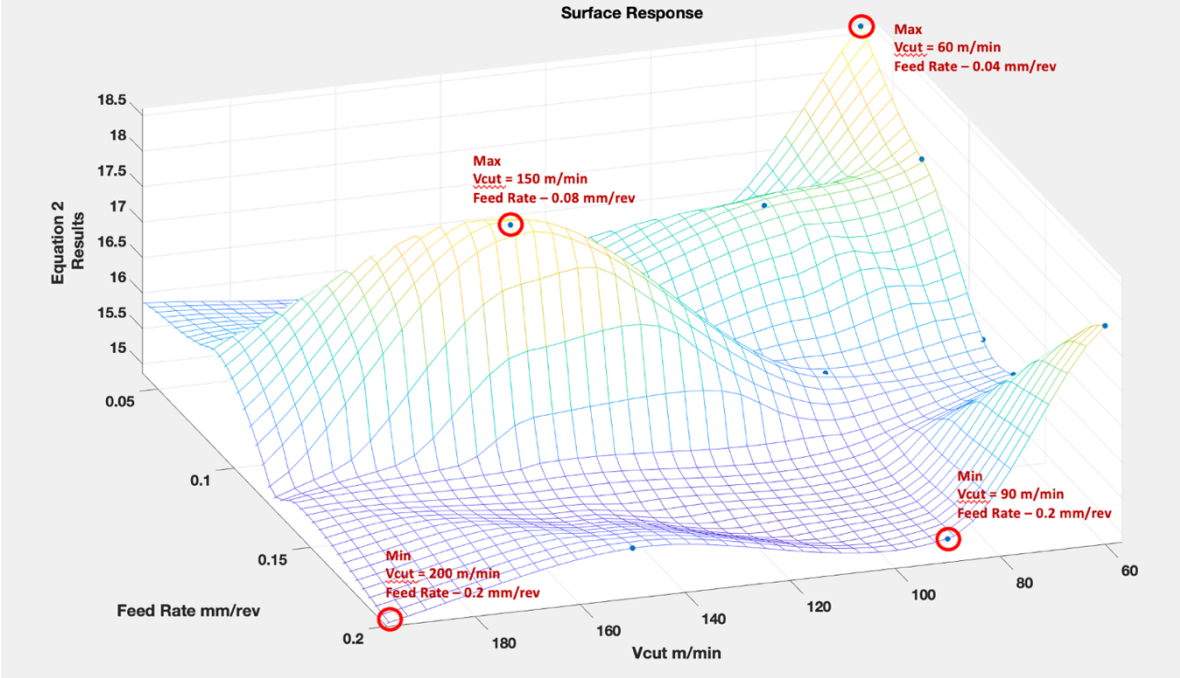

Figure 36: Surface response of cutting speed, feed rate and *Delamination size*

The results of *Delamination size* shows that the maximum delamination size is observed in low cutting speed of 60 m/min and feed rate of 0.04 mm/rev and moderate cutting speed of 150 m/min and feed rate of 0.12 mm/rev.

The minimum delamination size is observed higher cutting speed of 200m/min and feed rate of 0.2 mm/rev. Furthermore, it is also observed that minimum delamination size can be obtain for higher feed rate of 0.2mm/rev and cutting speed of 90 m/min.

Equation 2 also shows a tendency of decreasing delamination in mm for high cutting speed and higher feed rate combination comparing to moderate and lower cutting speeds.

3.4.3 Result of equation 3

Equation 3 represents the 2D delamination factor where A_{del} is the delamination area and A_{nom} is the nominal area of the drilled hole. Comparing to equation 1 & 2, equation 3 focuses on delamination area.

$$F_a = \left(\frac{A_{del}}{A_{nom}}\right)\% \qquad (3)$$

Delamination area is generated in image processing model for 20 conducted test and each result is used to calculate F_a, where the A_{nom} is the same value for each test and defined by the area created by drilling tool without any deviations from ideal.
Figure 37 shows that the maximum delamination area over nominal area is observed in test 1 and 5, and the minimum delamination area over nominal area is observed in test number 15, 19 and 20. The related cutting parameters and the results of equation 3 is represented by response surface method and represented in Figure 38.

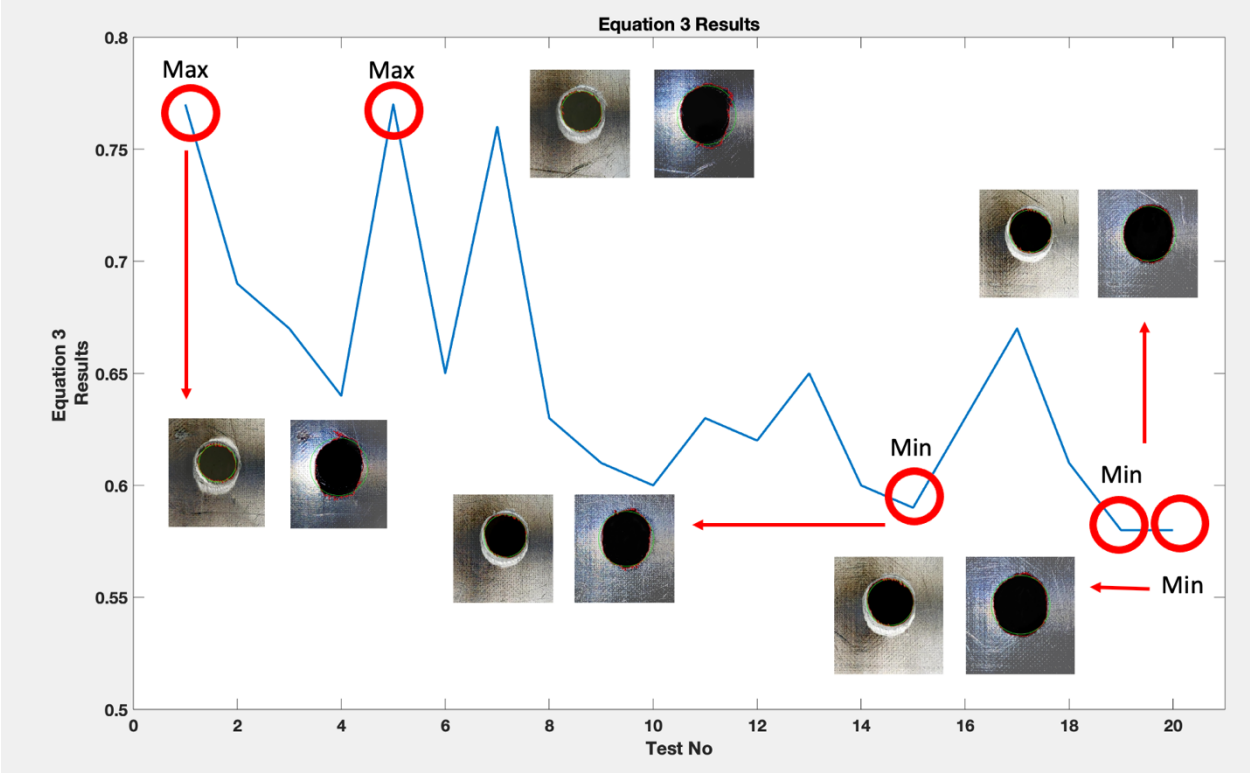

Figure 37: Conducted test number and $\boldsymbol{F_a}$ value

Equation 3 results shows that the maximum delamination area over nominal area is observed in low cutting speed of 60 m/min and feed rate of 0.04 mm/rev and for the same cutting speed and feed rate of 0.2 mm/rev. Even though the higher feed rate results in lower delamination, for a lower cutting speed, delamination area is still observed to be severe.

The minimum delamination size is observed in higher cutting speed of 200m/min and feed rate of 0.2 mm/rev and 0.14 mm/rev.

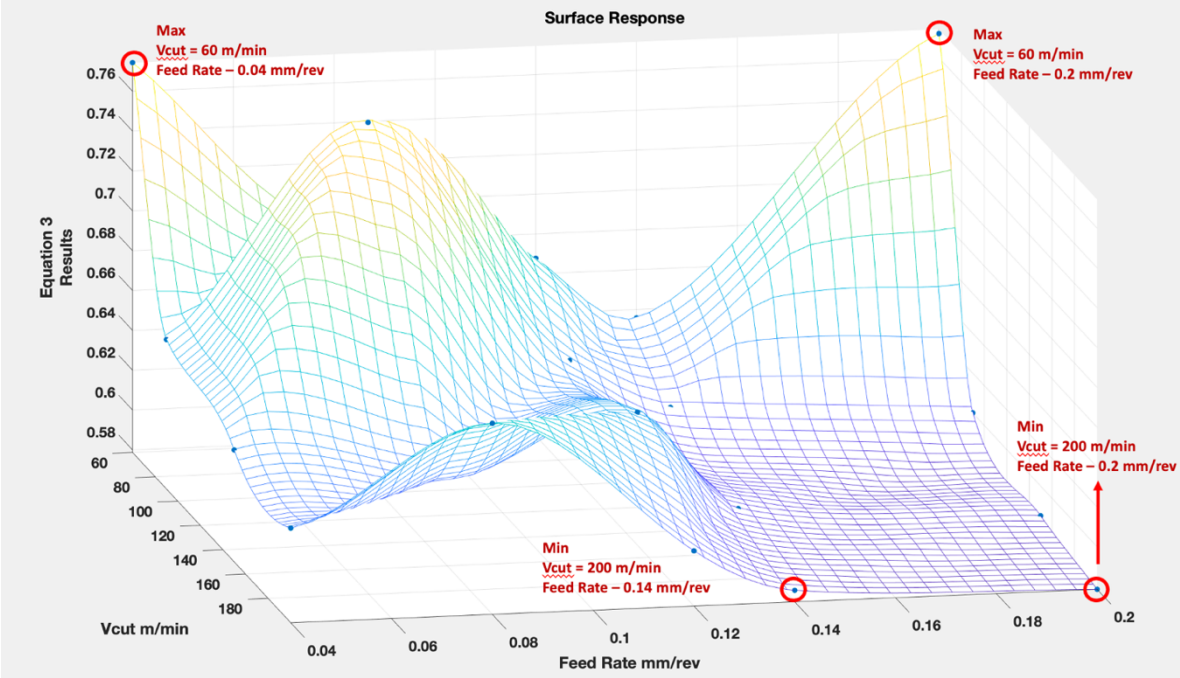

Figure 38: Surface response of cutting speed, feed rate and $\boldsymbol{F_a}$ value

F_a values also shows a tendency of decreasing delamination area for high cutting speed and higher feed rate combination comparing to moderate and lower cutting speeds.

3.4.4 Result of equation 4

Equation 4 represents the equivalent delamination factor where D_e is the equivalent delamination factor and calculated by

$$F_e = \left(\frac{D_e}{D}\right), \quad D_e = \sqrt{\frac{4(A_{del} + A_{nom})}{\pi}} \qquad \text{(Eq.4)}$$

Comparing to equation 1, 2 and 3, equation 4 focuses on both delamination area and delamination diameter

Results shows that the maximum equivalent delamination factor is observed in test 1 and 5, and the minimum delamination area over nominal area is observed in test number 15, 19 and 20. The related cutting parameters and the results of equation 3 is represented by

response surface method. Figure **39** shows the corresponding minimum and maximum F_e value results.

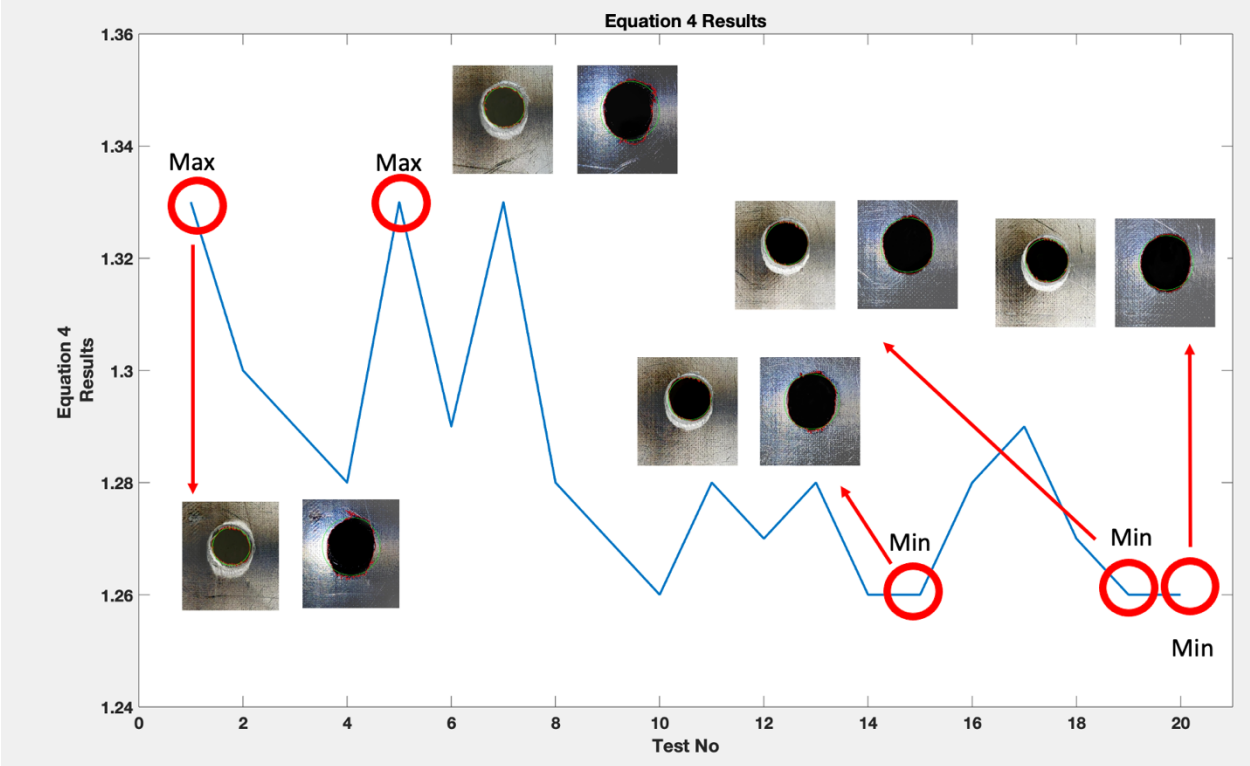

Figure 39: Conducted test number and $\boldsymbol{F_e}$ value

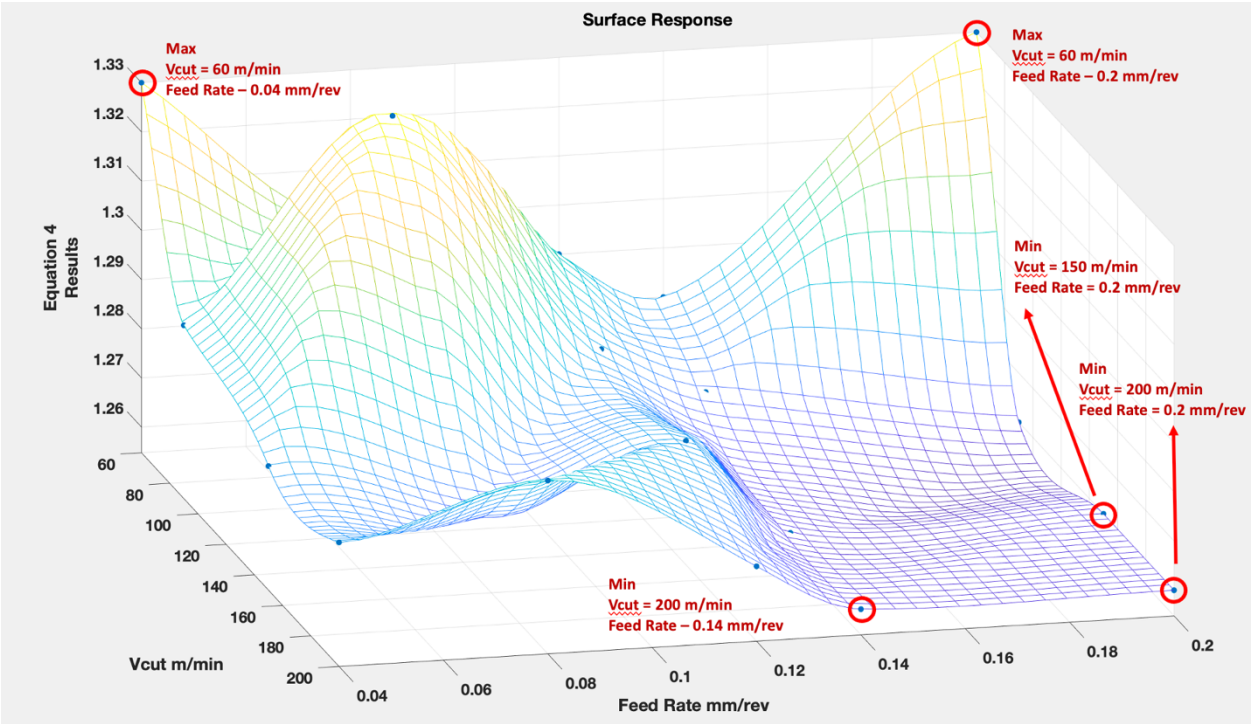

Figure 40: Surface response of cutting speed, feed rate and F_e value

The results of F_e shows that the maximum delamination size is observed in low cutting speed of 60 m/min. The minimum delamination size is observed in higher cutting speed of 200m/min and feed rate higher than of 0.14 mm/rev.

Equation 4 also shows a tendency of decreasing F_e value for high cutting speed and higher feed rate combination comparing to moderate and lower cutting speeds.

3.5 Results of GLM

In literature, there are conflicting views on how cutting speed affects delamination during drilling operations. To gain a better understanding of this relationship, ANOVA General Linear Model (GLM) is used to compare the effect of machining parameters on different delamination assessment methods. The goal is to find a correlation between cutting speed and feed rate, and to identify a delamination equation that best represents this relationship. GLM uses a least squares regression approach to determine the statistical relationship between the predictor variables (cutting speed and feed rate) and the response variable (delamination). The model can also be determined by using stepwise regression to predict

values for new observations and identify the combination of predictor values that optimize delamination. The F-values and P-values obtained from GLM are used to determine if cutting speed and feed rate are related to the delamination equation. By the result of GLM model runed for each equation and given in Figure 41, Figure 42,

Figure 43 and Figure 44 only the p-values of cutting speed in equation 3 and equation 4 are less than alpha level of 5%, it can be statistically concluded that the predictor, cutting speed in this case, has a significant effect on delamination representation. However, p-value for feed rate does not show any correlation for any of the delamination formulations.

General Linear Model: Equation 1 versus Vcut; Feed Rate

Factor Information

Factor	Type	Levels	Values
Vcut	Fixed	4	60; 90; 150; 200
Feed Rate	Fixed	5	0,04; 0,08; 0,12; 0,14; 0,20

Analysis of Variance

Source	DF	Adj SS	Adj MS	F-Value	P-Value
Vcut	3	0,02278	0,007593	3,03	0,071
Feed Rate	4	0,01137	0,002842	1,13	0,386
Error	12	0,03007	0,002506		
Total	19	0,06422			

Model Summary

S	R-sq	R-sq(adj)	R-sq(pred)
0,0500583	53,18%	25,86%	0,00%

Figure 41: GLM model for Equation 1

General Linear Model: Equation 2 versus Vcut; Feed Rate

Factor Information

Factor	Type	Levels	Values
Vcut	Fixed	4	60; 90; 150; 200
Feed Rate	Fixed	5	0,04; 0,08; 0,12; 0,14; 0,20

Analysis of Variance

Source	DF	Adj SS	Adj MS	F-Value	P-Value
Vcut	3	8,650	2,8833	3,03	0,071
Feed Rate	4	4,276	1,0689	1,12	0,391
Error	12	11,416	0,9513		
Total	19	24,341			

Model Summary

S	R-sq	R-sq(adj)	R-sq(pred)
0,975358	53,10%	25,74%	0,00%

Figure 42: GLM model for Equation 2

General Linear Model: Equation 3 versus Vcut; Feed Rate

Factor Information

Factor	Type	Levels	Values
Vcut	Fixed	4	60; 90; 150; 200
Feed Rate	Fixed	5	0,04; 0,08; 0,12; 0,14; 0,20

Analysis of Variance

Source	DF	Adj SS	Adj MS	F-Value	P-Value
Vcut	3	0,02900	0,009667	4,81	0,020
Feed Rate	4	0,01633	0,004083	2,03	0,154
Error	12	0,02411	0,002009		
Total	19	0,06945			

Model Summary

S	R-sq	R-sq(adj)	R-sq(pred)
0,0448253	65,28%	45,03%	3,56%

Figure 43: GLM model for Equation 3

General Linear Model: Equation 4 versus Vcut; Feed Rate

Factor Information

Factor	Type	Levels	Values
Vcut	Fixed	4	60; 90; 150; 200
Feed Rate	Fixed	5	0,04; 0,08; 0,12; 0,14; 0,20

Analysis of Variance

Source	DF	Adj SS	Adj MS	F-Value	P-Value
Vcut	3	0,004135	0,001378	4,61	0,023
Feed Rate	4	0,002530	0,000633	2,11	0,142
Error	12	0,003590	0,000299		
Total	19	0,010255			

Model Summary

S	R-sq	R-sq(adj)	R-sq(pred)
0,0172964	64,99%	44,57%	2,76%

Figure 44: GLM model for Equation 4

GLM R-square results for equation 3 and equation 4 shows that the 65% of the model can be explained by the cutting speed effect. For materials like CFRP, 65% of R-square value is a statistically good prediction due to the fact that delamination can be related with many factors and each assessment formulation of delamination has different dimensions and complexity.

In conclusion, equation 3 and equation 4 are both capable of showing correlation between delamination and cutting speed and equation 3 and equation 4 performs well when the delamination area is the main focus of the study.

Chapter 4

Machining dust studies of composite material

Chip produced from machining of CFRPs are largely a dust or powder-like materials and some portion of the powder-like materials has been shown to be an aerosol. This topic is an area of concern for workers and environment. The effect of carbon fiber dust in the workplace and aerosol science are still a research topic. The work discussed in this chapter aims to develop a system with an internal vacuuming system starting from the machining tool itself to collect the dust forming in machining operations of CFRP and its efficiency to use in industry. Furthermore, the results are analytically examined to determine the effect of the spindle and to optimize the suction capacity of the system by using different machining parameters.

The spindle system developed is designed by SIMUT and the special too used for this spindle is designed and produced by ZUBIOLA and the spindle is integrated to KUKA KR216 multi axis robotic machining unit.

4.1 Material

The workpiece used in this experiment is a CFRP plate in which the prepregs are stacked and cured in 0° and 90° degree sequence resulting in final thickness of 8 mm.

4.2 Cutting tools

All tests were conducted with new unused flat end mill tool that is designed by ZUBIOLA. The flat end mill tool used in these tests has a special geometry to increase the efficiency of suction during the edge trimming operations. The tool is designed with an end-to-end hole inside connected to the vacuuming system of the spindle. Furthermore, the teeth of the flat end mill have gaps in between the four teeth to create more space for vacuuming. The edge trimming tool having the special suction gaps is shown in Figure 45.

Figure 45: Designed tool with vacuuming gaps

4.3 Experimental Methodology and Dust collection

The wrapping paper between the CFRP plate and the fixture is used to collect the dust that is generated by the edge trimming operation. The wrapping paper is selected as the collective material for the edge trimming test mainly for two reasons: the weight of the wrapping papers are nearly the same so that the weight of the wrapping paper can be

subtracted from the total weight of the collected dust and paper after each edge trimming test and the due to the material nature of the wrapping paper, dust can be consolidated in the center of the paper making the collection much easier.

In each experiment, wrapping paper is changed and a new wrapping paper is replaced between the material and the fixture. The leftover dust is collected by taking the paper out. The paper containing the dust is then folded and weighted to analyse the effect of the suction system. The cutting tests were conducted with vacuuming system and without vacuuming system to analyse the suction performance in each case. Figure 46 and Figure 47 shows the setup for dust collection and the dust generated after the edge trimming test.

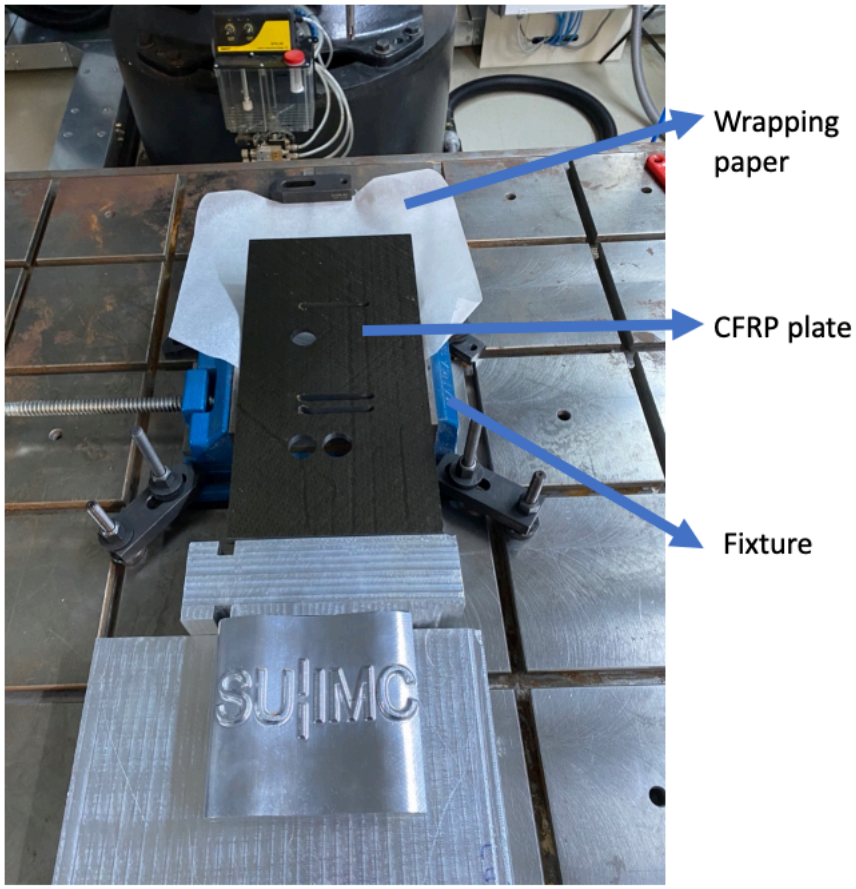

Figure 46: Dust collection set-up

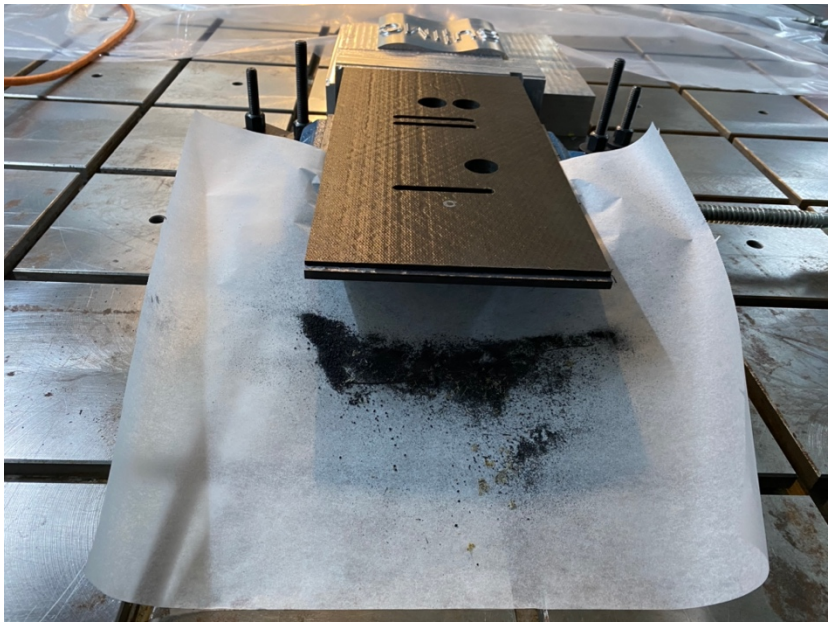

Figure 47: Dust generated by the edge trimming operation

4.4 The spindle designed for dust collection

The spindle used for vacuuming performance test is designed by SIMUT to increase the dust collection with an end to end suction gap and an external vacuuming system that is connected to the suction unit of the KUKA KR16 multi axis machining robotic unit. The prototype of the spindle is shown in Figure 48.

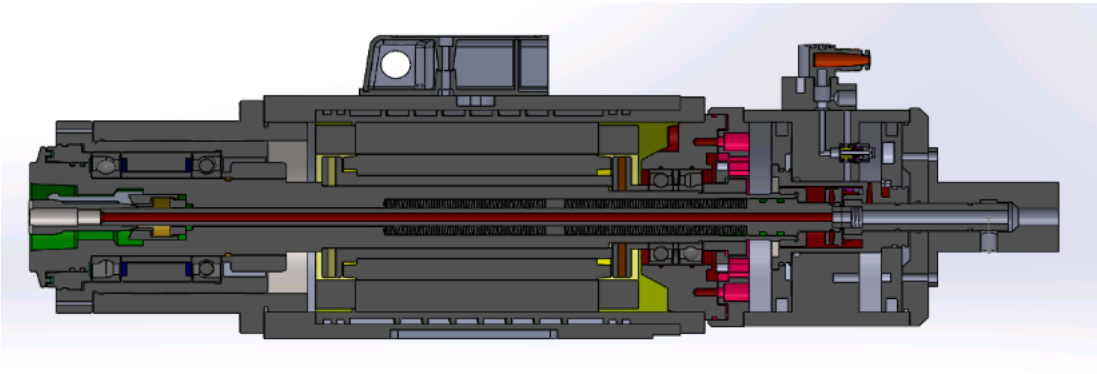

Figure 48: Technical drawing of the prototype spindle for dust collection

4.5 Parameter Selection & Test Matrix

Parameters used in the cutting tests are dynamically selected. In the first test group, test number 1, 2, 3, and 4 the spindle speed is kept constant while the feed rate values are selected 720, 1200, 1800 and 2400 mm/min consecutively. First group of cutting tests are conducted under vacuuming condition where the same test matrix is used under the non-vacuuming condition in the following test group (Test number 5, 6, 7, and 8). After conducting same cutting condition with vacuum and non-vacuum options, the best suction performance is analysed and the feed rate from the best performance is selected as the constant feed rate for further cutting tests.

Cutting condition hence the suction performance highly depends on the selection of machining parameters such as feed rate, spindle speed, axial depth, and radial depth. For the sake of the experiment, the axial depth is kept as 1,5 mm in each test where the radial depth is used 10%, 50% and 100%. The change in radial depth highly effects the vacuuming nature of the spindle hence the performance is also highly dependent to radial depth of the cutting tests.

The parameters list used for fixing the feed rate for each radial depth (%10, %50 and %100) is the same for every conducted test. The attempt of fixing the feed rate for upcoming test group is aimed to simplify the examination and the complexity of the relation between cutting parameter and the suction performance

The common test matrix used to fix the feed rate for upcoming test group analysis for each radial depth is listed in the Table 9.

Table 9: The common test matrix used for dynamic parameter selection

Test No	Test Condition	Spindle Speed (rpm)	Feed Rate (feed/tooth)	Axial Depth (mm)	Vcut (mm/min)	Vfeed (mm/min)
1	With suction	6000	0.03	1.5	188.4	720
2	With suction	6000	0.05	1.5	188.4	1200
3	With suction	6000	0.075	1.5	188.4	1800
4	With suction	6000	0.1	1.5	188.4	2400
5	Without suction	6000	0.03	1.5	188.4	720
6	Without suction	6000	0.05	1.5	188.4	1200
7	Without suction	6000	0.075	1.5	188.4	1800
8	Without suction	6000	0.1	1.5	188.4	2400

The performance result according to test parameters and the procedure of fixing the feed rate for different radial depth values are detailly examined in section 4.6

4.6 Performance of the vacuuming system

Parameters used in the edge trimming tests are dynamically selected according to the current suction performance. The performance of the vacuuming system highly depends on the test parameters such as feed rate, cutting speed, spindle speed and radial depth. In order to examine the effect of the radial depth, cutting tests are conducted in 3 different radial depth condition: %10, %50 and %100. It is observed that for each radial depth value, the cutting mechanism and the nature of the tool and the work piece interaction is different. The first group of cutting test group under vacuuming and non-vacuuming conditions are used for each radial depth condition. The following test matrix is determined according to the observations and the calculated performance after each test. In this section, radial depths of %10, %50 and %100 are separately examined.

4.6.1 Suction performance of radial depth of %10

In the performed edge trimming tests, as it is already given in section 4.5, to detect the effect of feed rate, spindle speed and hence the cutting speed kept the same where the feed rate values in each test for vacuuming and non-vacuuming condition are varied. Following table shows the cutting parameter for the first 4 test under vacuuming condition. The same cutting parameters are then used for non-vacuuming condition and compared to find the best suction performance for given feed rate values. After fixing the feed rate, tests are conducted by changing the other machining parameters (except feed rate) such as spindle speed and cutting speed values for vacuuming and non-vacuuming condition to determine the best parameter selection for higher vacuuming performance.

Parameter list for determining best feed rate value for suction performance and collected dust weight for %10 radial depth are given in Table 10.**Error! Reference source not found.**

Table 10: Parameter list for dynamic selection (for radial depth of 10%) and suction performance

Test Condition	**Test No**	**Spindle Speed (rpm)**	**Feed Rate (mm/rev/teeth)**	**Vcut (m/min)**	**Vfeed (mm/min)**	**Dust Weight (gr)**	**Suction Performance(%)**
With Suction	1	6000	0,030	188,4	720	0,3691	
With Suction	2	6000	0,050	188,4	1200	0,2492	(min dust weight)
With Suction	3	6000	0,075	188,4	1800	0,3675	
With Suction	4	6000	0,100	188,4	2400	0,3875	
Without Suction	5	6000	0,030	188,4	720	0,3896	5,2618
Without Suction	6	6000	0,050	188,4	1200	0,6950	64,1439
Without Suction	7	6000	0,075	188,4	1800	0,8389	56,1926
Without Suction	8	6000	0,100	188,4	2400	0,4208	7,9135

As it is given in the Table 10, in the first 8 test, the spindle speed is kept as 600 rpm and cutting speed is calculated for the cutting tool having a 10 mm diameter with 4 teeth is 188,4 m/min. Feed rate values are used as 0.03, 0.05, 0,075 and 0.1 mm/rev/tooth consecutively.

Test number 1, 2, 3, and 4 are conducted under vacuuming condition where test number 5, 6, 7, and 8 are the same as the first 4 test except the non-vacuuming condition. By conducting the cutting tests as such, it is possible to determine the suction performance by comparing the weight of the dust collected from wrapping paper and analytically define the best performing feed rate value to fix for further cutting tests.

From the conducted first 8 tests, it is observed that the minimum dust weight is recorded under the cutting conditions of 0.05 mm/rev/tooth feed rate. After performing the edge trimming tests with the given tests parameters, the dust that are not collected by the suction system of the spindle is weighted around 0.25 gram. Furthermore, the dust weight under vacuuming and non-vacuuming conditions are analytically compared and the best suction performance of 64% is found with the feed rate of 0.05 mm/rev/tooth.

For suction performance calculation, the dust weight collected from the table after each edge trimming test is compared for the same cutting conditions. For example, dust weight collected from test 1 (vacuuming condition) and dust weight collected from test 5 (non-vacuuming condition) is compared to find the suction performance for the same cutting parameters. Since test 1 and test 5 has the same cutting parameter except the vacuuming condition, the result of this comparison provides the performance of the vacuuming system.

After determining the best performing feed rate value , 0.05 mm/rev/tooth in this case, and fixing the feed rate to this value for the upcoming tests, the test matrix used for the following test is dynamically updated as given in Table 11.

Table 11: Dynamically updated parameter list (for radial depth of 10%) and suction performance

Test Condition	**Test No**	**Spindle Speed (rpm)**	**Feed Rate (mm/rev/teeth)**	**Vcut (m/min)**	**Vfeed (mm/min)**	**Dust Weight (gr)**	**Suction Performance(%)**
With Suction	9	16000	0,050	502,4	1200	0,0866	
With Suction	10	8000	0,050	251,2	1200	0,2455	
With Suction	11	4000	0,050	125,60	1200	0,3161	

With Suction	12	2000	0,050	62,80	1200	0,3541	
Without Suction	13	8000	0,050	251,2	1200	0,4864	49,52713816
Without Suction	14	4000	0,050	125,6	1200	0,5877	46,21405479
Without Suction	15	2000	0,050	62,8	1200	0,6791	47,8574584

The following test group of test number 9, 10, 11, and 12 are conducted after fixing the feed rate value to 0.05 mm/rev/tooth. Spindle speed values for this group of cutting test is selected as 16000, 8000, 4000 and 2000 rpm consecutively.

After performing the test 9, it is observed that spindle speed of 16000 rpm is not suitable for the nature of the cutting test due to the extensive spread of dust to the outer side of the dust collection mechanism. It is also observed that the minimum dust weight is collected for the highest spindle speed. However, this observation is biased due to the extensive spread of the dust even under the vacuuming condition. Hence, the spindle speed of 16000 rpm is decided not to use in the following cutting tests. Test number 10, 11 and 12 are conducted under vacuuming condition and test 13, 14 and 15 are conducted by using the same test parameter as used in the previous test group but under non vacuuming condition.

After analytically calculating the suction performance, for radial depth of 10% and axial depth of 1.5 mm, it is observed that up to %49.5 of dust can be collected by the suction system integrated to the spindle by using feed rate value of 0.05mm/rev/tooth, spindle speed of 8000 rpm and cutting speed of 251 m/min.

The same cutting test structure and approach is performed for radial depth of %50 and detailly examined in the following section of 4.6.2

4.6.2 Suction performance of radial depth of %50

The same methodology used for examining the effect of %10 radial depth is also used to examine the effect of %50 radial depth. The same test condition used in the first 8 test is also used for %50 radial depth to determine the best performed feed rate value for following test to calculate the best suction performance for given cutting test parameters.

Parameter list for determining best feed rate value for suction performance and collected dust weight for %50 radial depth are given in Table 12.

Table 12: Parameter list for dynamic selection (for radial depth of 50%) and suction performance

Test Condition	**Test No**	**Spindle Speed (rpm)**	**Feed Rate (mm/rev/teeth)**	**Vcut (m/min)**	**Vfeed (mm/min)**	**Dust Weight (gr)**	**Suction Performance(%)**
With Suction	1	6000	0,030	188,4	720	1,36	
With Suction	2	6000	0,050	188,4	1200	1,03	min dust weight
With Suction	3	6000	0,075	188,4	1800	1,42	
With Suction	4	6000	0,100	188,4	2400	1,59	
Without Suction	5	6000	0,030	188,4	720	2,47	44,9393
Without Suction	6	6000	0,050	188,4	1200	2,77	62,8159
Without Suction	7	6000	0,075	188,4	1800	2,68	47,0149
Without Suction	8	6000	0,100	188,4	2400	2,27	29,9559

In order to determine the best performed feed rate value by comparing the suction performance for radial depth of %50, the spindle speed value is kept as 6000 rpm for each test and the cutting speed value is kept still as 188,4 m/min where the feed rate values are selected as 0.03, 0.05, 0.075 and 0.1 respectively.

After collecting the dust after each edge trimming test, the minimum collected dust weight is calculated in test number 2 under vacuuming condition. The same cutting test parameters are used in test number 5, 6, 7 and 8 under non-vacuuming condition. It is observed that comparing to vacuuming and non-vacuuming conditions, %62 of the dust can be collected by the suction system integrated to the spindle in test number 6 where the feed rate is 0.05 mm/rev/tooth. Hence, the feed rate is fixed as 0.05 mm/rev/tooth for the following cutting tests and the test matrix used for the following test is dynamically updated as given in Table 13.

Table 13: Dynamically updated parameter list (for radial depth of 50%) and suction performance

Test Condition	**Test No**	**Spindle Speed (rpm)**	**Feed Rate (mm/rev/teeth)**	**Vcut (m/min)**	**Vfeed (mm/min)**	**Dust Weight (gr)**	**Suction Performance(%)**
With Suction	9	16000	0,050	502,4	1200	0,91	
With Suction	10	8000	0,050	251,2	1200	1,45	
With Suction	11	4000	0,050	125,60	1200	1,4	
With Suction	12	2000	0,050	62,80	1200	0,67	
Without Suction	13	8000	0,050	251,2	1200	2,5452	43,03001729
Without Suction	14	4000	0,050	125,6	1200	2,392	41,47157191
Without Suction	15	2000	0,050	62,8	1200	2,76	75,72463768

After fixing the feed rate to 0.05mm/rev/tooth, spindle speed values are used as 16000, 8000, 4000 and 2000 rpm respectively. However, the same observation for %10 radial depth for 16000 also observed in radial depth of %50 case where the dust generated in the cutting test is extensively spread outside of the dust collection area hence 16000 rpm of spindle speed is decided to not to be used in the following cutting tests.

The comparison of the vacuuming and non-vacuuming condition showed that the up to %76 of the dust generated in the cutting test with 2000 rpm of spindle speed, 0.05 mm/rev/tooth feed rate and 62.8 m/min of cutting speed can be collected by using the suction system integrated in the spindle.

The same cutting test structure and approach that is used for radial depth of %10 and %10 is also performed for radial depth of %100 and detailly examined in the following section of 4.6.3

4.6.3 Radial depth of %100

The same methodology used for examining the effect of %10 and %50 radial depth given in section 4.6.1 and 4.6.2 is also used to examine the effect of %100 radial depth. The same test condition used in the first 8 test is also used for %100 radial depth to determine the best performed feed rate value for upcoming tests to dynamically update the test parameters and to calculate the best suction performance accordingly.

Parameter list for determining best feed rate value for suction performance and collected dust weight for %100 radial depth are given in Table 14.

Table 14: Parameter list for dynamic selection (for radial depth of 100%) and suction performance

Test Condition	**Test No**	**Spindle Speed (rpm)**	**Feed Rate (mm/rev/teeth)**	**Vcut (m/min)**	**Vfeed (mm/min)**	**Dust Weight (gr)**	**Suction Performance(%)**
With Suction	1	6000	0,030	188,4	720	2,2152	min dust weight
With Suction	2	6000	0,050	188,4	1200	2,5888	
With Suction	3	6000	0,075	188,4	1800	2,7115	
With Suction	4	6000	0,100	188,4	2400	2,9948	
Without Suction	5	6000	0,030	188,4	720	6,0096	63,1390
Without Suction	6	6000	0,050	188,4	1200	5,7482	54,9633
Without Suction	7	6000	0,075	188,4	1800	4,2503	36,2045
Without Suction	8	6000	0,100	188,4	**2400**	**4,7146**	36,4782

In order to determine the fix value of feed rate by comparing the suction performance for radial depth of %100, the spindle speed value is kept still as 6000 rpm for each test and the cutting speed value is kept still as 188,4 m/min where the feed rate values are selected as 0.03, 0.05, 0.075 and 0.1 respectively.

After collecting the dust weight after each edge trimming test, the minimum collected dust weight is calculated in test number 2 under vacuuming condition. The same cutting test parameters are used in test number 5, 6, 7 and 8 under non vacuuming condition in order to determine the fixed feed rate values and best suction performance. It is observed that by comparing to vacuuming and non-vacuuming conditions, %63 of the dust can be

collected by suction system integrated in spindle in test number 5 where the feed rate is 0.03 mm/rev/tooth. Hence, the feed rate is fixed as 0.03 mm/rev/tooth for the following cutting tests and the test matrix used for the following test is dynamically updated as given in Table 15.

Table 15: Dynamically updated parameter list (for radial depth of 100%) and suction performance

Test Condition	**Test No**	**Spindle Speed (rpm)**	**Feed Rate (mm/rev/teeth)**	**Vcut (m/min)**	**Vfeed (mm/min)**	**Dust Weight (gr)**	**Suction Performance(%)**
With Suction	9	8000	0,030	251,2	720	2,34	
With Suction	10	4000	0,030	125,60	720	1,0195	
With Suction	11	2000	0,030	62,80	720	0,3957	
Without Suction	12	8000	0,030	251,2	720	5,0775	53,91432792
Without Suction	13	4000	0,030	125,60	720	5,0015	79,61611517
Without Suction	14	2000	0,030	62,80	720	4,1769	90,526467

After fixing the feed rate to 0.03mm/rev/tooth, spindle speed values are used as 8000, 4000 and 2000 rpm respectively. Spindle speed of 16000 rpm is decided not to be used for %100 radial depth for this cutting test due to the extensive spreading tendency observed in radial depth of %10 and %50 cutting tests.

The comparison of the vacuuming and non-vacuuming condition showed that the up to %90 of the dust generated in the cutting test with 2000 rpm of spindle speed, 0.03 mm/rev/tooth feed rate and 62.8 m/min of cutting speed can be collected by using the suction system integrated in the spindle.

4.7 Test results on the performance of the vacuuming system

The suction system integrated in the spindle is examined for different cutting conditions. The cutting test parameters are design to analyse the effect of spindle speed, feed rate, cutting speed and radial depth of cut to the suction performance.
To decrease the complexity and the repetition of the cutting tests, the test matrix is dynamically degenerated by fixing the spindle speed and cutting speed values at the first group of tests to determine a fixed feed rate value. After determining the fixed feed rate value for each radial depth of cut of %10, %50 and %100 emerging conditions, the optimum spindle speed and cutting speed values are determined by calculating the suction performance of the integrated system. The details of the dust collection system and the methodology to calculate the suction performance are explained in section 4.2, 4.3, and 4.5, and the results from cutting test are examined in section 4.6

As it can be predicted by analysing the nature of the edge trimming operation and the structure of the cutting tool, the suction system integrated end to end in the spindle performs best with the lower feed rate and lower spindle speed values. Furthermore, the radial depth of cut also plays a crucial role in the suction performance. It is observed that the suction performance can be increased by increasing the radial depth of cut where the interaction area between the cutting tool and the work piece is also increased, resulting an enlarged area for dust collection.

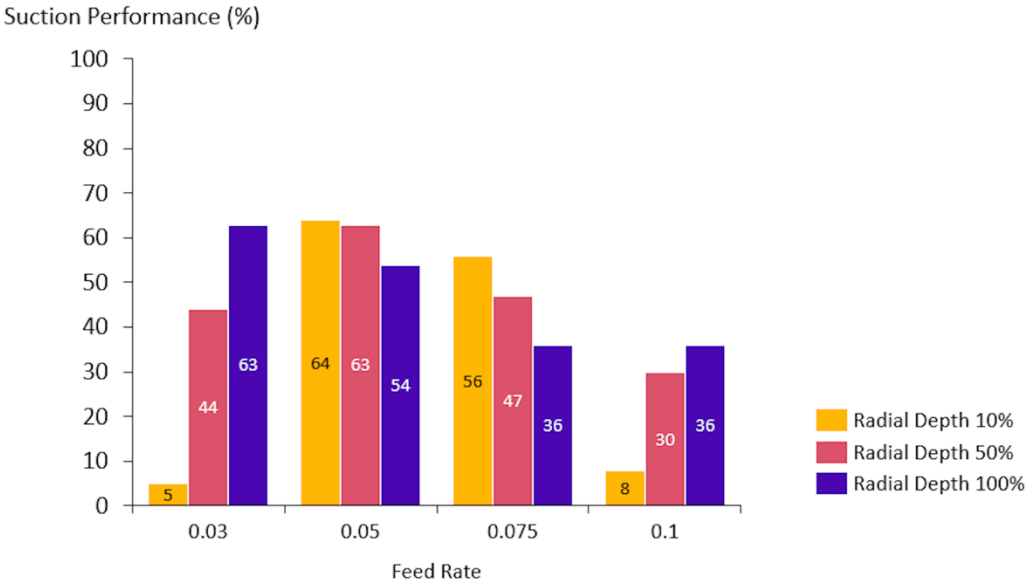

Figure 49: Suction performance result for given radial depth and feed rate, Spindle speed is 6000rpm

The cutting parameter list is dynamically updated according to the result of the common matrix that is used for every radial depth of cut. Figure 49 shows the suction performance results of the common matrix before dynamically updating for the further edge trimming operations. It is observed that the maximum suction performance can be achieved in moderate and low feed rate values while using lower radial depth of cut. However, it is not safe to say that the best suction performance can only be obtained in these conditions due to the fact that a change in radial depth and feed rate highly affects the material removal rate (MRR) and the comparison between different MRR and suction performance can be misleading. Hence, the dynamically selected parameter list and the suction performance for each radial depth is also visualized for further insight.

Once the dynamically updated parameters are completed respected to the best performed feed rate value, it is observed that for radial depth of 10% and 50%, feed rate of 0.05mm/rev/tooth, and for radial depth of 100%, feed rate of 0.03mm/rev/tooth are found to be the best performing value and fixed for different values of spindle speed.

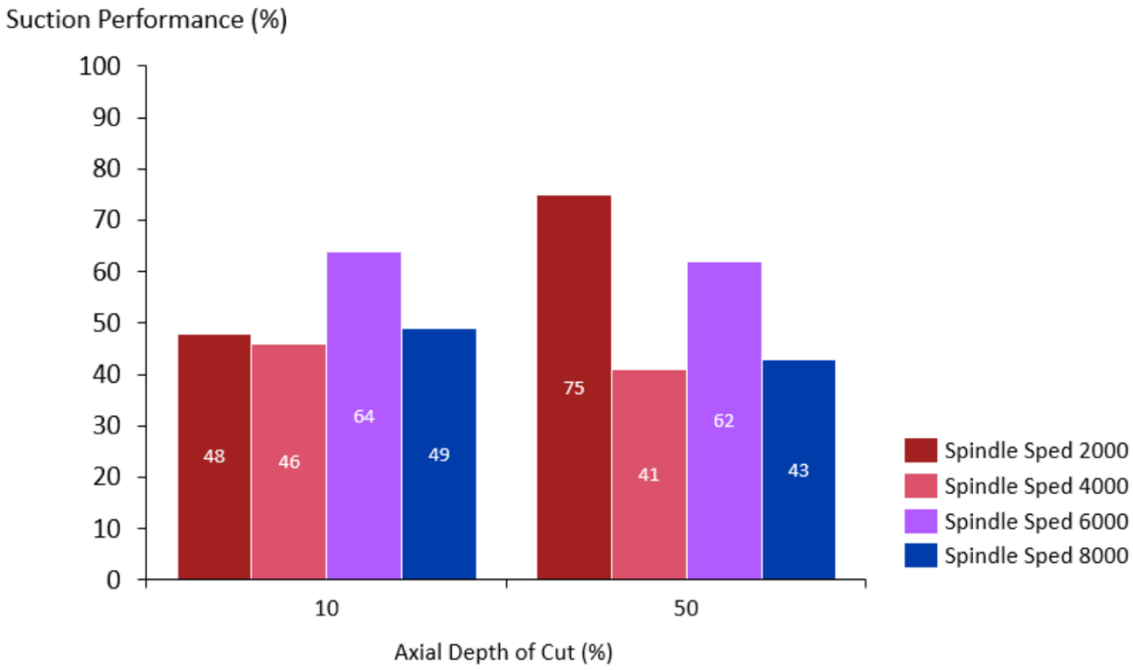

Figure 50: Suction performance of given spindle speed and axial depth values, Feed rate is 0.04mm/rev/tooth

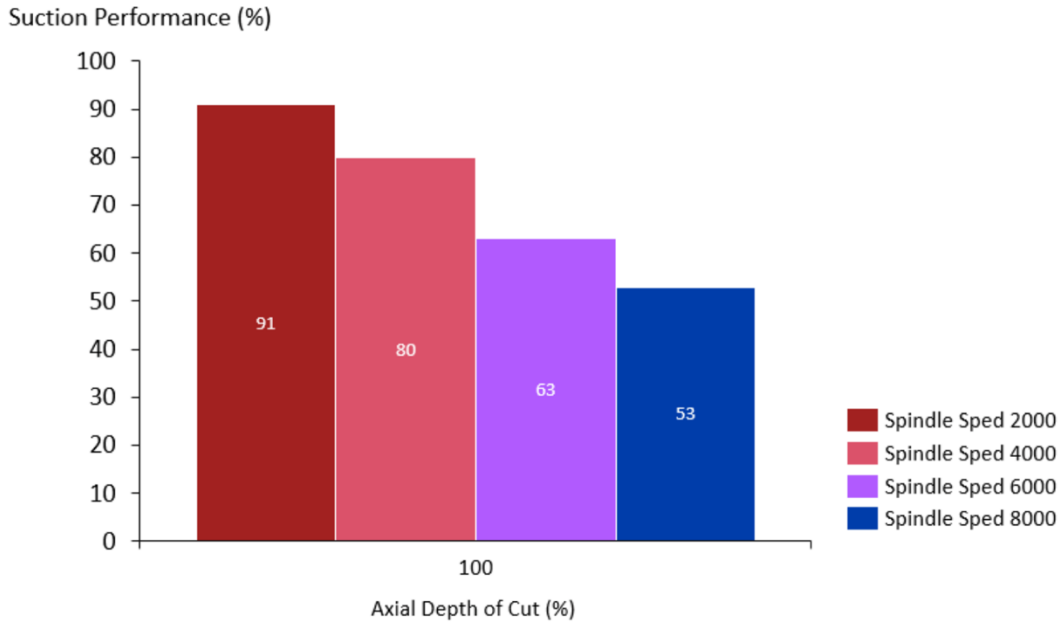

Figure 51: Suction performance of given spindle speed and axial depth values, Feed rate is 0.03mm/rev/toot

Figure 50 and Figure 51 shows the result of calculated suction performance according to the updated cutting test parameters. It is possible to say that, in each case, the vacuuming set-up performs well and more than 40% of the dust generated during the

edge trimming operations are collected by the vacuuming system. By comparing 10% and 50% of axial depth of cut, for lower spindle speed and higher axial depth of cut, it is possible to collect up to 75% of the dust generated during the edge trimming operations. Moreover, for full engagement of cutting tool and workpiece (100% radial depth) and lower feed rate of 0.03mm/rev/tooth, up to 91% of the dust generated during edge trimming operations can be collected. It is convenient to find best performing machining parameter for higher axial depth of cut, lower spindle speed and feed rate values due to the fact that an increase in engagement area, increases the likelihood to collect dust particles and decrease in spindle speed prevents dust particles to spread and lower feed rate values decreases MRR hence dust formation is inhibited.

Chapter 5

Edge trimming Tests

Edge trimming is a common process for roughing and finishing carbon fiber composite parts. The experimental procedure conducted in this chapter involves edge trimming of CFRP plates with a roughing tool under different machining parameters and conditions. The goal of this study is to investigate the relationship between the force required during edge trimming of carbon fiber composite materials and the parameters of the machining process. Specifically, the experiments focus on measuring the force required during edge trimming and how it is affected by different machining parameters in order to minimize damage to the material.

5.1 Edge trimming test setup

The goal of the experiments discussed in this chapter is to study the relationship between machining parameters and the forces generated during edge trimming of CFRP plates using a roughing tool. The experiments were conducted using a six-axis robotic machining unit, where various spindle speeds, feed rates, and radial depths were used while keeping the tool constant. The cutting tool used was a 12mm diameter end-mill with 6 cutting edges, specially designed for roughing operations. The cutting direction was upwards and the cutting was stopped at the center of the plate. In total, 10 edge trimming operations are performed according to design of experiment and cutting parameters.

Figure 52 shows the cutting tool used in the experiment, Figure 53 show the CFRP plate connected to KISTLER dynamometer via 4 drilled whole at the center of the plate and clamping screw, and the fixture holding the dynamometer above the cutting frame of the six-axis machining unit.

Figure 52: Sandvik 2P350-1200-OA O12M Tool

Figure 53: CFRP plate, fixture, and dynamometer

Design of experiment is conducted according to the suggested cutting parameters of the tool and the full factorial test matrix to examine the effect of each varying component to the cutting force is developed. Table 16 shows the DoE values for parameters that are matched with one another to obtain coherent results and Table 17 show the resulting test parameters of the consolidated design of experiment matrix. During the edge trimming experiments, the input variables were the machining parameters such as spindle speed, feed rate, and radial depth. The most important output from these experiments was the force generated during the process.

Table 16: DoE values for parameters

Parameter	**Unit**	**Values**
Spindle Speed	rpm	1062, 2123, 3981, 6635, 9289
Feed/tooth	mm	0.015, 0.03, 0.075, 0.120
Vcut	m/min	40, 80, 150, 250, 350
Radial depth	%	25, 50, 75

Table 17: Full factorial test matrix

Test No	Spindle Speed (rpm)	Feed/tooth (mm)	Vcut (m/min)	Radial depth (%)	Vfeed
1	2123	0.015	80	50	191
2	2123	0.03	80	50	382
3	2123	0.075	80	50	955
4	2123	0.120	80	50	1529
5	1062	0.015	40	50	96
6	3981	0.015	150	50	358
7	6635	0.015	250	50	597
8	9289	0.015	350	50	836
9	2123	0.015	80	25	191
10	2123	0.015	80	75	191

Once the test matrix was completed, the toolpath was generated according to the DoE parameters to demonstrate the force generation trends in machining quality and simulated in Siemens NX CAD/CAM environment for the six-axis robotic machining unit of KUKA KR16 given in Figure 54. Close up look of the simulated tool path is given in Figure 55 and Figure 56.

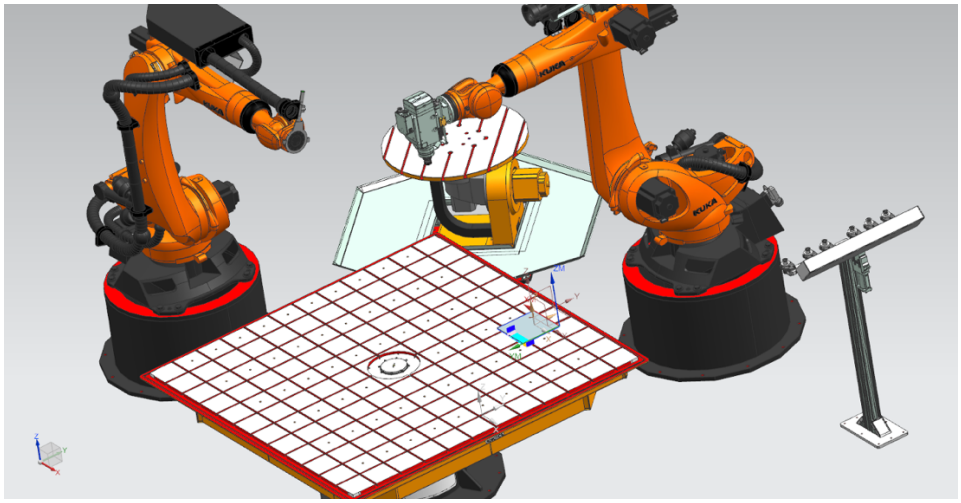

Figure 54: Tool path simulation

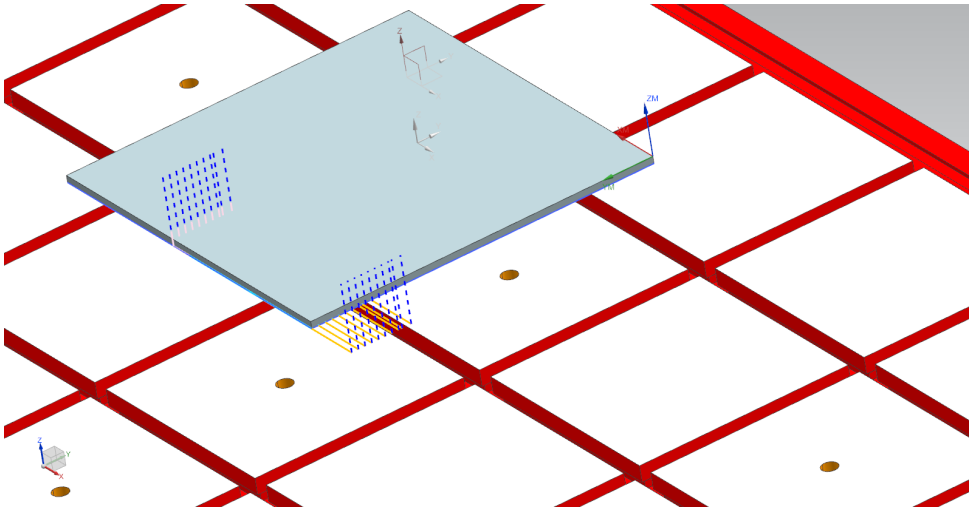

Figure 55 Tool path simulation close up (1)

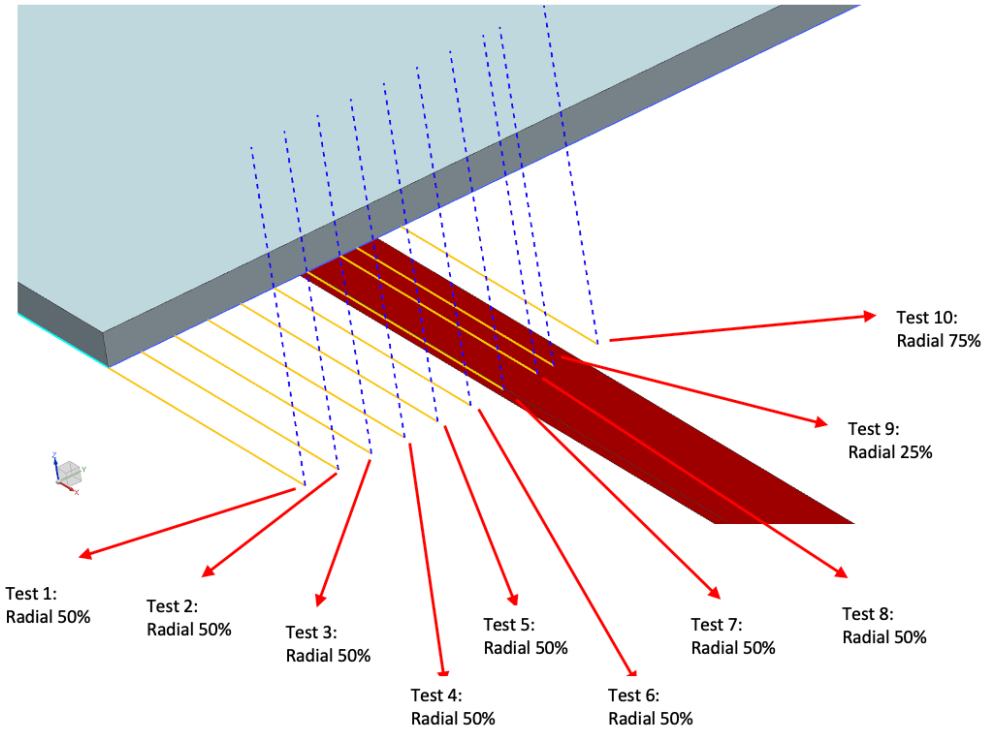

Figure 56: Tool path simulation close up (2)

Machining quality greatly depends on cutting force generated along X, Y and Z direction. To examine this effect and conclude on the most effective test parameter on force generation, force along X, Y and Z directions are collected during the experiment by using a KISTLER dynamometer, amplifier, and NI DAQ equipment as shown in Figure 57. Initial state of the CFRP plate connected to dynamometer and the fixture before the

edge trimming test and the trimmed region after the edge trimming operations are given in Figure 58 and Figure 59.

Figure 57: Amplifier and the NI DAQ equipment

Figure 58: CFRP plate before edge trimming operation

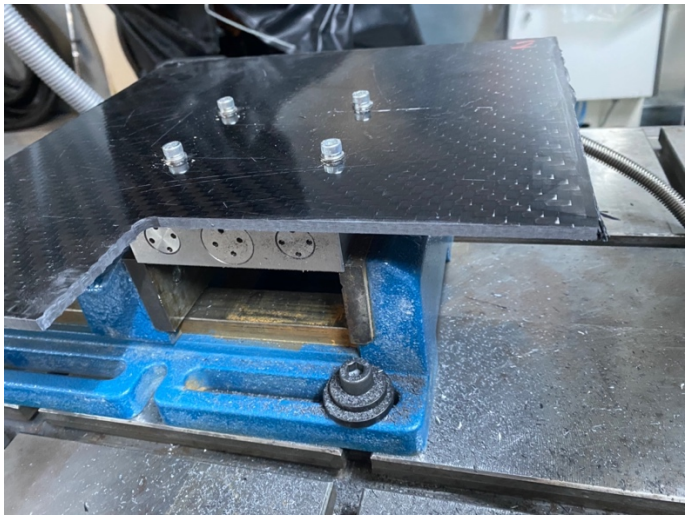

Figure 59: CFRP plate and trimmed zone after edge trimming operations

5.3 Edge trimming test results

Machining parameters in the full factorial test matrix is used and corresponding force values are collected during the edge trimming tests. Table 18 shows the related force values collected during edge trimming operations.

Table 18: Force data collected during edge trimming operations

Test no	Spindle Speed	Feed Rate mm/rev/tooth	Vcut (m/min)	Radial (%)	Force X (Avg)	Force Y (Avg)	Force Z (Avg)	Cumulative Force (X&Y)
1	2123	0,015	80	50	25	120	40	123
2	2123	0,03	80	50	27	180	25	182
3	2123	0,075	80	50	40	380	37	382
4	2123	0,12	80	50	50	520	50	520
5	1062	0,015	40	50	50	140	25	149
6	3981	0,015	150	50	45	125	30	133
7	6635	0,015	250	50	40	110	50	117
8	9289	0,015	350	50	40	108	27	115
9	2123	0,015	80	25	5	85	20	85
10	2123	0,015	80	75	70	140	25	157

To analyse the effect of feed rate to force along X, Y and Z direction, first four test are used to generate scatterplot of cumulative force values along X &Y and feed rate.

Test no	Spindle Speed	Feed Rate mm/rev/tooth	Vcut (m/min)	Radial (%)	Force X (Avg)	Force Y (Avg)	Force Z (Avg)	Cumulative Force (X&Y)
1	2123	0,015	80	50	25	120	40	123
2	2123	0,03	80	50	27	180	25	182
3	2123	0,075	80	50	40	380	37	382
4	2123	0,12	80	50	-20	520	50	520

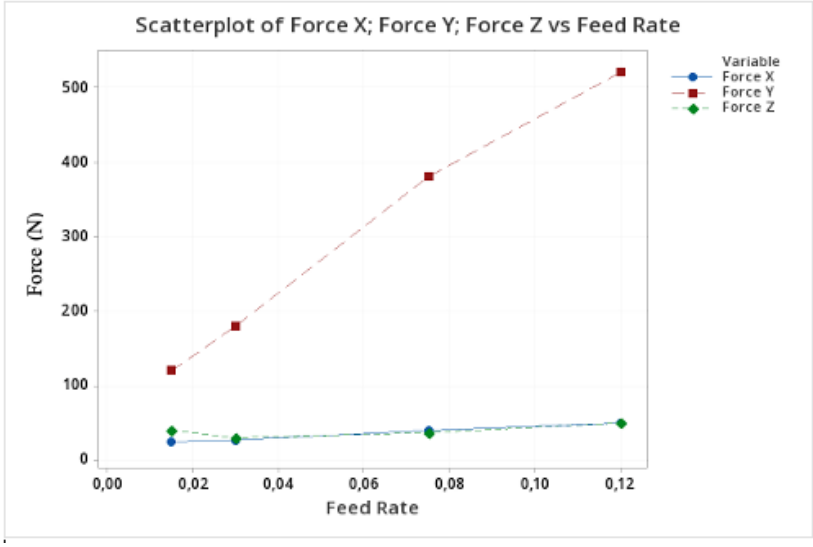

Figure 60: Force along X, Y and Z for given Feed rate

By comparing the feed rate effect on force along X, Y and Z direction, it is observed that the increase in feed rate results a visible increase in force along X and Y direction for the same spindle speed and cutting speed and radial depth. Figure 60 shows the scatterplot of force along X, Y and Z for the same spindle speed, cutting speed and radial depth of cut.

The relation between Force along X and Y with the feed per tooth is also separately analysed. It is observed that the feed rate is strongly effective/correlated with the force component along Y axis.

Since the cutting tool is designed for roughing operations, the surface of the CFRP plate after cutting operations has the same quality without any fiber pull-out or delamination however by inspection, it is observed that an increase in feed rate also increases the machining sound which indicates that there might be tool wear in the long run.

In order to examine the effect of cutting speed on force, Test number 5, 6, 7 and 8 are selected.

In this group of tests given in table below, the feed rate and radial depth of cut was 0.015 mm/tooth and 50% respectively. The only variant cutting parameter is the cutting speed with a range of 40 m/min to 350 m/min.

Test no	Spindle Speed	Feed Rate mm/rev/tooth	Vcut (m/min)	Radial (%)	Force X (Avg)	Force Y (Avg)	Force Z (Avg)	Cumulative Force (X&Y)
5	1062	0,015	40	50	50	140	25	149
6	3981	0,015	150	50	45	125	30	133
7	6635	0,015	250	50	40	110	50	117
8	9289	0,015	350	50	40	108	27	115

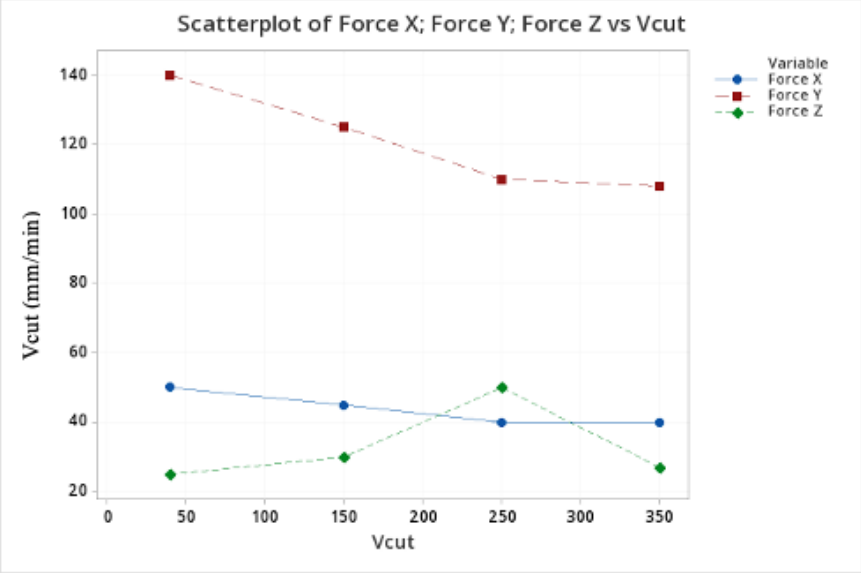

Figure 61: Force along X, Y and Z for given Cutting Speed

It is observed that as the cutting speed increases, force along X & Y axis decreases. For a roughing tool having a special geometry for composite machining, the result shows the expected output. We observed the same trend in looking separately to force along X and Y as given in Figure 61. However, this trend is not observable in force along Z direction.

To examine the effect of radial depth of cut on force applied to CFRP, test number 1, 9 & 10 selected. The only variant parameter among these tests is the radial depth of cut. It is observed that increasing radial depth of cut from 25% (3mm engagement) to 75% (8mm engagement) the force applied in X and Y direction increases from 5N to 70N and 85N to 140N for X and Y respectively. The effect of radial depth of cut(%) on force change is visualized in Figure **62**.

Test no	Spindle Speed	Feed Rate mm/rev/tooth	Vcut (m/min)	Radial (%)	Force X (Avg)	Force Y (Avg)	Force Z (Avg)	Cumulative Force (X&Y)
1	2123	0,015	80	50	25	120	40	123
9	2123	0,015	80	25	5	85	20	85
10	2123	0,015	80	75	70	140	25	157

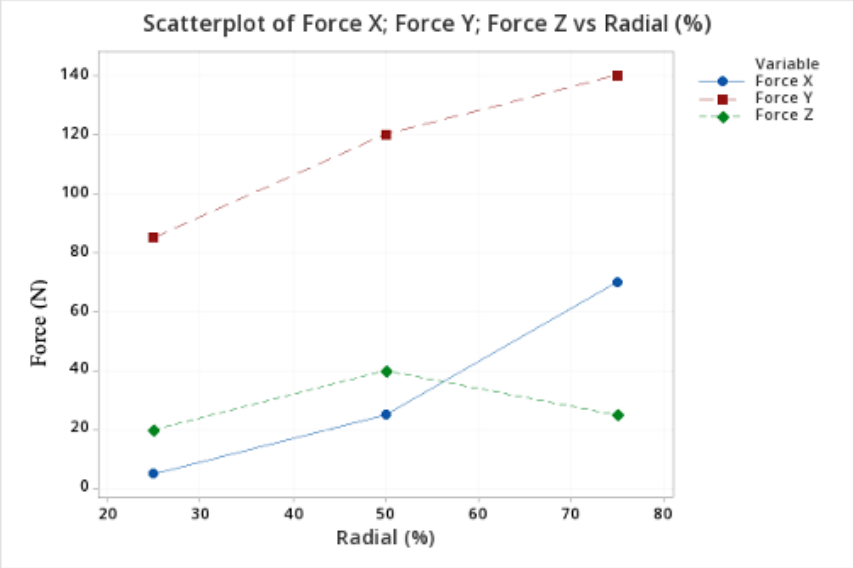

Figure 62: Force along X, Y and Z for given radial depth of cut (%)

In order to select the most effective parameter on cutting force, Minitab ANVOVA general linear model analysis is used.

The force analysis is especially important for CFRP materials. Even though the tool used in this experiment is designed for roughing operations and has a special design for eliminating fibre pull out and delamination, it is known that an increase in force can cause

machining induced errors such as vibration, delamination, wavy surface etc. Hence it is crucial for CFRP machining processes to define the most effective cutting parameters on force applied/generated on CFRP workpiece during the machining operations of composite materials.

GLM is a statistical method that uses a least squares regression approach to analyze the relationship between one or more independent variables (predictors) and a dependent variable (response). It is used to determine whether there is a correlation between the predictors and the response, and if so, how strong the correlation is. The p-values in GLM are used to test the significance of the coefficients of the independent variables, with a high p-value indicating that the coefficient is unreliable and a low p-value suggesting that the coefficient is statistically significant.

GLM is developed individually for the force along each axis since the nature of machining has different effect in each axis hence the related machining parameter effecting the force generation in each axis can be highly different.

For the force generation along X axis, first, the effect of feed rate and radial depth of cut is compared. The main reason for comparing two parameter at once but not every parameter is that the number of test is not enough to generate a result that can be statistically examined and interpreted to generate a model. The results showed that according to the p-value of the analysis of variance, radial depth of cut is highly and statistically effective on force generation along X axis where the effect of feed rate is not statistically observable.

Since the nature of machining has different effects in each axis, the corresponding machining parameter affecting the force generation in each axis might be very varied, GLM is create separately for the force along each axis.

First, the impact of feed rate and radial depth of cut is contrasted for the force generation along the X axis. The findings shown that, in contrast to the influence of feed rate, which is not statistically detectable, radial depth of cut is substantially and statistically effective on force generation along the X axis. As the Figure 63 shows that the model can explain

87% of the relation between force generated along X axis and the cutting parameter of feed rate and radial depth of cut.

General Linear Model: Force X versus Feed Rate; Radial (%)

Method

Factor coding (-1; 0; +1)

Factor Information

Factor	Type	Levels	Values
Feed Rate	Fixed	4	0,015; 0,030; 0,075; 0,120
Radial (%)	Fixed	3	25; 50; 75

Analysis of Variance

Source	DF	Adj SS	Adj MS	F-Value	P-Value
Feed Rate	3	267,9	89,29	1,02	0,472
Radial (%)	2	2121,4	1060,71	12,12	0,020
Error	4	350,0	87,50		
Total	9	2737,6			

Model Summary

S	R-sq	R-sq(adj)	R-sq(pred)
9,35414	87,22%	71,23%	*

Figure 63: GLM for force along X, Feed rate vs Radial depth of cut

Now that the GLM model states the effect of radial depth of cut is statistically higher than the effect pf feed rate, cutting speed and radial depth of cut are compared to determine the most effective parameter on the force generation along X axis.

General Linear Model: Force X versus Radial (%); Vcut

Method

Factor coding (-1; 0; +1)

Factor Information

Factor	Type	Levels	Values
Radial (%)	Fixed	3	25; 50; 75
Vcut	Fixed	5	40; 80; 150; 250; 350

Analysis of Variance

Source	DF	Adj SS	Adj MS	F-Value	P-Value
Radial (%)	2	2117,8	1058,92	7,69	0,066
Vcut	4	204,9	51,22	0,37	0,818
Error	3	413,0	137,67		
Total	9	2737,6			

Model Summary

S	R-sq	R-sq(adj)	R-sq(pred)
11,7331	84,91%	54,74%	*

Figure 64: GLM for force along X, Radial depth of cut vs Cutting speed

Again, as the result of GLM to compare the effect of radial depth of cut and cutting speed given in Figure 64, radial depth of cut is statistically has more effect on the generation of force along X axis compared to cutting speed and feed rate.

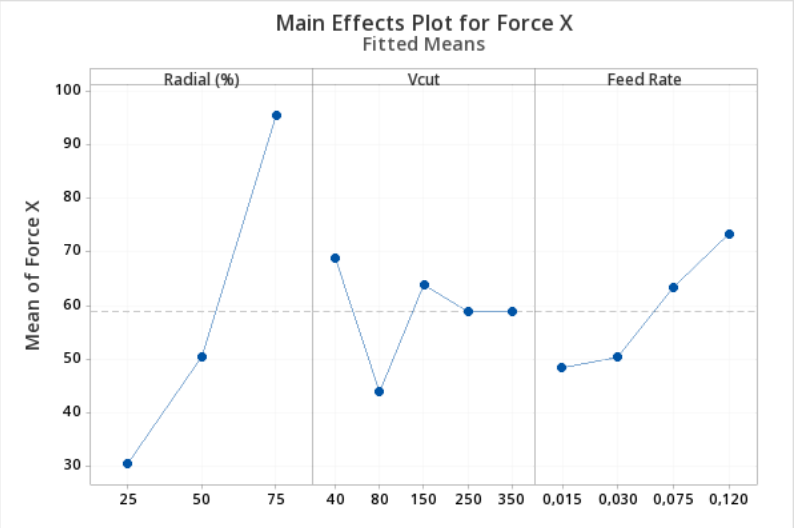

Figure 65: Factorial plot for force along X

Factorial plot for force along X axis is generated to visualize the individual effect of cutting parameters and their correlation with the Force generation along X as it is given in Figure 65. The effect of radial depth of cut can be observed as a positively correlated with the force generation along X axis where the effect of feed rate can also be interpreted as a positively correlated relation with the force generation along X axis.

The same approach is also followed for the force generation along Y axis. First, the relation between feed rate and radial depth of cut to force generation along Y axis is investigated by developing GLM model. Unlike the relation found in force along X direction, feed rate is statistically the most effective cutting parameter compared to radial depth of cut. The statistical significance that is represented by p-value is lower than 0,05 meaning that the association is statistically significant. The result of GLM is given in Figure **66**.

General Linear Model: Force Y versus Feed Rate; Radial (%)

Method

Factor coding (-1; 0; +1)

Factor Information

Factor	Type	Levels	Values
Feed Rate	Fixed	4	0,015; 0,030; 0,075; 0,120
Radial (%)	Fixed	3	25; 50; 75

Analysis of Variance

Source	DF	Adj SS	Adj MS	F-Value	P-Value
Feed Rate	3	165861	55286,9	331,46	0,000
Radial (%)	2	1606	803,1	4,81	0,086
Error	4	667	166,8		
Total	9	183368			

Model Summary

S	R-sq	R-sq(adj)	R-sq(pred)
12,9151	99,64%	99,18%	*

Figure 66: GLM for force along Y, Feed rate vs radial depth of cut

Furthermore, R-sq value of 99,64% shows that the model fits to the data set and it explains 99.64 % of the variation in the force along Y axis.

The effect of feed rate and cutting speed on force generation along Y axis is also separately investigated. The results are given in Figure 67.

General Linear Model: Force Y versus Feed Rate; Vcut

Method

Factor coding (-1; 0; +1)

Factor Information

Factor	Type	Levels	Values
Feed Rate	Fixed	4	0,015; 0,030; 0,075; 0,120
Vcut	Fixed	5	40; 80; 150; 250; 350

Analysis of Variance

Source	DF	Adj SS	Adj MS	F-Value	P-Value
Feed Rate	3	148438	49479,2	63,84	0,015
Vcut	4	723	180,9	0,23	0,899
Error	2	1550	775,0		
Total	9	183368			

Model Summary

S	R-sq	R-sq(adj)	R-sq(pred)
27,8388	99,15%	96,20%	*

Figure 67: GLM for force along Y, Feed rate vs cutting speed

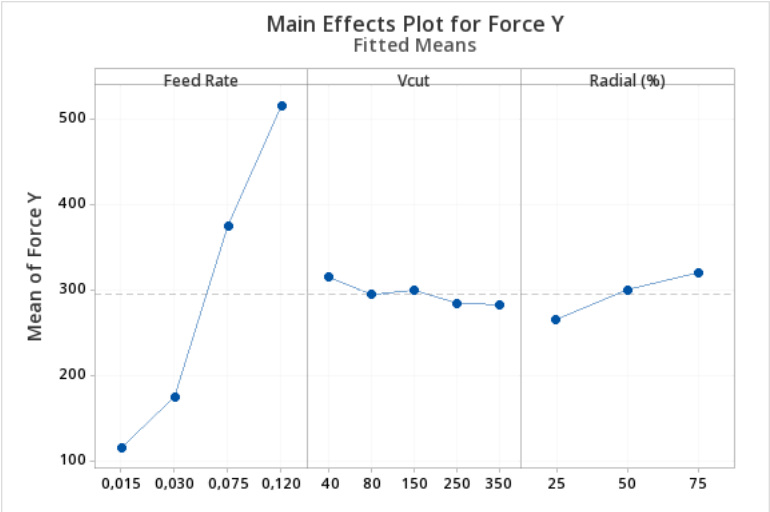

Figure 68: Factorial plot for force along Y

As Figure 67and Figure 68 shows, feed rate is positively correlated with the force generation along Y axis. This effect is visualiazed in factorial plot and statistically proven to be correct in GLM model.

It is convenient to observe that force along X axis is highly affected by radial depth of cut while the force along Y axis is mostly affected by feed rate. Morever, this effect on force along Y axis is happen to be statistically more accurate due to the R-sq of the GLM model.

The same approach is finally followed for the force generation along Z axis. First, the relation between feed rate and cutting speed to force generation along Z axis is investigated by developing GLM model.

General Linear Model: Force Z versus Feed Rate; Vcut

Method

Factor coding (-1; 0; +1)

Factor Information

Factor	Type	Levels	Values
Feed Rate	Fixed	4	0,015; 0,030; 0,075; 0,120
Vcut	Fixed	5	40; 80; 150; 250; 350

Analysis of Variance

Source	DF	Adj SS	Adj MS	F-Value	P-Value
Feed Rate	3	500,00	166,67	6,67	0,133
Vcut	4	507,71	126,93	5,08	0,171
Error	2	50,00	25,00		
Total	9	950,40			

Model Summary

S	R-sq	R-sq(adj)	R-sq(pred)
5	94,74%	76,33%	*

Figure 69: GLM for force along Z, Feed rate vs cutting speed

General Linear Model: Force Z versus Feed Rate; Radial (%)

Method

Factor coding (-1; 0; +1)

Factor Information

Factor	Type	Levels	Values
Feed Rate	Fixed	4	0,015; 0,030; 0,075; 0,120
Radial (%)	Fixed	3	25; 50; 75

Analysis of Variance

Source	DF	Adj SS	Adj MS	F-Value	P-Value
Feed Rate	3	287,7	95,89	0,95	0,498
Radial (%)	2	152,5	76,26	0,75	0,528
Error	4	405,2	101,30		
Total	9	950,4			

Model Summary

S	R-sq	R-sq(adj)	R-sq(pred)
10,0648	57,37%	4,07%	*

Figure 70: GLM for force along Z, Feed rate vs Radial depth of cut

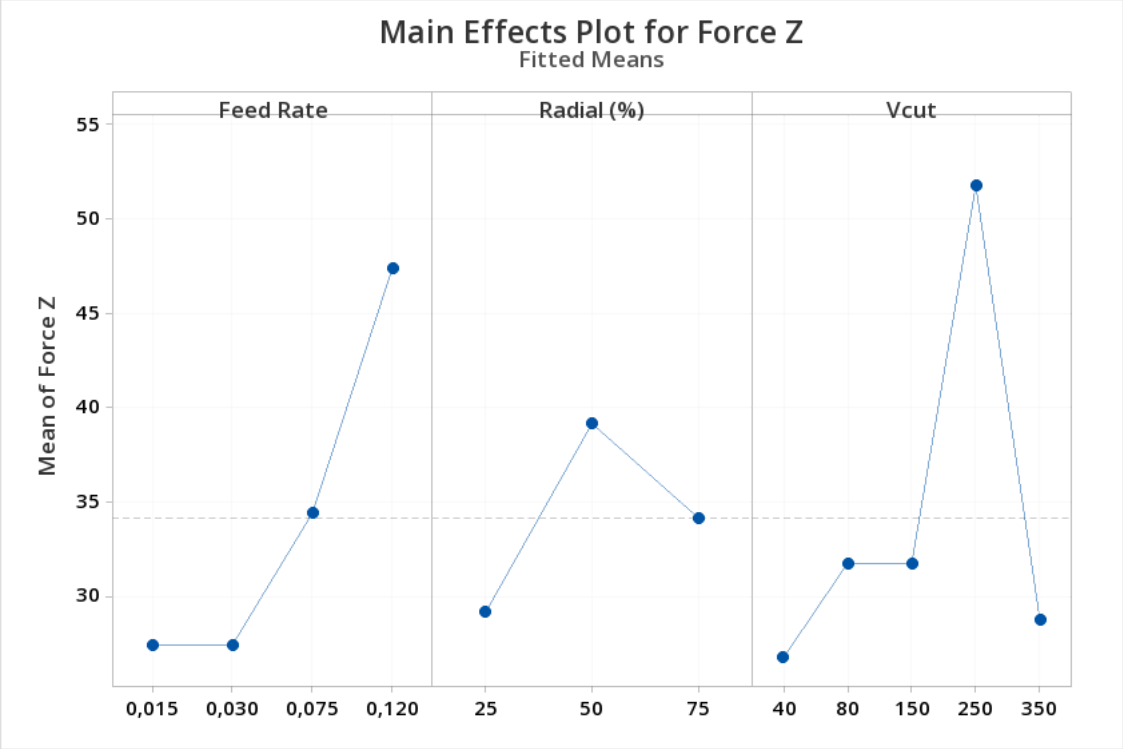

Figure 71: Factorial plot for force along Z

In the first run of the GLM model for force along Z axis, the effect of feed rate and cutting speed are compared. As it is given in Figure 69, both parameter has higher p-values meaning that the effect is not statistically significant. This phenomenon can be caused by

the insufficient number of test that has been conducted, the complexity of DoE and the number of parameter that can affect the force generation along Z direction.

The same investigation is generated for feed rate and radial depth of cut and as it is given in Figure 70, again the p-values for both the parameter is not statistically significant to conclude that the force along Z axis is definitely affected by one machining parameter given in experimental setup.

Figure 71 visualizes a positive correlation between force along Z axis and feed rate. Even though this phenomenon cannot be explained statistically due to the insufficient data set, the effect can visually be observed for insight generation.

In edge trimming operations, the forces acting on an object along the x, y, and z axes will depend on the specific details of the operation and the materials being trimmed. Some factors that can affect the magnitude and direction of the force acting on an object in edge trimming operations include the material being trimmed, the cutting tool, the cutting speed, the clamping force and the feed rate. These are just a few examples of factors that can affect the force acting on an object in edge trimming operations. There may be other factors that are specific to the particular operation being performed. In this experiment, it is observed that the force generation in each direction is separately affected by different machining parameters.

CHAPTER 6

Conclusion and Future Work

The purpose of this study was to provide an overview of recent research on CFRP machining, various delamination assessment formulation generated for different use cases are examined, a detailed explanation of each process parameter for the chosen manufacturing process, identify the relationships between the key parameters, assess how

each parameter affected the final product's machining quality, and offer a suitable parameter selection strategy. Within this study, drilling operations are performed to measure drilling quality in a machine shop setting and identify the impact of machining parameters without the use of high-tech cameras, edge trimming operations are conducted to assess the performance of suction system designed to vacuum airborne CFRP dust and again, edge trimming operations are performed to analyse the effect of machining parameter to force generation during the machining operation which is known to be highly related with the formation of machining induced damaged in CFRP materials.

It was concluded that an increase in engagement area increases the likelihood of collecting dust particles generated during the machining operation and a decrease in spindle speed prevents dust particles from spreading hence increases the suction performance. Furthermore, since a decrease in feed rate decreases material removal rate, dust formation is by nature inhibited and it is convenient to find the best performing machining parameter for higher axial depth of cut, lower spindle speed and lower feed rate values.

Image processing technique and image processing model developed to assess the drilling quality has been proven to be an appropriate method to quickly determine the severity of the delamination without the need for highly developed laboratory cameras. Moreover, the result of the model is implemented in the delamination formulations that are used in the literature to select the best fitting formulation for similar experiments.

It is observed that the nature of force generation in edge trimming operation is correlated with different machining parameter in each axis and to minimize the effect of high force generation, related machining parameter for that special axis should be selected accordingly.

CFRP materials are important because of their combination of high strength, stiffness, fatigue resistance, corrosion resistance, high temperature resistance, and customizability and optimizing the machining of CFRP materials is important because it can help to improve the efficiency, accuracy, and cost-effectiveness of the manufacturing process, as well as the quality and performance of the finished parts. It requires specialized tools and techniques to achieve good results, and it is generally considered to be more challenging

than machining metal materials due to the abrasive nature of the carbon fibers in the composite. In literature, there are many studies focused to understand the machining nature of CFRP and optimize the machining process in perspective of defect and efficiency. This study will enlighten the researchers in terms of choosing the machining parameters that suits best for the purpose and improve the visibility of the machining operation for higher performance.

References

[1] Davim JP, editor. Machining composites materials. John Wiley & Sons; 2013 Oct 28.

[2] Soutis C. Fibre reinforced composites in aircraft construction. Progress in aerospace sciences. 2005 Feb 1;41(2):143-51.

[3] Mouritz AP. Introduction to aerospace materials. Elsevier; 2012 May 23.

[4] Che D, Saxena I, Han P, Guo P, Ehmann KF. Machining of carbon fiber reinforced plastics/polymers: a literature review. Journal of Manufacturing Science and Engineering. 2014 Jun 1;136(3).

[5] Giasin K, Ayvar-Soberanis S. An Investigation of burrs, chip formation, hole size, circularity and delamination during drilling operation of GLARE using ANOVA. Composite Structures. 2017 Jan 1;159:745-60.

[6] Giasin K, Hodzic A, Phadnis V, Ayvar-Soberanis S. Assessment of cutting forces and hole quality in drilling Al2024 aluminium alloy: experimental and finite element study. The International Journal of Advanced Manufacturing Technology. 2016 Nov;87(5):2041-61.

[7] Clyne TW, Hull D. An introduction to composite materials. Cambridge university press; 2019 Jul 11.

[8] Strong AB. Fundamentals of composites manufacturing: materials, methods and applications. Society of manufacturing engineers; 2008.

[9] Liu D, Tang Y, Cong WL. A review of mechanical drilling for composite laminates. Composite structures. 2012 Mar 1;94(4):1265-79.

[10] Wang GD, Kirwa MS. Comparisons of the use of twist, pilot-hole and step-drill on influence of carbon fiber-reinforced polymer drilling hole quality. Journal of Composite Materials. 2018 May;52(11):1465-80.

[11] Niu C, Niu MC. Airframe structural design: practical design information and data on aircraft structures. Conmilit Press; 1988.

[12] Hocheng H, Puw HY, Huang Y. Preliminary study on milling of unidirectional carbon fibre-reinforced plastics. Composites Manufacturing. 1993 Jun 1;4(2):103-8.

[13] Wang XM, Zhang LC. An experimental investigation into the orthogonal cutting of unidirectional fibre reinforced plastics. International journal of machine tools and manufacture. 2003 Aug 1;43(10):1015-22.

[14] Palanikumar K. Modeling and analysis for surface roughness in machining glass fibre reinforced plastics using response surface methodology. Materials & design. 2007 Jan 1;28(10):2611-8.

[15] Gao C, Xiao J, Xu J, Ke Y. Factor analysis of machining parameters of fiber-reinforced polymer composites based on finite element simulation with experimental investigation. The International Journal of Advanced Manufacturing Technology. 2016 Mar;83(5):1113-25.

[16] Gao H, Bao YJ, Feng ZM. A study of drilling uni-directional carbon/epoxy composites. International Journal of Abrasive Technology. 2011 Jan 1;4(1):1-3.

[17] Ahmad J.S, Machining of polymer composites, Boston: MA,2009.

[18] Feito N, Díaz-Álvarez J, Díaz-Álvarez A, Cantero JL, Miguélez MH. Experimental analysis of the influence of drill point angle and wear on the drilling of woven CFRPs. Materials. 2014 May 30;7(6):4258-71.

[19] Giasin K, Ayvar-Soberanis S, Hodzic A. An experimental study on drilling of unidirectional GLARE fibre metal laminates. Composite Structures. 2015 Dec 1;133:794-808.

[20] KoPlev AA, Lystrup A, Vorm T. The cutting process, chips, and cutting forces in machining CFRP. composites. 1983 Oct 1;14(4):371-6.

[21] Santhanakrishnan G, Krishnamurthy R, Malhotra SK. Machinability characteristics of fibre reinforced plastics composites. Journal of Mechanical Working Technology. 1988 Aug 1;17:195-204.

[22] Karpat Y, Bahtiyar O, Değer B. Mechanistic force modeling for milling of unidirectional carbon fiber reinforced polymer laminates. International Journal of Machine Tools and Manufacture. 2012 May 1;56:79-93.

[23] Wang DH, Ramulu M, Arola D. Orthogonal cutting mechanisms of graphite/epoxy composite. Part I: unidirectional laminate. International Journal of Machine Tools and Manufacture. 1995 Dec 1;35(12):1623-38.

[24] Teti R. Machining of composite materials. CIRP Annals. 2002 Jan 1;51(2):611-34.

[25] Groover MP. Fundamentals of modern manufacturing: materials, processes, and systems. John Wiley & Sons; 2020 Jul 15.

[26] Singh R. Introduction to basic manufacturing processes and workshop technology. New Age International; 2006.

[27] Shaw MC, Cookson JO. Metal cutting principles. New York: Oxford university press; 2005.

[28] Knight WA, Boothroyd G. Fundamentals of metal machining and machine tools. CRC Press; 2005 Nov 1.

[29] Azmi AI, Lin RJ, Bhattacharyya D. Machinability study of glass fibre-reinforced polymer composites during end milling. The International Journal of Advanced Manufacturing Technology. 2013 Jan;64(1):247-61.

[30] Davim JP, Reis P, Antonio CC. A study on milling of glass fiber reinforced plastics manufactured by hand-lay up using statistical analysis (ANOVA). Composite structures. 2004 Jun 1;64(3-4):493-500.

[31] Mathivanan NR, Mahesh BS, Shetty HA. An experimental investigation on the process parameters influencing machining forces during milling of carbon and glass fiber laminates. Measurement. 2016 Sep 1;91:39-45.

[32] Hintze W, Cordes M, Koerkel G. Influence of weave structure on delamination when milling CFRP. Journal of Materials Processing Technology. 2015 Feb 1;216:199-205.

[33] Haddad M, Zitoune R, Bougherara H, Eyma F, Castanié B. Study of trimming damages of CFRP structures in function of the machining processes and their impact on the mechanical behavior. Composites Part B: Engineering. 2014 Feb 1;57:136-43.

[34] Sheikh-Ahmad J, Urban N, Cheraghi H. Machining damage in edge trimming of CFRP. Materials and Manufacturing Processes. 2012 Jul 1;27(7):802-8.

[35] Sheikh-Ahmad J, Shahid AH. Effect of edge trimming on failure stress of carbon fibre polymer composites. International Journal of Machining and Machinability of Materials. 2013 Jan 1;13(2-3):331-47.

[36] Khan ZM. A study of the drilling of advanced carbon fibre composites (Doctoral dissertation, University of Salford).

[37] PMelentiev R, Priarone PC, Robiglio M, Settineri L. Effects of tool geometry and process parameters on delamination in CFRP drilling: An overview. Procedia Cirp. 2016 Jan 1;45:31-4.

[38] Davim JP, Reis P. Drilling carbon fiber reinforced plastics manufactured by autoclave—experimental and statistical study. Materials & design. 2003 Aug 1;24(5):315-24.

[39] Abrão AM, Faria PE, Rubio JC, Reis P, Davim JP. Drilling of fiber reinforced plastics: A review. Journal of Materials Processing Technology. 2007 May 7;186(1-3):1-7.

[40] Abrao AM, Rubio JC, Faria PE, Davim JP. The effect of cutting tool geometry on thrust force and delamination when drilling glass fibre reinforced plastic composite. Materials & Design. 2008 Jan 1;29(2):508-13.

[41] Shyha IS, Aspinwall DK, Soo SL, Bradley S. Drill geometry and operating effects when cutting small diameter holes in CFRP. International journal of machine tools and manufacture. 2009 Oct 1;49(12-13):1008-14.

[42] Palanikumar K. Experimental investigation and optimisation in drilling of GFRP composites. Measurement. 2011 Dec 1;44(10):2138-48.

[43] Rajakumar IP, Hariharan P, Srikanth I. A study on monitoring the drilling of polymeric nanocomposite laminates using acoustic emission. Journal of composite materials. 2013 Jun;47(14):1773-84.

[44] Krishnaraj V, Prabukarthi A, Ramanathan A, Elanghovan N, Kumar MS, Zitoune R, Davim JP. Optimization of machining parameters at high speed drilling of carbon fiber reinforced plastic (CFRP) laminates. Composites Part B: Engineering. 2012 Jun 1;43(4):1791-9.

[45] Marques AT, Durão LM, Magalhães AG, Silva JF, Tavares JM. Delamination analysis of carbon fibre reinforced laminates: evaluation of a special step drill. Composites Science and Technology. 2009 Nov 1;69(14):2376-82.

[46] Tsao CC. Investigation into the effects of drilling parameters on delamination by various step-core drills. Journal of materials processing technology. 2008 Sep 12;206(1-3):405-11.

[47] Quan Y, Zhong W. Investigation on drilling-grinding of CFRP. Frontiers of Mechanical Engineering in China. 2009 Mar;4(1):60-3.

[48] Gaitonde V, Karnik SR, Rubio JC, Correia AE, Abrao AM, Davim JP. Analysis of parametric influence on delamination in high-speed drilling of carbon fiber reinforced plastic composites. Journal of materials processing technology. 2008 Jul 18;203(1-3):431-8.

[49] Durão LM, Gonçalves DJ, Tavares JM, de Albuquerque VH, Vieira AA, Marques AT. Drilling tool geometry evaluation for reinforced composite laminates. Composite structures. 2010 Jun 1;92(7):1545-50.

[50] Grilo TJ, Paulo RM, Silva CR, Davim JP. Experimental delamination analyses of CFRPs using different drill geometries. Composites Part B: Engineering. 2013 Feb 1;45(1):1344-50.

[51] Davim JP, Reis P, Antonio CC. Experimental study of drilling glass fiber reinforced plastics (GFRP) manufactured by hand lay-up. Composites Science and Technology. 2004 Feb 1;64(2):289-97.

[52] Davim JP, Reis P. Study of delamination in drilling carbon fiber reinforced plastics (CFRP) using design experiments. Composite structures. 2003 Mar 1;59(4):481-7.

[53] Kilickap E. Optimization of cutting parameters on delamination based on Taguchi method during drilling of GFRP composite. Expert systems with applications. 2010 Aug 1;37(8):6116-22.

[54] Khashaba UA, El-Sonbaty IA, Selmy AI, Megahed AA. Machinability analysis in drilling woven GFR/epoxy composites: Part I–Effect of machining parameters. Composites Part A: Applied Science and Manufacturing. 2010 Mar 1;41(3):391-400.

[55] Mishra R, Malik J, Singh I, Davim JP. Neural network approach for estimating the residual tensile strength after drilling in uni-directional glass fiber reinforced plastic laminates. Materials & Design. 2010 Jun 1;31(6):2790-5.

[56] Ho-Cheng H, Dharan CK. Delamination during drilling in composite laminates.

[57] Jain S, Yang DC. Delamination-free drilling of composite laminates.

[58] Tsao CC, Hocheng H. Taguchi analysis of delamination associated with various drill bits in drilling of composite material. International Journal of Machine Tools and Manufacture. 2004 Aug 1;44(10):1085-90.

[59] Chen WC. Some experimental investigations in the drilling of carbon fiber-reinforced plastic (CFRP) composite laminates. International Journal of Machine Tools and Manufacture. 1997 Aug 1;37(8):1097-108.

[60] Shyha I, Soo SL, Aspinwall D, Bradley S. Effect of laminate configuration and feed rate on cutting performance when drilling holes in carbon fibre reinforced plastic composites. Journal of materials processing technology. 2010 Jun 1;210(8):1023-34.

[61] Khashaba UA. Delamination in drilling GFR-thermoset composites. InInternational conference on aerospace sciences and aviation technology 2003 May 1 (Vol. 10, No. 10th International Conference On Aerospace Sciences & Aviation Technology, pp. 461-481). The Military Technical College.

[62] Faraz A, Biermann D, Weinert K. Cutting edge rounding: An innovative tool wear criterion in drilling CFRP composite laminates. International Journal of Machine Tools and Manufacture. 2009 Dec 1;49(15):1185-96.

[63] Davim JP, Rubio JC, Abrao AM. A novel approach based on digital image analysis to evaluate the delamination factor after drilling composite laminates. Composites Science and Technology. 2007 Jul 1;67(9):1939-45.

[64] Scott IG, Scala CM. A review of non-destructive testing of composite materials. NDT international. 1982 Apr 1;15(2):75-86.

[65] Silva DN. Image processing methodology for assessment of drilling induced damage in CFRP (Doctoral dissertation, Faculdade de Ciências e Tecnologia).

[66] Hocheng H, Tsao CC. The path towards delamination-free drilling of composite materials. Journal of materials processing technology. 2005 Aug 30;167(2-3):251-64.

[67] Lazar MB, Xirouchakis P. Experimental analysis of drilling fiber reinforced composites. International Journal of Machine Tools and Manufacture. 2011 Dec 1;51(12):937-46.

[68] Tsao CC, Hocheng H. Effects of exit back-up on delamination in drilling composite materials using a saw drill and a core drill. International Journal of Machine Tools and Manufacture. 2005 Sep 1;45(11):1261-70.

[69] Capello E. Workpiece damping and its effect on delamination damage in drilling thin composite laminates. Journal of Materials Processing Technology. 2004 May 15;148(2):186-95.

[70] Stone R, Krishnamurthy K. A neural network thrust force controller to minimize delamination during drilling of graphite-epoxy laminates. International Journal of Machine Tools and Manufacture. 1996 Sep 1;36(9):985-1003.

[71] Hocheng H, Tsao CC. Effects of special drill bits on drilling-induced delamination of composite materials. International Journal of Machine Tools and Manufacture. 2006 Oct 1;46(12-13):1403-16.

Appendix

Drilling Test Results

Test	Image processing internal contour		Image processing external contour
1	Calculated by Circle Fit approach: ---------- Diameter=12.2154mm Area=117.1946mm^2 Found from area: ---------- Diameter=8.6893mm Area=59.3mm^2	Diameter max Diameter min	Calculated by Circle Fit approach: ---------- Diameter=18.8496mm Area=279.0586mm^2 Found from area: ---------- Diameter=12.7179mm Area=127.0333mm^2
2	Calculated by Circle Fit approach: ---------- Diameter=12.4652mm Area=122.0355mm^2 Found from area: ---------- Diameter=8.8552mm Area=61.5869mm^2		Calculated by Circle Fit approach: ---------- Diameter=18.3584mm Area=264.7023mm^2 Found from area: ---------- Diameter=12.4155mm Area=121.0653mm^2
3	Calculated by Circle Fit approach: ---------- Diameter=12.5396mm Area=123.4981mm^2 Found from area: ----------		Calculated by Circle Fit approach: ---------- Diameter=17.535mm Area=241.4907mm^2 Found from area: ----------

	Diameter=8.9525mm Area=62.948mm^2	Diameter=12.3301mm Area=119.4057mm^2
4	Calculated by Circle Fit approach: ---------- Diameter=12.645mm Area=125.5825mm^2 Found from area: ---------- Diameter=9.0098mm Area=63.756mm^2	Calculated by Circle Fit approach: ---------- Diameter=17.511mm Area=240.8316mm^2 Found from area: ---------- Diameter=12.2113mm Area=117.1145mm^2
5	Calculated by Circle Fit approach: ---------- Diameter=12.6527mm Area=125.7358mm^2 Found from area: ---------- Diameter=9.0483mm Area=64.3014mm^2	Calculated by Circle Fit approach: ---------- Diameter=18.5244mm Area=269.5132mm^2 Found from area: ---------- Diameter=12.7103mm Area=126.8824mm^2
6	Calculated by Circle Fit approach: ---------- Diameter=12.2699mm Area=118.2414mm^2 Found from area: ---------- Diameter=8.7067mm Area=59.5388mm^2	Calculated by Circle Fit approach: ---------- Diameter=17.5752mm Area=242.5986mm^2 Found from area: ---------- Diameter=12.278mm Area=118.3977mm^2
7	Calculated by Circle Fit approach: ---------- Diameter=12.6058mm Area=124.8038mm^2 Found from area: ---------- Diameter=8.9882mm Area=63.45mm^2	Calculated by Circle Fit approach: ---------- Diameter=18.1616mm Area=259.0588mm^2 Found from area: ---------- Diameter=12.6608mm Area=125.8965mm^2
8	Calculated by Circle Fit approach: ---------- Diameter=12.8202mm Area=129.0858mm^2 Found from area: ---------- Diameter=9.0956mm Area=64.9761mm^2	Calculated by Circle Fit approach: ---------- Diameter=17.4235mm Area=238.4301mm^2 Found from area: ---------- Diameter=12.2074mm Area=117.0404mm^2
9	Calculated by Circle Fit approach: ---------- Diameter=12.9487mm Area=131.6858mm^2 Found from area: ---------- Diameter=9.2419mm Area=67.083mm^2	Calculated by Circle Fit approach: ---------- Diameter=17.2056mm Area=232.5039mm^2 Found from area: ---------- Diameter=12.1114mm Area=115.207mm^2

10	Calculated by Circle Fit approach: ---------- Diameter=13.137mm Area=135.544mm^2 Found from area: ---------- Diameter=9.3571mm Area=68.7655mm^2	Calculated by Circle Fit approach: ---------- Diameter=17.1524mm Area=231.0691mm^2 Found from area: ---------- Diameter=12.0772mm Area=114.5573mm^2
11	Calculated by Circle Fit approach: ---------- Diameter=12.5277mm Area=123.2639mm^2 Found from area: ---------- Diameter=9.0238mm Area=63.9548mm^2	Calculated by Circle Fit approach: ---------- Diameter=17.3841mm Area=237.3526mm^2 Found from area: ---------- Diameter=12.2079mm Area=117.051mm^2
12	Calculated by Circle Fit approach: ---------- Diameter=12.4376mm Area=121.4962mm^2 Found from area: ---------- Diameter=9.1209mm Area=65.3378mm^2	Calculated by Circle Fit approach: ---------- Diameter=17.5557mm Area=242.0625mm^2 Found from area: ---------- Diameter=12.1544mm Area=116.027mm^2
13	Calculated by Circle Fit approach: ---------- Diameter=12.7937mm Area=128.5533mm^2 Found from area: ---------- Diameter=9.214mm Area=66.6782mm^2	Calculated by Circle Fit approach: ---------- Diameter=18.7254mm Area=275.392mm^2 Found from area: ---------- Diameter=12.2472mm Area=117.8041mm^2
14	Calculated by Circle Fit approach: ---------- Diameter=13.1473mm Area=135.7582mm^2 Found from area: ---------- Diameter=9.3955mm Area=69.331mm^2	Calculated by Circle Fit approach: ---------- Diameter=17.2107mm Area=232.6401mm^2 Found from area: ---------- Diameter=12.0581mm Area=114.1956mm^2
15	Calculated by Circle Fit approach: ---------- Diameter=13.387mm Area=140.7532mm^2 Found from area: ---------- Diameter=9.599mm Area=72.3679mm^2	Calculated by Circle Fit approach: ---------- Diameter=17.3376mm Area=236.0855mm^2 Found from area: ---------- Diameter=12.0204mm Area=113.4813mm^2
16	Calculated by Circle Fit approach: ---------- Diameter=12.9801mm	Calculated by Circle Fit approach: ---------- Diameter=17.4854mm

	Area=132.3253mm^2	Area=240.1269mm^2
	Found from area: --- Diameter=9.3373mm Area=68.4755mm^2	Found from area: --- Diameter=12.1754mm Area=116.4274mm^2
	Calculated by Circle Fit approach: --- Diameter=12.9853mm	Calculated by Circle Fit approach: --- Diameter=17.5849mm
17	Area=132.4318mm^2	Area=242.8668mm^2
	Found from area: --- Diameter=9.3462mm Area=68.6057mm^2	Found from area: --- Diameter=12.3553mm Area=119.8944mm^2
	Calculated by Circle Fit approach: --- Diameter=13.0797mm	Calculated by Circle Fit approach: --- Diameter=17.0661mm
18	Area=134.3646mm^2	Area=228.7496mm^2
	Found from area: --- Diameter=9.3481mm Area=68.633mm^2	Found from area: --- Diameter=12.101mm Area=115.0084mm^2
	Calculated by Circle Fit approach: --- Diameter=13.3334mm	Calculated by Circle Fit approach: --- Diameter=17.1577mm
19	Area=139.6282mm^2	Area=231.212mm^2
	Found from area: --- Diameter=9.5615mm Area=71.8028mm^2	Found from area: --- Diameter=12.0183mm Area=113.4435mm^2
	Calculated by Circle Fit approach: --- Diameter=13.3956mm	Calculated by Circle Fit approach: --- Diameter=16.9851mm
20	Area=140.934mm^2	Area=226.5836mm^2
	Found from area: --- Diameter=9.6187mm Area=72.6653mm^2	Found from area: --- Diameter=11.9961mm Area=113.0234mm^2

Image processing MATLAB Code (Partially):

Function used to calculate hole diameter:

```
function [diaMMCF alanCF diaMMAC alanAC]=delikCapiHesapla(strImage)
%clc
Irgb=imread(strImage);
close all;
I=Irgb;
Igr = rgb2gray(I);
level = graythresh(Igr);
Ibw = im2bw(I,level^2);
Ibwx=imcomplement(Ibw);
% close all
figure;Ibwx2 = imcomplement(Ibwx);imshow(Ibwx2);title('BW Image');
```

```
Ibw2 = bwareaopen(Ibwx,
100000);Ibw=Ibw2;figure;imshow(imcomplement(Ibw));title('Small objects
removed')


Ibw2 = imfill((Ibw2),'holes');
figure;Ibw2x = imcomplement(Ibw2);imshow(Ibw2x);title('Filled Holes');

Alan1=sum(sum(Ibw2x))

Alan2=sum(sum(Ibw2))

Ibwx=Ibw2;

[features, count_circles, centers, separation12,diameterx] =
findcircles(Ibw2);

diameterEski=diameterx;

offset=0;
testSonuc=0;

diameterx=diameterx+1;

diameter=diameterx;
figure;
imshow(Irgb);
hold on;
xler=[];
yler=[];
for i=0:1:360
    xler=[xler centers(2)+offset+cosd(i)*diameter/2];
    yler=[yler centers(1)+offset+sind(i)*diameter/2];
end

xler=[];
yler=[];
for i=0:1:360
    xler=[xler centers(2)+offset+cosd(i)*diameterEski/2];
    yler=[yler centers(1)+offset+sind(i)*diameterEski/2];
end

diameterOrt=(diameter+diameterEski)/2;
xler=[];
yler=[];
for i=0:1:360
    xler=[xler centers(2)+offset+cosd(i)*diameterOrt/2];
    yler=[yler centers(1)+offset+sind(i)*diameterOrt/2];
end
%plot(xler,yler,'c-.','LineWidth',2);


[B,L,N,A] = bwboundaries(Ibw);
boundary = B{1};

noktalar=[];
for i=1:size(boundary,1)
    noktalar=[noktalar; double(boundary(i,2))+offset,
double(boundary(i,1))+offset];
end
```

```
[z, r, residual] = fitcircle(noktalar');
z
r
residual

xler=[];
yler=[];
for i=0:1:360
    xler=[xler z(1)+offset+cosd(i)*r];
    yler=[yler z(2)+offset+sind(i)*r];
end
plot(xler,yler,'g.','LineWidth',2);

plot(boundary(:,2)+offset, boundary(:,1)+offset, 'r', 'LineWidth', 2)
display([' '])
radiusPixel=r;
radiusMM=radiusPixel/24*2.5/14;
diaMMCF=2*radiusMM;
alanCF=pi*radiusMM*radiusMM;
display(['Circle Fit ile Bulunan:'])
display(['-------------'])
display([' Cap=' num2str(2*radiusMM) 'milimetre'])
display(['Alan=' num2str(alanCF) 'milimetrekare'])
display([' '])


Radius1x=sqrt(Alan1/pi);
Radius2x=sqrt(Alan2/pi);
radiusPixel=Radius2x;
radiusMM=radiusPixel/24*2.5/14;
diaMMAC=2*radiusMM;
alanAC=pi*radiusMM*radiusMM;
display(['Alandan Bulunan:'])
display(['-------------'])
display([' Cap=' num2str(2*radiusMM) 'milimetre'])
display(['Alan=' num2str(alanAC) 'milimetrekare'])
display([' '])
```

Function used to fit the best fitting circle:

```
function y = imcircle(n)

if rem(n,1) > 0,
   disp(sprintf('n is not an integer and has been rounded to
%1.0f',round(n)))
   n = round(n);
end

if n < 1     % invalid n
   error('n must be at least 1')

elseif n < 4 % trivial n
   y = ones(n);

elseif rem(n,2) == 0,  % even n

   DIAMETER = n;
   diameter = n-1;
   RADIUS = DIAMETER/2;
   radius = diameter/2;
```

```
    height_45 = round(radius/sqrt(2));
    width = zeros(1,RADIUS);
    semicircle = zeros(DIAMETER,RADIUS);

    for i  = 1 : height_45
        upward = i - 0.5;
        sine = upward/radius;
        cosine = sqrt(1-sine^2);
        width(i) = ceil(cosine * radius);
    end

    array = width(1:height_45)-height_45;

    for j = max(array):-1:min(array)
        width(height_45 + j) = max(find(array == j));
    end

    if min(width) == 0
       index = find(width == 0);
       width(index) = round(mean([width(index-1) width(index+1)]));
    end

    width = [fliplr(width) width];

    for k  = 1 : DIAMETER
        semicircle(k,1:width(k)) = ones(1,width(k));
    end

    y = [fliplr(semicircle) semicircle];

else   % odd n

    DIAMETER = n;
    diameter = n-1;
    RADIUS = DIAMETER/2;
    radius = diameter/2;
    semicircle = zeros(DIAMETER,radius);
    height_45 = round(radius/sqrt(2) - 0.5);
    width = zeros(1,radius);

    for i  = 1 : height_45
        upward = i;
        sine = upward/radius;
        cosine = sqrt(1-sine^2);
        width(i) = ceil(cosine * radius - 0.5);
    end

    array = width(1:height_45) - height_45;

    for j = max(array):-1:min(array)
        width(height_45 + j) = max(find(array == j));
    end

    if min(width) == 0
       index = find(width == 0);
       width(index) = round(mean([width(index-1) width(index+1)]));
    end

    width = [fliplr(width) max(width) width];
```

```
    for k  = 1 : DIAMETER
        semicircle(k,1:width(k)) = ones(1,width(k));
    end

    y = [fliplr(semicircle) ones(DIAMETER,1) semicircle];

end
```